Unitat de Química Física
Departament de Química
Universitat Autònoma de Barcelona

ACTIVATION OF AMINO ACIDS AND PEPTIDES BY INTERACTION OF Cu^{+} AND Cu^{2+} CATIONS AND ALUMINOSILICATE SURFACES

Albert Rimola Gibert

March 2007

Els sotasignants **Dra. Mariona Sodupe i Roure** i **Dr. Luis Rodríguez i Santiago**

Certifiquem

Que **Albert Rimola i Gibert** ha realitzat sota la nostra direcció al Departament de Química de la Universitat Autònoma de Barcelona la tesi doctoral que porta per títol

Activation of amino acids and peptides by interaction of Cu^{+} and Cu^{2+} cations and aluminosilicate surfaces

que es presenta en aquesta memòria per optar al grau de doctor per la Universitat Autònoma de Barcelona dins del programa de Química Teòrica i Computacional.

Mariona Sodupe i Roure

Luis Rodríguez i Santiago

Bellaterra, Març 2007

Aquesta tesi doctoral s'ha pogut realitzar gràcies als aports financers de:

- Beca predoctoral per a la Formació de Personal Investigador de la UAB.

- Contracte de profesor ajudant de la UAB.

- Projecte «Grup d'Estructura i Reactivitat Química», (2001SGR-00812).

- Projecte «Ionización y activación por cationes metálicos de sistemas de interés bioquímico. Estudios teóricos y de espectrometría de masas», (BQU2002-04112-C02-01).

- Projecte «Grup d'Estudis Teòrics d'Activació de Biomolècules», (SGR2005-00244).

- Projecte «Activación de biomoléculas. Estudios computacionales y de espectrometría de masas», (CTQ2005-08797-C02-02/BQU).

Els ideals són com els estels,
no els assolim però il·luminen el nostre camí
Demòcrit

Als pares, germans, i a la Itzi

A tots aquells que m'han donat una oportunitat.

Als que m'han ensenyat i a qui jo he ensenyat.

Als que m'han ajudat i a qui he ajudat.

Als que m'han fet costat i a qui he fet costat.

Als que m'han escoltat i a qui he escoltat.

Als que m'han fet riure i a qui he fet riure.

Als que ja no són aquí.

Amb els que compartim, valorem, aprenem i confiem.

Als que m'estimen i a qui estimo.

Amb els que encara continuem somiant desperts

Moltes gràcies a tots!

CONTENTS

OUTLOOK

When starting a PhD degree in the field of theoretical and computational chemistry it is usual to establish both the problem to study and the methodology to employ. However, a thesis is not independent of itself so the results obtained in the step *n* can affect the direction of the step *n+1*. In this sense, a thesis is like a person: birth, growth, reproduction and death.

Since some years ago, our research group addresses theoretical studies of the activation of small biomolecules. Initially this subject focused on the activation of, on one hand, nucleobases, nucleosides and nucleotides, and on the other hand, amino acids and peptides induced by metal cation interactions and by UV or oxidising radiation. Additionally, other studies carried out in our group treated the interaction of small molecules with mineral surfaces such as zeolites, which can also be potential activator agents for biomolecules. Understanding the fundamental nature of the interaction of biological molecules and inorganic substrates present an enormous interest in many fields such as prebiotic chemistry, astrobiology, or bionanotechnology. In the present thesis, the activation, which in principle affects the reactivity of these biological interesting molecules, is studied by means of sophisticated quantum chemical calculations.

This thesis presents an exhaustive study of the activation of amino acids and peptides by Cu^{+} and Cu^{2+} binding. In addition, it provides the first results obtained in the group on the activation of amino acids by silica-based materials. Consequently, it involves a great variety of areas that come from the gas phase chemistry to homogeneous and heterogeneous catalysis. Despite of that, the introduction has been mainly focused on the context of the gas phase chemistry of metal-containing systems since nowadays is the main research topic of the group and because the most extense part of the work presented here refers to this subject.

The present thesis is divided in 7 chapters. Chapter 1 is an introduction of the gas phase ion chemistry: the relevance of mass spectrometry when studying biological systems and the role that theoretical calculations play in this area. Chapter 2 focuses on the technical aspects of mass spectrometry (generation, detection and fragmentation of the ions in the gas phase) as well as on the brief description of several mass spectrometry techniques to obtain valuable thermodynamic and structural information. Chapter 3 concerns to the methodological aspects when treating with transition metal-containing systems, from both theoretical and gas phase experimental point of view. The subsequent

three chapters describe the three different studies included in this thesis. Each chapter will present a specific introduction to the problem, the goals of the study, the methodology employed and a discussion of the obtained results. Chapter 4 is related to an experimental and theoretical study of the coordination properties of AA_{arom} (AA_{arom} = phenylalanine, tyrosine, triptophane and histidine) to $Cu^{+/2+}$ as well as the reactivity induced by Cu^{+} when interacting with these amino acids. I would like to mention that the experimental results were obtained in a short stay of three months during the spring of 2004 at the Université of Évry-Val d'Essonne under the supervision of Dr. Jeanine Tortajada. Chapter 5 concerns to a computational study of the structure, relative energies and binding energies of the complexes formed by the interaction of $Cu^{+/2+}$ with the $(glycyl)_n$glycine (n = 1-3) oligomers. The results exposed in chapter 6 address to the activation of glycine to form peptide bonds with other amino acids. In this line, the role of Cu^{2+} and aluminosilicates has been examined. I would like to comment that the study in which aluminosilicates are used as catalytic supports has been carried out in a close collaboration of the group leaded by Dr. Piero Ugliengo from the Università degli Studio di Torino, where I did a short stay of three months during the spring of 2005. Finally, in chapter 7 the main conclusions of the studies presented along this thesis are exposed. Additionally, there is an appendix section in which supplementary information related to the subject and results of the present thesis is provided.

ABBREVIATIONS

AA_{arom}	Aromatic amino acids
Aβ	Amyloide-β
AD	Alzheimer's disease
$Al(III)_{cus}$	Coordinatively unsaturated aluminium atom
AM1	Austin model 1
AMBER	Assisted Model Building with Energy Refinement
B	Becke's 1988 pure exchange functional
B3	Becke's three parameter nonlocal hybrid exchange functional
BDE	Bond dissociation energy
BH	Becke's half-and-half nonlocal hybrid exchange functional
CAD	Collision-activated dissociation or decomposition
CCSD(T)	Coupled cluster singles and doubles with a perturbational estimate of the connected triples
CID	Collision-induced dissociation or decomposition
COSMO	Conductor-like screening solvation model
CPCM	Conductor polarized continuum model
DFT	Density functional theory
DP	Declustering potential
EPR	Electron paramagnetic resonance
ESI	Electrospray ionization
FAB	Fast atom bombardment
FD	Field desorption
FTICR	Fourier Transform ICR
G2	Gaussian-2
G3	Gaussian-3
G96	Gill 96 exchange functional

GG	Glycylglycine
GGA	Generalized-gradient approximation
GGG	Glycylglycylglycine
GGGG	Glycylglycylglycylglycine
Gly	Glycine
HF	Hartree-Fock
His	Histidine
ICR	Ion cyclotron resonance
IE	Ionization energy
IRC	Intrinsic reaction coordinate
IRMPD	Infrared multiple-photon dissociation
LDA	Local density approximation
LYP	Lee, Yang and Parr correlation functional
m/z	Mass-to-charge ratio
MALDI	Matrix-assisted laser desorption ionization
MCMM	Monte Carlo multiple minumum
MCPF	Modified coupled pair functional
MNDO	Modified Neglect of Differential Overlap
MP	Moller-Plesset correlation energy correction
MPW1	One-parameter modified Perdew-Wang exchange functional
MR-ACPF	Multi-Reference-Averaged Coupled Pair Functional
MS/MS	Tandem mass spectrometry
ONIOM	Our-own N-layered Integrated molecular Orbital and Molecular mechanics
P86	Perdew 86 local correlation functional
PCI-80	Parametrized configuration interaction (with parameter 80)
PD	Plasma desorption
PES	Potential energy surface

Phe	Phenylalanine
PW91	Perdew-Wang 91 correlation functional
RF	Radiofrequency
SI	Self-interaction
SIPF	Salt induced peptide formation
SVWN	Slater exchange and Vosko, Wilk and Nusair correlation functional
TOF	Time-of-flight
Trp	Tryptophane
Tyr	Tyrosine

1. INTRODUCTION

1.1 THE GAS PHASE METAL ION CHEMISTRY

The area of gas phase metal ion chemistry has experienced a considerably growth during the last decades. Parallel to this increasing interest, the fast development of new instrumentation and methods has positioned the gas phase techniques as invaluable tools into the research laboratories of a vast array of disciplines.

When referring to gas-phase ion chemistry, mass spectrometry enjoys a central position.[1, 2] Indeed, nowadays gas phase systems are mainly generated experimentally by means of such techniques, whose main idea lies in the production of gas-phase ions of a given compound and the separation and detection according to their mass-to-charge ratio. Generation of the gas phase ions can be achieved by different manners, such as by direct ionization of a neutral molecule, by protonation or by coordination through metal ions. However, a metal ion complex is often more amenable to experimental study than the corresponding non-metal system due to the ease of detection of the metal and the fact that endothermic reactions can be driven to threshold by accelerating the ions. Generating ions from neutral molecules requires some more aggressive ionization techniques (i. e. ionization by electron impact), a fact that induces extensive fragmentations so the molecular ions are not always observed. Hereafter, the chemistry of the metal ion-containing systems in gas phase will be closely related to mass spectrometry techniques.

The study of metal-containing ions in gas phase is of great importance because it enables us to get information on their intrinsic chemical and physical properties in the absence of complicating factors such as solvation or ion-pairing effects. These studies can provide important clues to understand the behaviour of more complicated mechanisms occurring on condensed phases or surfaces by identifying crucial steps or potential intermediates. On the other hand, metal cation interactions with neutral compounds implies a reorganization of the charge density of the neutral moiety, which leads to an activation of some particular bonds that can affect ultimately their reactivity.[3-5] Such an activation is usually manifested in bond-weakening and/or bond-reinforcement processes, which can be demonstrated under mass spectrometry conditions and rationalized (sometimes unavoidly) through the use of appropriate theoretical techniques.

During the decades of the 70s and 80s, mass spectrometry evolved as an important tool for solving problems in organic and inorganic chemistry. In particular, the studies of

metal-ligand systems were focused basically on the organometallic field as a consequence of the available instrumental techniques: ion cyclotron resonance (IRC)[6] and Fourier transformer ICR (FTICR)[7] spectrometers, ion-beam experiments and collision-induced decomposition (CID) processes.[8, 9] In that vein, especially attention was focused on the activation of the C-H and C-C bonds,[10-19] processes that are not easily achieved in homogeneous or heterogeneous catalysis. These techniques could not be applied in the study of biomolecules because ion generation was too aggressive for this kind of systems. However, in the early 80s the appearance of fast atom bombardment (FAB),[20] field desorption (FD)[21] or plasma desorption (PD)[22] ionization techniques led the first breakthrough for mass spectrometry in the field of biomolecules and began to push their techniques, specially FAB, into applications of peptide sequencing and molecular weight determination of biological systems of about 10,000 Daltons.[23, 24] However, it was not until the beginning of the 90s, with the invention of electrospray ionization (ESI)[25] and matrix-assisted laser desorption ionization (MALDI)[26, 27] techniques that was possible to generate large biological systems between 100,000 and 300,000 Daltons in the gas phase. The coupling of these ionization techniques with advanced analyzers such as the triple quadropole or the time of flight (TOF) allowed the high-precision analysis of biomolecules of very high molecular weight and opened the door to mass spectrometry to assume a primary role in biological research, particularly in proteomics. In fact, the discipline of mass spectrometry has experienced a leap in activity with the chemical-physical studies of proteins, oligodeoxynuclotides, and other biological compounds in the gas phase.

1.2 THE GAS PHASE CHEMISTRY OF METAL-CONTAINING BIOLOGICAL SYSTEMS

It is well-known that metal cations are crucial in living organisms because of its functionality in some biochemical processes.[28, 29] One can find alkali, alkaline-earth as well as transition metal cations. The presence or not of filled *d* orbitals determines the way and the magnitude of the interaction with biological macromolecules, two factors that influence the role of the metals in each system. The absence of filled *d* orbitals in alkali and alkaline-earth metal cations allows the interaction with the ligands to occur without excessive geometric restrictions, basically given by the ligand-ligand repulsion, which allows high numbers of coordination. The type of interaction is electrostatic so that its chemistry is focused basically on ionic tasks such as counterions or charge loading. In contrast, the presence of *d* electrons in transition metal cations gives rise to geometric restrictions that

characterise the interactions with the macromolecules and lead to a rich chemistry that varies according to the oxidation state, the spin of the metal or the environment.[30] Owing to the obvious inherent importance and the rich chemistry given in metal containing biological systems, during the last years enormous efforts has been focused on the study of such systems.

1.2.1 RELEVANCE IN PROTEOMICS

The term proteome was colied by Mark Wilkins[31] in 1995 and is used to describe the entirety of proteins found in a given biological system at a given time. A cellular proteome is the collection of proteins found in a particular cell type under a particular set of environmental conditions. Proteomics is the large-scale study of the proteome, that is the knowledge of i) the structure of the proteins in the proteome, so-called as protein expression and ii) the functional interaction between the proteins.

The rapid growth of proteomics has been possible thanks to the development of mass spectrometry techniques coupled with database searches for protein identifications. The information produced by the mass spectrometer can be manipulated and compared with protein data stored in databases. The peptide mass fingerprint procedure identifies an unknown protein by cleaving it into short peptides using residue-specific endoproteases, and then deduces the protein's identity by matching the observed peptide masses against a sequence database.[32] The tandem mass spectrometry technique, alternatively, can get protein sequence information by isolating individual peptides from the unknown protein and by colliding them with a nonreactive gas. This causes fragmentations along the peptide backbone and generates a series of short amino acids sequences (the sequence tag) whose different mass values are compared with theoretical peptide libraries in order to identify the protein expression.[33]

These two above-mentioned methods are only plausible when the fragments generated were previously identified and the data stored in a peptide sequencing database. Otherwise, 'de novo' peptide sequencing is required. This procedure implies the performance of the pepetide sequencing without prior knowledge of the amino acid. The most common peptide fragments observed in a tandem mass spectrometry of an unknown protein are the *y*, *b* and *a* fragments of Figure 1.1. Thus, 'de novo' sequencing looks for peaks that appear to extend from the N-terminus (*b* fragments) and from the C-terminus (*y* fragments). The peaks belonging to the *y* or *b* family (*y1* and *y2* or *b1* and *b2*) will appear to

differ by the approximate mass of one amino acid residue. Accordingly, a ladder built by the set of *y* or *b* fragments allows to establish the protein sequence.

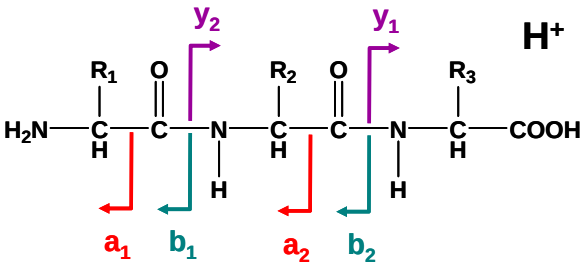

Figure 1.1 The most common fragments observed in low energy collions: *y*, *b* and *a*.

Proteomics was traditionally invoked to proceed via protonation of the analyte. Protonation ideally occurs at random in the peptide chain in such a way that series of backbone fragments that differ by the mass-to-charge ratio of one or more amino acids residues are provided. However, gaps in the series of product ions are observed in some amino acid sequences, a fact that complicates the sequenciation. To overcome the inconveniences of protonation, the interaction of proteins with transition metal cations has been proposed to be an alternative strategy to the 'random' fragmentation because it enables more specific cleavages. For example, strategies involving Ag^+ or Cu^+ metal cations have been developed.[34-37] As a first step, to understand specific fragmentations and the coordination properties of metal cations to small peptides is of great interest.

1.2.2 RELEVANCE IN BIOCHEMISTRY

The knowledge of metal cation binding sites when interacting with peptides is not only of interesting in proteomics but also to get fundamental information of metalloproteins, which are involved in a broad range of processes, for example, photsynthesis and electron transport,[38, 39] oxygen binding and transport,[40] metal chelation,[41] activity of antibiotic[42] and anti-Alzheimers agents,[43] pathological redox chemistry[44] and the synthesis of DNA binding agents.[45]

The study of the detailed mechanistic pathways in protein active sites relies on the generation of stable intermediates that can be characterized by X-ray crystallography. However, the conclusions from such studies can be ambiguous and often further studies are required to confirm the mechanistic implications.[46-49] An alternative strategy for investigating the mechanism in protein active sites involves the study of smaller model systems that only include the transition metal and chelating ligands and can hence mimic

the structure and function of the active site. Such systems are also known as biomimetics, and their structural study is usually carried out in the condensed phase using X-ray crystallography, FTIR, and electron paramagnetic resonance (EPR). Due to the relatively small size of biomimetics, such complexes lead themselves to structural elucidation in the gas phase (i. e. in the absence of solvent or other effects), which can be directly compared to condensed-phase structures. Thus, since one of the ways of ionizing the analytes in mass spectrometry, especially the ESI technique, is via cationization (i. e. charging the analyte by adding metal cations in the sample) during the last two decades some studies in mass spectrometry have been directed towards metal-containing biomimetic systems in the gas phase. These studies are the first step for understanding the role played by these cations in more real biological environments; i. e. binding sites, magnitude of interaction, metal exchange, activation and reactivity, etc.

1.2.3 *AB-INITIO* CALCULATIONS APPLIED TO PROBLEMS OF METAL-LIGAND GAS PHASE CHEMISTRY

Nowadays, the recent advances in theoretical methodology as well as in computational hardware has allowed quantum chemical methods to be powerful tools in many areas of research. In this respect, gas phase ion chemistry is a fertile ground for the interface between theory and experiment.[50] Indeed, most of the experimental techniques used in this field work under very low-pressure regimes so the conditions to have isolated gas-phase systems are achieved. These situations are quite close to the true isolated systems that are often the object of study using theoretical calculations.

Therefore, the fruitful interplay between theory and experiments given by the combination of different mass spectrometry techniques with theoretical approaches allows: i) the evaluation of binding energy values obtained both by experiments and theory, ii) the anchoring of absolute gas-phase metal cation affinities scales for different ligands, iii) the prediction of different isomers and their relative energies for a given ion, and iv) the formulation of possible reaction mechanisms trough a detailed analysis of the topology of the corresponding potential energy surface (PES), that is, computing the reactants, products, intermediates and transition structures that connect them.

The synergy between theory and experiment has its implications when studying metal-containing biological systems. On one hand, as aforementioned, since the early nineties, mass spectrometry has been considered a well-suited tool to study biological systems in the gas phase, in which the recourse of using biomimetic models are often

employed. On the other hand, the study of whole biological systems using quantum-chemical calculations is nowadays challenging, especially in presence of transition metal cations so that it is more practicable the treatment of models that involve those regions chemically more interesting (i. e. regions rich in electron donor atoms such as N, O and S capable of coordinating the metal cations). In view of these two statements, the idea is now to assembly the study of metal containing biological systems from the insights of mass spectrometry measurements and theoretical calculations. According to this, some pioneer works combining experimental and theoretical methodology appeared up to the end of the 90s. They were mainly addressed to the interaction of metal cations with small biomolecules;[51-76] that is, systems composed by basic constituents of fundamental relevance of more complicated biological systems, such as amino acids, nucleobases or small peptides. These studies have demonstrated the enormous utility of theoretical tools in gas phase studies by rationalizing the experimental results and also have allowed the calibration of theoretical methods by determining the optimal ones that reproduce accurately the experimental results.

1.3 PREVIOUS STUDIES

Studies addressed to the interaction of metal cations with small biomolecules, both from experimental and theoretical point of view, can be considered as a first step for understanding the behaviour of bigger and more realistic biological systems. Focusing on the field of metalloproteins, the models consist on systems with metal cations interacting with amino acids and small peptides in order to represent the active sites. In this section some previous works of paramount importance in which the present thesis has been inspired are presented. Additionally, they are good examples to show the fruitful interplay between theory and experiment in the gas phase chemistry.

1.3.1 ESTIMATION OF METAL-LIGAND AFFINITIES

There are a great number of experimental works that focus on measuring the metal cation affinity of different amino acids and peptides, the cations being mainly alkali [77-88] and transition metal cations.[80, 89, 90] Obtaining such affinities were carried out either by the kinetic method,[91], where one obtains the relative cation affinities of a set of ligands, or by threshold collision-induced dissociation method,[92] which allows to determine the bond dissociation energy of a metal-ligand system.

A nice example of the synergy between theory and experiment is the determination of the Cu^+ affinities of natural amino acids. In 1995 Cerda and Wesdemiotis[89] determined the relative Cu^+ affinities of amino acids in the gas phase using the kinetic method. They established a ladder of the Cu^+ affinities for the different amino acids tested and found that the reference system was Cu^+-glycine, since the weakest interaction was given between Cu^+ and glycine. Complementary to this work, in 1997 Hoyau and Ohanessian[93] performed a theoretical study in order to establish the absolute Cu^+-amino acid affinities in gas phase. This work explored the possible isomers of the Cu^+-glycine system in order to determine the most stable one and computed the absolute Cu^+-glycine binding energy from the lowest energy isomer, which allowed to establish the absolute Cu^+ affinity ladder using the experimental relative binding energies. To assess the reliability of the theoretical ladder, the absolute binding energies of the Cu^+-serine and Cu^+-cysteine systems (with the consequent conformational analysis for each one) were also computed, showing that the ab-initio calculations were in close agreement with the experimental results. This case reflects the powerful synergy between theory and experiment because on one hand, the absolute Cu^+ affinities for the 20 natural amino acids was able to be determinated using theoretical methods and supported by the experimental data and on the other hand, the reliability of the methods employed was able to be tested benchmarking the experimental values against the theoretical ones.

Experimental absolute binding energies for these biomimetic systems have also been reported in the literature, most of these works carried out by Armentrout and Rodgers[94] These values were determined by means of the threshold collision-induced dissociation method and compared by the results from theoretical calculations, which were usually used to confirm the accuracy of the experimentally measured bond energies. One can find a great variety of systems, the most relevants for this thesis being those that involve the interaction of alkali and singly charged transition metal cations with amino acids[77, 78, 80, 81] or with the aromatic rings that mimic the side chains of aromatic amino acids.[95-100] However, other interesting results are those that provide accurate bond dissociation energies of metal ions with small molecules that represent simpler models of functional groups present in a peptide.[94, 101]

1.3.2 STRUCTURAL CHARACTERIZATION OF THE ION COMPLEXES

By means of the above-exposed experimental methods one can determine ion affinities, either relative or absolute values. However only having the binding energies it is not possible to determine which structure adopts the complex ion so the use of theoretical calculations is required. Biomolecules can present different binding sites according to the number and type of electron donor atoms, and consequently, for a unique metal-biomolecule complex several isomers can exist. Because all of them show different stabilities, the ground state isomer can be located by determining the relative energy between them. This procedure is inherently associated to an important aspect: the structural determination of the complex. Indeed, the conformational analysis enables us to determine the geometry and the coordinating atoms of the complex under study. Additionally, the theoretical binding energies can be computed and good agreements with the experimental ones can be used to confirm the reliability of the predicted structure.

According to this procedure, most of the experimental works cited in section 1.3.1 inspired theoretical studies to establish the structure of the metal-amino acid or peptide complex generated in the gas phase and compute their binding energies.[76, 93, 102-117] To exemplify that, the different isomers of Cu^+-glycine, -serine and -cysteine were distinguished.[93, 112] While the most stable isomer of Cu^+-glycine is a dicoordinated structure in which the N amino and the O carbonyl atoms attach to the metal cation, the lowest energy structures for the other two systems are tricoordinated, the interaction of the metal given by the same groups as in Cu^+-glycine plus the donor atoms from the lateral chain, O and S for serine and cysteine, respectively (Figure 1.2).

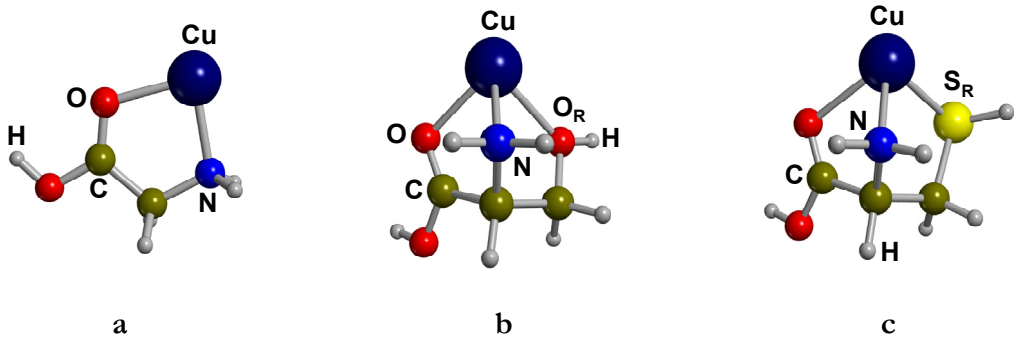

Figure 1.2 The most stable structures for the Cu^+-glycine (a), Cu^+-serine (b) and Cu^+-cysteine (c) systems. The subindex R indicates the donor atom from the lateral chain.

Sometimes the only experimental data available to assess the reliability of the theoretical results of the above-exposed procedure is the measurement of the binding energies, whose values sometimes depends on the experimental method employed, which often leads inconclusive data. To overcome such inconveniences, recently, a potential new technique has appeared for structural determination purposes: the infrared multiple-photon dissociation (IRMPD).[118, 119] The data obtained by this technique is an IRMPD spectrum, whose peaks are related to the vibrational modes of the complex in the gas phase; that is, data directly connected to the structural features of the complexes. Theoretical calculations are very useful for the structural characterization by means of IRMPD since they allow to perform a conformational search of the possible isomers of the complex, compute the vibrational spectrum for each isomer located and compare the simulated spectra with the IRMPD one. The isomer whose theoretical spectrum is the closest to the IRMPD one is taken as the structure of the complex. The validity of such structure can be reinforced by computing the relative energies of the different isomers, in which the predicted structure should be the most stable one. This is an elegant procedure that, in addition, allows to determine the presence of more than one isomer in gas phase when univocal vibrational characteristics of these isomers appear in the IRMPD spectrum. Just a few number of studies treating the interaction of metal cations (Na^+, K^+, Cr^+, Ag^+, Zn^{2+}) with amino acids and peptides[120-124] are reported in literature. As an example, Figure 1.3 shows the study of the interaction of Ag^+ ion with the phenylalanine amino acid.[124] Comparing the IRMPD spectrum with the computed ones it seems clear that Ag^+ interacts with this amino acid through the amino group, the carbonyl group and the aromatic ring, a fact that is confirmed when the computed relative energies of the isomers found are also considered.

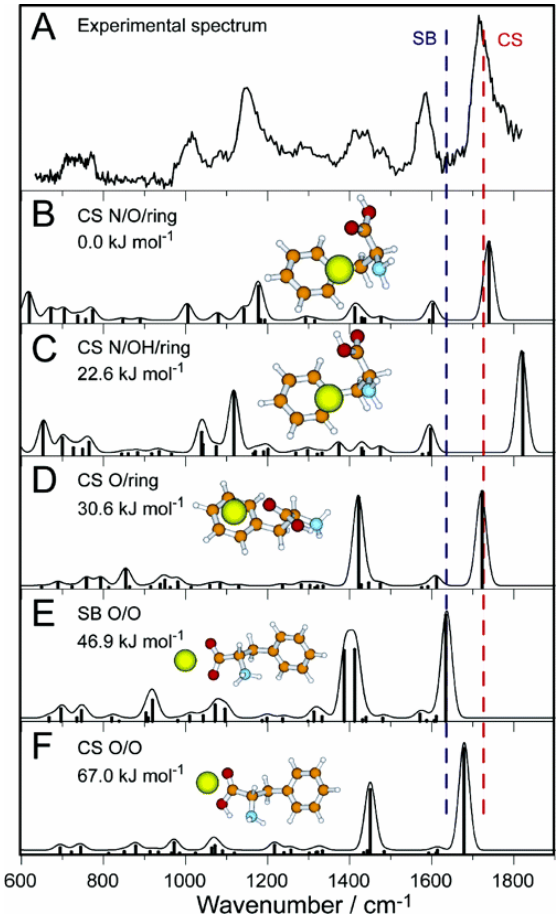

Figure 1.3 Experimental IRMPD spectrum of $[Ag\ Phe]^+$ complex and relative energetics and spectra for optimized structures (taken from reference [124]).

1.3.3 ACTIVATION AND REACTIVITY OF THE METAL-BIOMOLECULE COMPLEXES

The interaction of metal cations with neutral molecules is usually accompanied by a drastic reorganization of the electron density of the neutral moiety, whose changes derive to an activation of the bonds and consequently to a different reactivity. The reactions of the activated complexes can be studied using mass spectrometry collision activation techniques, which consist mainly in colliding a nonreactive gas towards the ion complex and, as a consequence of the internal energy transferred during the collision process, fragmentations of the ion take place. Since metal-molecule interactions are often metal-specific, an ion complex submitted under collisonal activation conditions leads to specific fragmentations that can indirectly provide structural information of the neutral molecules because one may expect relationships between the metal binding sites as well as the binding affinities with the fragmentation reactions. According to that, an uncountable number of

works concerning the fragmentation of metal ion-ligand complexes are available in literature. Among them, Harrison and coworkers studied the fragmentation of the Ni^+ and Cu^+ adducts of α-amino acids under conditions of FAB ionization,[125, 126] Lei at al. investigated the gas phase reactions of Cu^+ and Fe^+ with the 20 common amino acids ionizing the complexes generating the ions with LD,[127] Hoppilliard and coworkers performed a PD mass spectrometry study on the formation and fragmentation of α-amino acids complexed by Fe^+, Co^+, Ni^+ and Cu^+;[128, 129] and some studies involving the fragmentation of singly and doubly charged transition metal-cationazed amino acids and peptides employing the electrospray ionization technique were reported.[130-137]

Although the specific fragmentations of metal cationized systems involving small molecules of biochemical significance could provide a useful complement toward full structural characterization, there is still a lack of general understanding of the fragmentation pathways of cationized biomolecules. In view of that, fragmentations can be investigated by using theoretical methods in such a way that, examining different pathways, one can predict the most probable mechanism that takes place. Once the most favourable paths have been distinguished one can elucidate the structure of the product ions obtained as well as identify which neutral molecules have been lost as a result of the fragmentation processes. Therefore, calculations allow to rationalize the experimental findings through reliable description of the potential energy surfaces; that is, computing the local minima and the transitions states that connect them. Accordingly, the structure of the ion parents can also be determined because they should be consistent with the fragmentation mechanisms. Thus, these studies can also provide information on the bonding of the metal-biomolecule complexes.[53, 54, 56, 59, 63, 68, 138, 139] To exemplify that, Figure 1.4a shows the fragmentation spectrum of the Ni^+-glycine system generated in a FAB ion source and Figure 1.4b the PES for the loss of 46 u observed in the spectrum.[56] The mass of 46 u can correspond to the loss of HCOOH or to simultaneous loss of $CO+H_2O$ so that both fragmentation mechanisms were examined. Results showed that these fragmentations started with the Ni^+ insertion into the C-C bond of the ion parent. On the other hand, it was found that channel I (concerning to the loss of HCOOH) presents a higher barrier activation than channel II (concerning to the loss of $CO+H_2O$). In view of that, theoretical results suggested that i) the loss of 46 u observed in the experiment proceeded via consecutive loss of CO and H_2O; ii) the ion parent of this fragmentation should be a dicoordinated structure with the N amino and the O carbonyls atoms coordinating Ni^+, a fact that pointed this isomer as the most stable one for this system and iii) the observed

fragmentations do not correspond to the most stable products so the reaction follow a kinetic control. Similar fragmentations of Ni^+-glycine were found when studying the reactivity of the Cu^+-glycine ion complex in the gas phase,[138] while for Ag^+-phenylalanine additional fragments were observed.[68, 70]

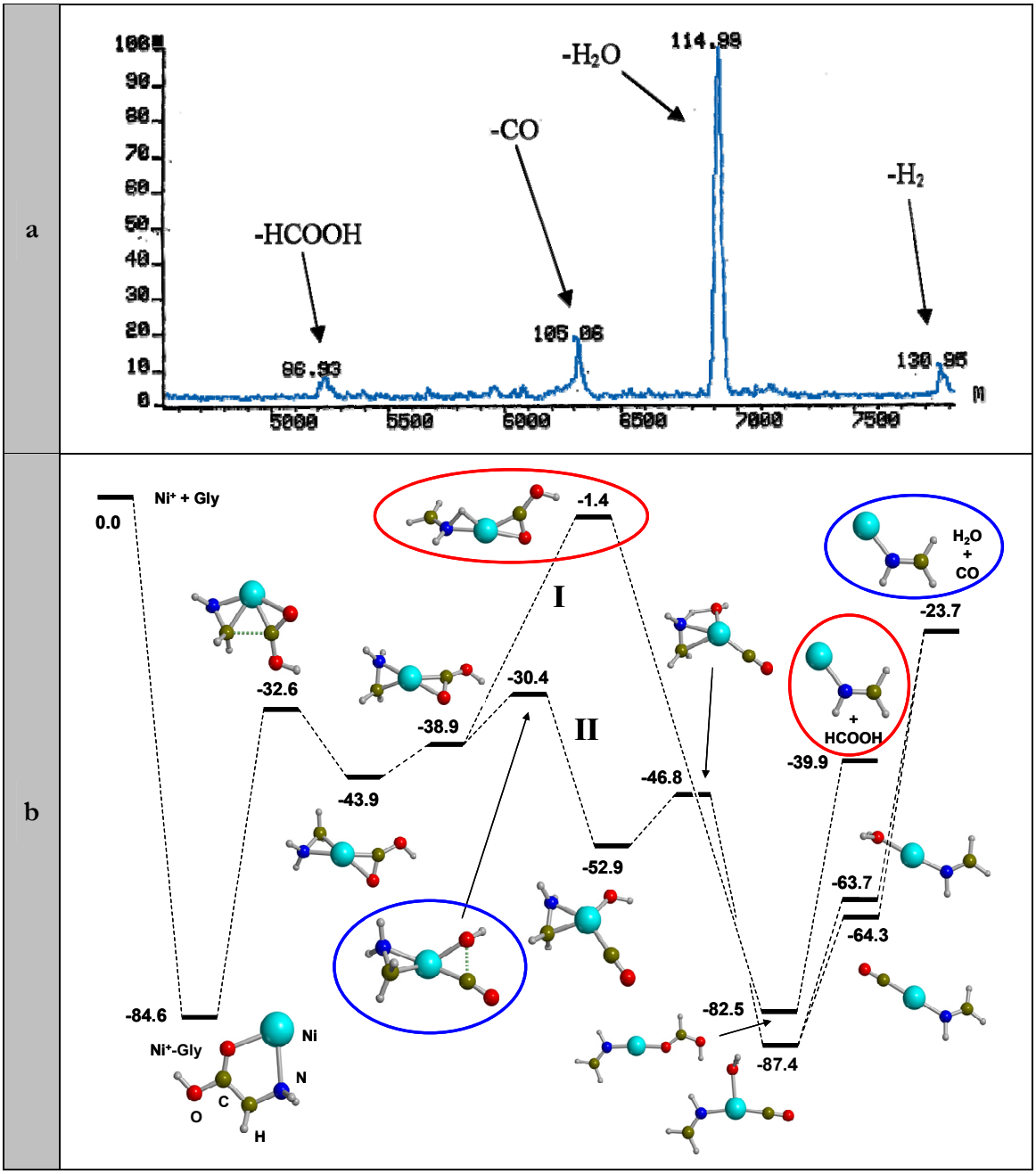

Figure 1.4 a) Fragemntation spectrum of the Ni^+-glycine complex at m/z 133. b) Potential energy surface for the loss of 46 u of the unimolecular reaction from the Ni^+-glycine system. Circles in red label the most representative structures for the loss of HCOOH; circles in blue label the most representative structures for the loss of CO+H_2O.

Furthermore, it was found that, in some cases, the activated complexes give rise intriguing fragments such as radical cations,[65, 74, 75, 140-144] whereas in others, reactions of biological relevance were suspected to occur during the collision process.[145, 146] Particularly interesting is the work carried out by Seto et al.[145] who, owing to the elimination of H_2O from the Cu^{2+}-(glycine)$_2$ complex submitted to low collisionally conditions, suggested that a condensation between the two glycines might take place; that is, the peptide bond formation was activated in the gas phase by the interaction of glycine molecules with the Cu^{2+} cation.

1.4 OBJECTIVES

To sum up, the gas phase metal ion chemistry is an important field involved in many areas of research. In that respect, mass spectrometry is considered as a central tool in the fields of proteomics and biochemistry: for the former because it allows obtaining protein sequences; for the latter because it can provide valuable information of the active sites of metalloproteins such as the metal binding sites. A well-suited strategy for studying these active sites is the use of small model systems that involve those regions chemically more interestings and that mimic larger and more complicated biological systems. Since these biomimetic models are generated in gas phase, the use of theoretical calculations has become an important (sometimes mandatory) tool to rationalize the experimental findings as well as to determine the intrinsic properties of the systems under study (such as obtaining the most stable structure of a given metal-ligand complex or the elucidation of some fragmentation paths). Accordingly, nowadays the fruitful interplay between theory and experiment in the area of the gas phase chemistry has leaded important steps to the knowledge and understanding of the metal-containing biological systems. Despite that, most of the theoretical works, or in combination with experiments, that are described in the literature treat with alkali and/or closed-shell transition metal cations and only few works address the interaction of open-shell transition metal cations with small biomolecules. The study of open-shell systems with biological relevance is of great importance since cations such as Cu, Ni, Co and Fe are present in metalloproteins that participate in processes of electron transfer or oxygen transport.

In view of the above-exposed, the following points summarize the objectives proposed for the present thesis:

1. To analyse the conformational properties of the closed-shell Cu^{+} (d^{10},^{1}S) and the open shell Cu^{2+} (d^{9},2D) metal cations interacting with the aromatic amino acids (AA_{arom}) of phenylalanine, tyrosine, tryptophane and histidine in order to establish the ground-state isomer for each system and to evaluate the cation-π interactions and the oxidative effects on their binding properties.

2. To generate experimentally the gas phase complexes arising from a mixture of $CuSO_4$ and the aromatic amino acids as well as to study its reactivity under collision-induced dissociation conditions in order to observe whether metal-specific fragmentations take place. To rationalize such fragmentations by means of DFT calculations.

3. To analyse the conformational properties of the $Cu^{+/2+}$-$(glycyl)_n$glycine (n = 1-3) oligomers in order to establish the ground-state isomer for each system and to determine the differences on the coordination properties as a function of the electronic configuration of the metal cation and to the length of the peptide chain.

4. To evaluate whether Cu^{2+} cations and aluminosilicates are good catalysts that activate the peptide bond formation reaction between two amino acids and to understand which factors may favour the process.

2. EXPERIMENTAL TECHNIQUES

2.1 MASS SPECTROMETRY

Mass spectrometry is an analytical spectroscopic tool primarily concerned to the separation of molecular species according to their mass. In order to achieve a mass separation on a practical scale it is necessary to ionize the species under investigation (the analyte) in such a way that the ions generated are distinguished according to their mass-to-charge ratio m/z and are detected in proportion to their abundance. A picture of a mass spectrometer diagram must always contain the following elements (see Figure 2.1): a) a device to introduce the analyte (nowadays usually by means of gas or liquid cromatography), b) a source to produce ions from the sample (so-called ion source), c) one or several analyzers to separate the various ions and, if desired, to select one specific ion to be fragmented, d) a detector to count the ions emerging from the last analyzer and to measure their abundance, and e) a computer to process the data, which produces the mass spectrum.

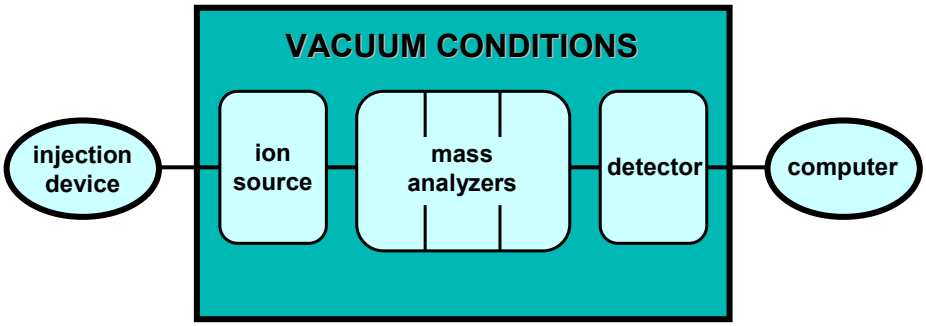

Figure 2.1 Basic diagram for a conventional mass spectrometer.

2.1.1 THE ELECTROSPRAY IONIZATION

There are a great variety of ionization techniques, which differ according to the internal energy transferred during the ionization process and the physicochemical properties of the analyte. The called 'strong' ionization techniques are very energetic and lead to massive fragmentation caused by the excess of internal energy transferred when ionizing the analyte. Electron ionization[147-149] and chemical ionization[150, 151] belong to this group and are only suitable for gas-phase ionization, so the compounds must be sufficiently volatile and thermally stable. In contrast, the called 'soft' ionization techniques allow to produce molecular ions in gas phase through their direct extraction from the condensed phases, both liquid-phase and solid-state. ESI corresponds to a gentle liquid-

phase ion source that involves the transfer of solution ions to the gas phase, and therefore typically yields molecular ions with little or no fragmentation.

The production of the ions by means of ESI[25] is achieved as follows (see Figure 2.2). The sample in solution is introduced in a capillary. Applying a potential difference between the containing-sample capillary and the counter-electrode (between 3 – 6 kV) a strong electric field is created (of the order of 10^6 V m^{-1}). This field induces a charge accumulation at the liquid surface located at the end of the capillary, which breaks to form highly charged droplets due to the high voltage. The solvent evaporates partially leading to a shrinking size of the droplet and, consequently, increasing the charge concentration at the droplet's surface. When the coulombic repulsion between the surface charges overcomes the droplet's surface tension, then the droplet explodes. This coulombic explosion forms a series of smaller, lower new charged droplets, creating thus an electrospray medium. The process of shrinking followed by explosions is repeated until individually charge naked analyte ions are formed. The later droplets pass through a curtain of heated inert gas (usually N_2) to remove the last solvent molecules.

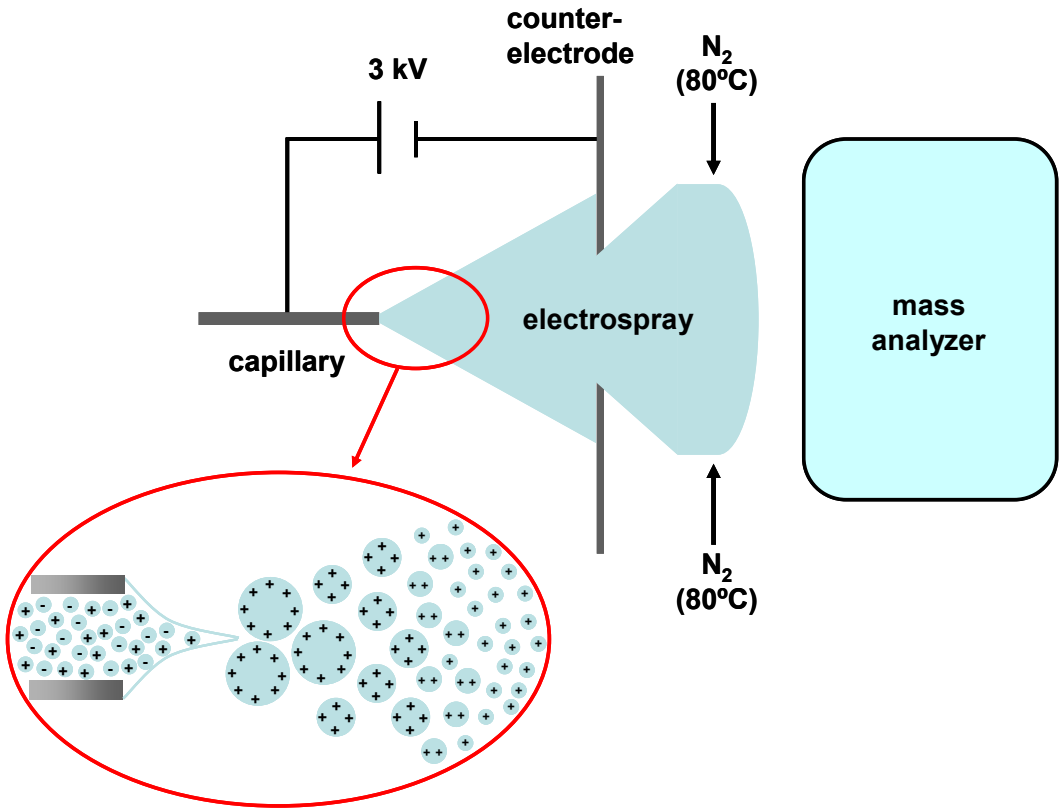

Figure 2.2 Diagram of ESI sources. The ionization-desolvation process at the tip of the capillary is emphasized.

One of the most used ways of ionizing proteins is via protonation because, since they are large molecules with several protonation sites, it is possible to produce multiply charged ions. Obtaining multiply charged ions is advantageous because it allows the analysis of high-molecular-weight molecules using analyzers with a weak nominal mass limit. Therefore, ESI allows the analysis of biological macromolecules such as obtaining molecular weights or determining peptide sequences, being thus one of the most used ion sources. Additionally, ESI also enables us obtaining charged metal-ligand complexes in gas phase by introducing through the capillary a solution composed by a mixture of a metallic salt and the ligand. In this case, the neutral ligand is ionized by cationization, that is, by the interaction with the metal cation, whose complex will be detected.

Finally, it should be mentioned that other ionization techniques such as fast atom bombardment (FAB)[20] and matrix-assisted laser desorption ionization (MALDI)[26] are also prone to be used for the analysis of biological systems. These are two solid-state ion sources in which the analyte is deposited on a matrix. The ions are generated by irradiation of the matrix that contains the analyte with energetic particles (FAB) or photons (MALDI) and extracted by an electric field.

2.1.2 QUADROPOLAR ANALYZERS

Once the ions have been produced they need to be separated according to their m/z. There are many different analyzers, just as there are a great variety of sources, but we will focus on the called quadropolar analyzer, since it is the one used in the present thesis.

An scheme of a quadrupolar mass analyzer,[152] is represented in Figure 2.3. A quadrupole is made up of four rods with a hyperbolic cross-section and in perfectly parallel disposition. Two opposite rods are at positive electric potential ($+\Phi_0$) while the other two at negative ($-\Phi_0$), which generate an electric field within the region delimited by the quadrupole.

$$+\Phi_0 = +(U - V\cos\omega t) \quad \textbf{Equation 2.1}$$

$$-\Phi_0 = -(U - V\cos\omega t) \quad \textbf{Equation 2.2}$$

where $+\Phi_0$ and $-\Phi_0$ represents the potential applied to the positive and negative rods, respectively, U is the direct potential and $V\cos(\omega t)$ represents an alternating radio frequency (RF) field of amplitude V and frequency ω. The applied potentials on the opposite pairs of rods varies sinusoidally as $\cos(\omega t)$ cycles with time t. A positive ion

entering the space between the rods will be drawn towards a negative rod. If the potential changes sign by varying U, V and ω before the ion discharges itself against this rod it will change direction. Thus specific combinations of the variables U, V and ω result in specific ion stable trajectories from the quadrupole to the detector. If ions with a particular m/z are in resonance with such stable trajectories then they will reach the detector (red path of Figure 2.3). Otherwise, these ions will be non-resonant and will hit the quadrupoles and not be detected (blue path of Figure 2.3). In order to build up the mass spectrum in which all the ions have been detected, the RF must be varied to bring ions of different m/z into focus on the detector.

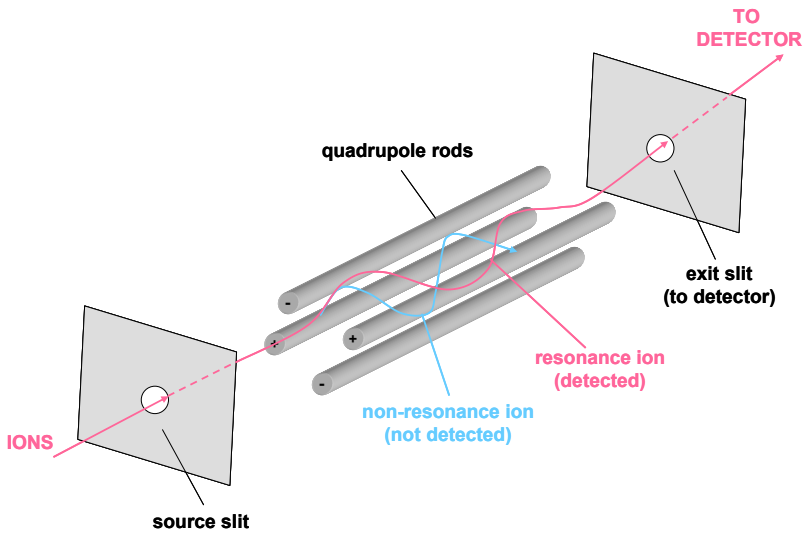

Figure 2.3 Simplified scheme of a quadrupole mass analyzer.

Finally, a brief comment referred to the time-of-flight (TOF)[153, 154] analyzer is noteworthy. It is based in a straightforward way of ion separation. All the ions are introduced with an equal initial kinetic energy and travel through a field free drift zone where they are separated by their masses. Lighter ions travel faster so that all ions of the same m/z arrive at the detector at the same time. As the ions are usually introduced directly from the source as a pulse, TOF is a well suited mass analyzer for the MALDI technique, in which the ionization is carried out by laser pulses, giving rise to MALDI-TOF mass spectrometry.[27]

2.1.3 TANDEM MASS SPECTROMETRY

With modern soft methods of ionisation, like ESI or MALDI, the spectra often only contain the ionised molecule with very little fragmentation. The information obtained is mainly which ions are or not generated. However, the ion source spectra are of little use

for structural characterisation and for that, induced fragmentations are required, which can be carried out via tandem mass spectrometry (MS/MS).

MS/MS is any general method involving at least two stages of mass analysis, either in conjunction with a dissociation process or a chemical reaction that causes a change in the mass or charge of an ion. In the most common MS/MS experiments a first analyzer (MS1) is used to isolate the desired ion. After selecting this precursor ion m_p^+, it undergoes, either spontaneously or by some activation, a fragmentation that yields product ions m_f^+ and neutral fragments m_n; i. e. $m_p^+ \rightarrow m_f^+ + m_n$. Finally, a second spectrometer (MS2) analyzes the product ions.

One of the most commonly available tandem mass spectrometers is the triple quadrupole instrument (QqQ).[155] The QqQ configuration indicates that the first (Q1) and the last (Q3) quadrupoles are mass analyzers, whereas the centre quadrupole (q2) is known as the collision cell. There are some varieties of experiments that can be performed using a triple quadrupole MS/MS instrument, the most important one probably being the so-called product ion scan, represented in Figure 2.4. In this type of MS/MS experiment, m_p^+ is focused in Q1 and transferred into the collision cell (q2). Here, a flow of gas is introduced in such a way that m_p^+ undergoes several collisions. If the collision gas is inert, a fraction of its kinetic energy is transferred and converted into internal energy of the m_p^+ ion. Consequently, m_p^+ fragments and the products are measured by Q3.

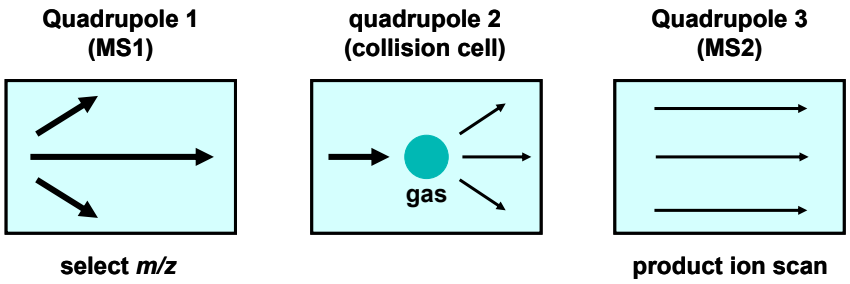

Figure 2.4 Schematic representation of the product ion scan MS/MS experiment.

2.2 EXPERIMENTAL DETERMINATION OF THERMODYNAMIC PROPERTIES AND STRUCTURAL INFORMATION

Mass spectrometry comprises a great variety of methods with manifolds applications. Some of them are widely used because they are capable of giving quantitative thermochemical information (such as metal ion-ligand binding energies)[101, 156] or provide valuable information related to the structure of the ions generated.[157] The comparison between theoretical and experimental data constitutes a cross-check in which sometimes calculations are used to gain complementary information from experimental results and in other cases experimental data help to assess the reliability of theoretical results. Consequently, in this section we have considered convenient to address some of the experimental techniques that supply thermochemical and structural information.

This section will only give a brief description of some of these techniques. However, if one is interested in having further information about them, the reader can find it in Appendix A, where a more comprehensive and exhaustive descriptions are exposed.

2.2.1 THE KINETIC METHOD

The kinetic method developed by Cooks and coworkers,[91] gives us the relative metal (M^+) affinities of two ligands (L1 and L2) by comparing the dissociation rates of the metal-bound heterodimer $[L1 + L2]M^+$ to each of the individual M^+-attached monomers:

$$[L1+L2]M^+ \xrightarrow{k_1} [L1]M^+ + L2$$

$$[L1+L2]M^+ \xrightarrow{k_2} L1 + [L2]M^+$$

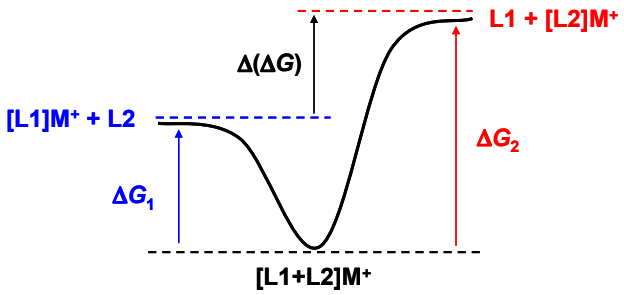

Figure 2.5 Top: competitive dissociation reactions involved in the kinetic method. Below: energy diagram of the dissociation reactions above-described.

Applying the thermodynamic formulation of transition state theory to the competing reactions one obtains the Equation 2.3,

$$\ln\left(\frac{I_{[L1]M^+}}{I_{[L2]M^+}}\right)=\ln\left(\frac{k_1}{k_2}\right)=\frac{\Delta(\Delta G)_{M^+L}}{RT_{eff}}\approx\frac{\Delta(\Delta H)_{M^+L}}{RT_{eff}} \quad \textbf{Equation 2.3}$$

which relates the natural logarithm of k_1/k_2 with the difference in metal ion enthalpies $\Delta(\Delta H)_{M^+L}$ between ligands L1 and L2. *R* is the ideal gas constant and T_{eff} a kinetic parameter called effective temperature. The abundance ratio of the $[L1]M^+$ and $[L2]M^+$ peaks in a given spectrum (their intensities) represents an approximate measure of the rate constant ratio k_1/k_2.

The validity of Equation 2.3 assumes that: i) the activation entropy variations for the two competitive channels are very similar so that their difference can be neglected, and ii) the reverse activation energies are negligible so that the relative enthalpy of activation can be approximate to the difference in binding enthalpies of M^+ to L1 and L2.

The representation of the $\ln(k_1/k_2)$ values measured in a stair-step form constitutes a M^+ affinity ladder, which is an elegant way to systematize the relative metal affinities for a set of ligands.

2.2.2 EQUILIBRIUM MEASUREMENTS

There are two types of equilibrium measurements according to the experimental conditions: high-pressure and low-pressure.

2.2.2.1 Low-pressure ion-molecule equilibrium

The most typical low-pressure ion-molecule equilibrium method is the ligand exchange equilibrium approach. In this procedure the reaction under study is a bimolecular transfer reaction,

$$XM^+ + Y \Leftrightarrow X + MY^+ \quad \mathrm{K}_{eq}$$

in which the species are M^+ the metal cation and X/Y the exchanged ligands. Unfortunately, since only the energetics associated with M^+ transfer can be obtained, measurements of exchange equilibrium do not directly yield absolute binding thermochemistry, but rather a relative scale of binding enthalpies may be derived.

Under these conditions the equilibrium constant is expressed as

$$\mathrm{K}_{eq}=\frac{I_{MY^+}p_X}{I_{XM^+}p_Y} \quad \textbf{Equation 2.4}$$

where p_X and p_Y are the partial pressures of species X and Y at equilibrium, respectively. According to the Van't Hoff equation, plots of $\ln(\mathrm{K}_{eq})$ versus 1/T obtained by different experiments varying temperature yield $\Delta(\Delta S)$ and $\Delta(\Delta H)$ values, in which the latter term corresponds to the relative M^+ binding enthalpies between X and Y.

2.2.2.2 High-pressure ion-molecule equilibrium

In high-pressure experiments direct clustering equilibria may be examined, and hence absolute binding energies derived

$$M^+ + A \Leftrightarrow MA^+ \quad \mathrm{K}_{MA^+}$$

At the equilibrium conditions, the equilibrium constant K_{MA^+} is related with the mass spectrometer intensities of the ions and the pressure of A according to Equation 2.5.

$$\mathrm{K}_{MA^+} = \frac{I_{MA^+}}{I_{M^+} p_A} \qquad \textbf{Equation 2.5}$$

where I_{MA^+} and I_{M^+} are the intensities of the cluster MA^+ and of the monomer M^+, respectively, and p_A is the pressure of neutral A. Therefore, the value of K_{MA^+} can be easily calculated. As exposed previously, measures of K_{MA^+} as a function of temperature allows the determination of the ΔS and ΔH values of the association process and hence absolute binding energies are obtained.

To obtain K_{MA^+} the ratio of the ion concentration must be known. However this is experimentally difficult. Indeed, the ion ratio may be distorted in the scape through the sampling orifice or later as a consequence of collision-induced decomposition processes caused by the high-pressure conditions.

2.2.3 THRESHOLD COLLISION-INDUCED DISSOCIATION

Threshold collision-induced dissociation (CID) measurements are ion beam experiments in which bond dissociation energies (BDEs) are obtained.[92]

In this technique the dissociation of the metal complex MA^+ is induced by collisioning with an inert rare gas (Rg) such as helium or argon.

$$MA^+ + Rg \rightarrow M^+ + A + Rg$$

The idea for obtaining the BDEs of MA^+ arises in studying the cross-section of endothermic CID reactions as a function of the reactant kinetic energy.

The total cross-section σ_{tot} is calculated using the ion intensities via Beer-Lambert law (Equation 2.6), while the reactant kinetic energy is approximated to reactant centre-of-mass energy, which is related to the laboratory ion energies through Equation 2.7.

$$I_{MA^+} = \left(I_{MA^+} + \sum I_P\right)\exp\left(-\sigma_{tot}\rho l\right) \quad \textbf{Equation 2.6}$$

$$E_{CM} = E_{lab}\left(\frac{m_{Rg}}{M_{MA^+} + m_{Rg}}\right) \quad \textbf{Equation 2.7}$$

In Equation 2.6, I_{MA^+} and I_P are the measured transmitted intensities of the reactant and product ions, respectively, ρ is the gas density, and l is the effective path length. In Equation 2.7 m_{Rg} and M_{MA^+} are the masses of the neutral and ion reactants, respectively.

The energy dependence of cross-sections can be analyzed using Equation 2.8

$$\sigma(E) = \sigma_0 \sum gi \frac{\left(E_{CM} + E_i - E_0\right)^n}{E_{CM}} \quad \textbf{Equation 2.8}$$

where σ_0 is an energy-independent scaling factor, E_{CM} is the centre-of-mass relative kinetic energy, E_0 is the reaction threshold and n an adjustable parameter that controls the shape of the energy dependence plot. The summation is over the ro-vibrational states of the reactant ions I_{MA^+} where E_i is the excitation energy of each state and g_i is the population of these states ($\sum g_i = 1$). Nonlinear least-squares analysis of the data is performed and by means of Equation 2.8 the optimized values for the parameters σ_0, E_0 and n are obtained. Thus, E_0 is derived, whose value can be approximated to the 0 K bond dissociation energy of the M^+-A complex.

2.2.4 COLLISION-ACTIVATED OR COLLISION-INDUCED DECOMPOSITION

Collision-induced processes can also be used to analyze decomposition reactions. Collision-activated and collision-induced decompositions (CAD and CID, respectively)[8, 9] refer to the same principal process, i. e. fragmentation of an ionic species accelerated to a certain kinetic energy upon collision with a quasi-stationary neutral target gas. Due to the

collision, the selected ion is fragmented, the product ions being used for structural purposes.

The fragmentation takes place when the precursor ion is excited via an energetic collision with neutral gaseous targets

$$m_p^+ + N \xrightarrow{1} \left[m_p^+\right]^* + N' \xrightarrow{2} m_f^+ + m_n + N'$$

where $\left[m_p^+\right]^*$ and *N'* represent the post-collision states of the precursor ion m_p^+ and the target N, respectively, and m_f^+ and m_n are the ionic and neutral products of the unimolecular decomposition. That is, under commonly used conditions CAD and CID are regarded as a two-step processes involving activation of the m_p^+ ion via one or more collisions (step 1) and a discrete unimolecular decomposition process (step 2).

CAD and CID applications are plentiful in the elucidation of structures, especially when treating with metal-containing biological systems. Indeed, it is well known that the interaction of transition metal cations with biological macromolecules depends strongly on the metal cation, especially on its electronic configuration. Consequently, when treating the metal-cationized system under collisional activation conditions metal-specific fragmentations occur. From the fragment ions one can indirectly obtain structural information by means of the well-known corresponding features for this class of compounds.[158] In this context, peptide sequencing is of particular relevance because of the clear-cut fragmentation at the peptide bonds allows straightforward sequence assignment.[157]

2.2.5 INFRARED MULTIPLE-PHOTON DISSOCIATION

Infrared multiple-photon dissociation (IRMPD)[118, 119] is a technique used in mass spectrometry to fragment molecules in gas phase usually for structural analysis of the parent ion. An infrared laser is directed where the ions are. The mechanism of fragmentation involves the absorption of multiple infrared photons by a given ion. This parent ion becomes excited into more energetic vibrational states until the bonds are broken resulting in gas phase fragments of the parent ion. Thus, IRMPD is a softer technique than CAD or CID methods to fragment the selected ions in the first analyzer.[159]

Aside from obtaining the fragmentation spectra for a given system, IRMPD presents additionally an enormous advantage compared to the CAD and CID techniques.

Indeed, by plotting the total fragmentation of the parent complexes as a function of the wavelength of the laser, the IRMPD spectra can be represented. Although IRMPD spectra are not identical to linear absorption spectra, the assumption that the IRMPD yield is linearly proportional to the IR absorption intensity is accepted as a useful approximation. Accordingly, the peaks observed in IRMPD spectra are associated to vibrational features of the parent ion (note that this is not true for the intensities of the bands, which should be compared only qualitatively). Overall, IRMPD is a very useful technique that can provide infrared spectra of ionic species so that direct structural information can be obtained.[120] The comparison of the IRMPD spectrum of a given metal ion complex with the simulated theoretically ones for various candidate isomers, allows to determine the structure of such a complex.

3. METHODOLOGICAL ASPECTS

The systems considered in this work present some difficulty from a theoretical point of view. First, the electronic structure of transition metal cations is complex due to their open shell nature and presence of low-lying electronic states. Thus, one must be cautious with the thereotical approaches chosen. On the other hand, amino acids and peptides are very flexible and may exist in many different conformations due to the high number of degrees of freedom. This fact is accentuated when the biomolecules interact with metal cations or are adsorbed on mineral surfaces because several isomers can arise from a given neutral conformation. Finally, modelling of surfaces is a challenge for computational chemistry so that different approaches are commonly used.

In this chapter these three points will be discussed, making special emphasis on the strategies employed along the present thesis.

3.1 ELECTRONIC STRUCTURE OF TRANSITION METAL CATIONS

Transition metal-ligand interactions are of paramount importance in biological systems and in organometallic catalytic processes. Because of that, the theoretical analysis of transition metal complexes is nowadays an area of wide interest. While the molecular properties (geometries, binding energies, etc.) for most of the main group elements can be described with good accuracy by using standard quantum chemical techniques, the determination of the same data and with the same accuracy for transition metal compounds is still considered an elusive goal and usually calls for very sophisticated treatments. The complexity when treating with transition metal-containing systems is due to the fact that transition metal atoms and ions have, in general, various low-lying electronic states, each with a different chemical behaviour, which arise from different occupations of the atomic n*d* (n+1)*s* (n+1)*p* valence orbitals.

At present, quantum chemical methods can provide accurate binding energies for transition metal-ligand systems. Moreover, since calculations are generally of nearly equal accuracy for all metal ions, they can reveal trends as well as possible experimental inaccuracies. In fact, some experimental results that were inconsistent with the theoretical trends have commonly been found to be in error so that theoretical methods have been particularly useful for identifying and explaining the unexpected trends.[160-168]

During the ninetines, detailed analysis of several M^+-L systems for an entire transition metal row and different representative ligands has revealed that besides the obvious electrostatic terms, many other competitive effects such as metal-ligand and ligand-ligand repulsion, dative interactions or the *d-d* exchange energy are important factors in the nature of bonding between transition metal cations and ligands,[101, 169] which consequently influence the optimal structures and binding energies. Especially important is the ability of transition metal cations to reduce the metal-ligand repulsion via *sd*σ or *dp*π hybridization (Figure 3.1a and Figure 3.1b, respectively), thereby shortening the metal-ligand distance and increasing the binding energy.

a **b**

Figure 3.1 Scheme of the formation of *sd*σ (a) and *dp*π (b) hybrid orbitals.

Because the great number of electrons and the open-shell character of transition metal complexes the methodology used to properly describe such species must treat accurately the electron exchange and correlation effects. In this sense, two general routes are available for the assessment of the electronic structure in transition metal containing species: i) *ab-initio* post-Hartree-Fock (post-HF) methods; and ii) density functional theory (DFT) methods. For small metal-ligand systems one can use highly accurate post-HF methods such as the coupled cluster singles and doubles with a perturbational estimate of the connected triples, CCSD(T), or multireference based approaches. However, for most problems of chemical and biochemical interest, these methods are impractical since they become extraordinarily expensive. In this context, density functional methods, especially the hybrid ones, offer a cost-effective alternative to optimise geometries and compute vibrational frequencies, since they account for electron correlation at a much lower computational cost than post-HF methods.

3.1.1 TRANSITION-METAL MONOCATIONS

In the last 15 years, the reliability of density functional methods has been analysed for many small metal-ligand systems by comparing the density functional results to high level wave function based methods or experimental data,[101, 170-176] which serve as benchmark values. For example, some cationic M^+-X complexes considered have X = H, CH_3 and CH_2, and $M^+ = Sc^+ - Cu^+$.

These studies showed that, for the $[M-H]^+$ systems[101, 170-172, 176] a large overestimation in the binding energies was observed when using the SVWN functional (LDA-typical overbinding) whereas gradient corrections introduced in the BP86 functional reduced the overbinding to some extent. The B3LYP hybrid performed much better and reduced the error present with GGA functionals. The Modified Coupled Pair Functional (MCPF) approach did not perform quite well as B3LYP but the empirical scaling within the Parametrized configuration interaction (PCI-80) scheme further improved the performance. Thus, the trend observed as a function of the best performance of binding energies in $[M-H]^+$ systems was PCI-80 > B3LYP > MCPF > BP86 > SVWN. For the $[M-CH_3]^+$ systems[101, 172, 173] the results obtained by B3LYP hybrid functional strongly depended on the basis set employed in such a way that using an extended basis set gave closer results to the experimental data and to high level post-HF values than using a small basis set, where quite large overestimations were obtained. The BHLYP hybrid functional was also tested and provided better results than the MCPF ones. The best performance of binding energies in $[M-CH_3]^+$ was PCI-80 ~ QCISD(T) > BHLYP ~ B3LYP (extended basis set) > MCPF > B3LYP (small basis set). Finally, for the $[M=CH_2]^+$ complexes,[101, 172, 174, 175] the poor performance of the MCPF approach suggested that these systems posses a severe near-degeneracy problem so that an appropriate rigorous wave-function based methods would have to invoke a multireference treatment. The BHLYP functional underestimated systematically the binding energies but the B3LYP one performed quite well. According to this results the best performance of binding energies for the $[M=CH_2]^+$ systems followed the trend PCI-80 > B3LYP > BHLYP > MCPF. Overall, these results concluded that the application of hybrid methods mixing Hartree-Fock and density functional exchange was a promising alternative to rigorous high level post-HF theory, being thus efficient and reliable tools for the evaluation of binding energies and other properties of transition metal complexes even with complicated electronic structures.

Finally, a brief methodological discussion about the Cu^+ cation deserves special attention since it is the main monocation considered along this thesis. The Cu^+ is a closed-shell d^{10} (^1S) ground state metal cation. It is often said that transition cations with this electronic configuration present similar behaviour as alkali and alkaline-earth cations, the interaction being mainly electrostatic. However, due to its d^{10} configuration other factors such as metal-ligand repulsion or charge transfer are also important.[101, 169] We need a reliable methodology to describe the Cu^+-systems because, on one hand, a great number of biochemical processes involving copper monocations (in which it is usually oxidised to

Cu^{2+}) exist, and on the other hand, despite its low reactivity, it is a very effective Lewis acid that strongly binds to molecules with accessible lone pairs. In that vein, the results previously reported when studying the small transition-metal complexes M^+-X are likewise valid. In addition, Luna et al.[177] computed the binding energies of a set of Cu^+-L systems (L = H, C, N, O, Si, CH_2, CH_3, NH_2, NH_3, H_2O, CO, SiH, SiH_2, SiH_3) at the G2(MP2), G2, CCSD(T) and B3LYP levels and the results were compared to the experimental binding energies reported in the literature. It is noteworthy that the set considered includes both open- and closed-shell species in order to have as many different situations as possible. The main conclusion of this work was that while the standard G2 methods presented dramatic failures when trying to reproduce the binding energies, the values obtained by the B3LYP functional, were in fairly good agreement with the experimental data. The deficient description by the G2 approach was attributed to a poor convergence of the Møller-Plesset perturbative series, the oscillations arising from the metal cation. Furthermore, a work of Irigoras et al.[178] evaluated the reaction path of Cu^+-$H_2O \rightarrow CuO^+ + H_2$, whose results confirmed B3LYP as a reliable method both to determine Cu^+ binding energies and reaction mechanisms in which this metal cation is involved.

3.1.2 TRANSITION-METAL DICATIONS

Doubly charged metal cations are of special interest for several reasons. On one hand they usually exhibit unusual structures, a fact that is accentuated in gas phase because of the formation of coordinatively unsaturated species. On the other hand, the stability of the M^{2+}-L complexes is intriguingly interesting and can be studied under mass spectrometry conditions, as is discussed as follows.[179-182] The formation of the doubly charged species is described according to Reaction 3.1

$$M^{2+} + L \rightarrow M^{2+}\text{-}L \quad \textbf{Reaction 3.1}$$

However, the stability of M^{2+}-L depends univocally on the second ionization energy (IE) of the metal (Reaction 3.2) and the first IE of the ligand (Reaction 3.3) in such a way that dissociation processes via charge separation, like Reaction 3.4 and governed by ΔE_{IP}, must be considered to evaluate the stability of the dicharged complex.

$M^+ \rightarrow M^{2+} + 1e^-$	IE_{M^+}	**Reaction 3.2**
$L \rightarrow L^+ + 1e^-$	IE_L	**Reaction 3.3**
$M^{2+} + L \rightarrow M^+ + L^+$	$\Delta E = -IE_{M^+} + IE_L$	**Reaction 3.4**

According to the values of ΔE, three cases may occur: i) $\Delta E > 0$, the M^{2+}-L complex is thermodynamically stable (Figure 3.2a), ii) $\Delta E < 0$, the charge dissociation is thermodynamically favoured but the M^{2+}-L complex is a minimum with a sizable barrier for dissociation (Figure 3.2b), and iii) $\Delta E < 0$ with a barrierless charge-separation process (Figure 3.2c). For case ii) it is said that the complex is kinetically stable with a Coulomb energy barrier, so that M^{2+}-L complex should exist. In contrast, in the later case, a charge-separation process via Coulomb explosion occurs.

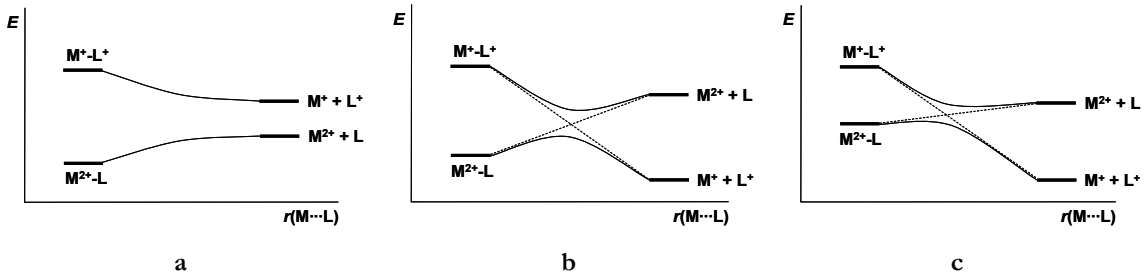

Figure 3.2 Schematic illustrations of electronic states for the M^{2+}-L system: a) with thermodynamic stability; b) with an energy minimum; c) barrierless dissociation respect to the $M^+ + L^+$ situation.

Since the usual high difference between the second IE of most of the transition metals and the first IE of small ligands, it is actually complicated to generate doubly charged metal-ligand complexes in gas phase, the attempts tested usually leading to an immediate charge-transfer dissociation process. In addition, proton transfer reactions are also commonly observed when trying to generate M^{2+}-L gas phase complexes. Indeed, the ligand often undergoes a deprotonation when interacting with the dication in such a way that the final complex detected is an overall monocharged system $[M^{2+}\text{-}(L\text{–}H)^-]^+$.

Since metal dications are of paramount relevance in a great number of biochemical systems and processes, jointly to the aforementioned difficulty for generating doubly (and multiply) metal-charged systems in gas phase with small ligands, it seems justified that theoretical methods can contribute giving clues and important information of the molecular properties and chemical behaviour of such systems. For that reason, it deserves to pay special attention to the reliability of the different theoretical techniques to the treatment of doubly metal-charged species.

As mentioned in the previous section, DFT/HF hybrid functionals seem to be reliable methods to describe singly-charged metal complexes. Nevertheless, methods that exhibit good results for both neutral and monocharged-metal species may fail when trying to describe metal dication complexes. Moreover, absolute assessments of the different theoretical procedures to reasonably describe M^{2+}-L complexes are scarcer than for monocations because of the lack of accurate experimental data as a consequence of the above-mentioned problems to generate such systems in gas phase. Therefore, the knowledge about the good/bad performance of the different theoretical approaches in this field is still nowadays somewhat incomplete and fragmentary.

Some works carried out by Corral et al., were focused on the interaction of Ca^{2+} with neutral molecules[183] as well as biomolecules.[184, 185] Assessments of theoretical procedures for this kind of systems concluded that the combination B3LYP/cc-pWCVTZ provides a good compromise between accuracy and computational cost. In a study of the first-row divalent transition metal monohydrates (from Sc^{2+} to Cu^{2+}) Trachtman et al.[186] showed that the MP2/6-311++G(d,p) and CCSD(T)/6-311++G(d,p)//MP2/6-311++G(d,p) methods provided the same electronic configurations for the ground states and that both computational levels estimated similar binding enthalpies for the corresponding states. In contrast, Schröder et al.[187] observed that the theoretical results of a set of dicationic vanadium compounds computed at B3LYP, CCSD(T) and Multi-Reference-Averaged Coupled Pair Functional (MR-ACPF) levels were in considerable spread, the CCSD(T) method being the only one that estimated results in reasonably agreement with the experimental ones, concluding thus that there was no still any cost-effective methods that provided results of benchmark quality. Therefore, the controversial behaviour of transition metal dication complexes dealt with different quantum-chemical methods demonstrates that a reassessment of the different DFT methods using a large test set of systems is quite needed.

In view of that, the next section addresses the reliability of some DFT methods to be used in Cu^{2+} containing systems. Cu^{2+}-H_2O has been chosen as the reference system and its ground and low-lying electronic states have been computed at different levels of theory to test the methods employed.

3.1.3 THE Cu^{2+}-H_2O SYSTEM

At the beginning of this work the only theoretical studies on Cu^{2+}-H_2O performed with DFT methods were the works of El-Nahas, who showed that although the Cu^{2+}-H_2O

is unstable with respect to the charge separation asymptote of $Cu^{+} + H_2O^{\bullet+}$, it is kinetically stable by a coulomb energy barrier of about 7 kcal/mol (see Figure 3.2b).[188, 189] These studies were important because the existence of Cu^{2+}-H_2O in gas phase was the subject of controversy. Early experiments indicated that Cu^{2+}-$(H_2O)_3$ was the smallest stable cluster in gas phase,[190] whereas more recent mass spectrometry experiments found that Cu^{2+}-H_2O could be generated as a long-lived dication.[191, 192] Additionally, the potential energy curves corresponding to the dissociation into $Cu^{+} + H_2O^{\bullet+}$ were obtained at the CCSD(T)/6-311+G(3df,2p)//BHLYP/6-311+G(d,p) level, concluding that Cu^{2+}-H_2O should be produced in gas phase[193] and thus, confirming the theoretical results of El-Nahas. Although these theoretical studies provided very valuable information on the stability of the Cu^{2+}-H_2O system, the lowest electronic state of this complex was not reported and the ground-state structure at the B3LYP level was found to have C_s symmetry.[188, 189, 191, 192] This fact contrasts to the most M^{n+}-H_2O systems (also to Cu^{2+}-H_2O) treated at the MP2[186] level which were shown to present C_{2v} symmetry, as expected considering that the planar structure provides the optimal ion-dipole interaction.

Cu^{2+} is an open-shell system with a d^9 (^{2}D) ground state metal cation. When interacting with water, the five *d* orbitals of Cu^{2+} split, which leads to different low-lying electronic states depending on the metal *d* occupation. Although the energy order of these states is largely determined by the different overlap of the five *d* orbitals with H_2O, other factors such as 4*s*-3*d* and 4*p*-3*d* mixing or charge-transfer processes can also contribute to determining the ground state of Cu^{2+}-H_2O. Thus, assuming C_{2v} symmetry, geometric optimizations and frequency calculations for Cu^{2+}-H_2O in different symmetry electronic states have been performed. Table 3.1 shows the relative energies and the optimized Cu-O distances obtained with the density functionals of G96LYP, [194, 195] BLYP, [195, 196] B3LYP, [195, 197] MPW1PW91[198-200] and BHLYP, [195, 201] as well as with the highly correlated CCSD(T) post-HF method, [202] using the 6-311++G(d,p) basis set for O and H and the supplement basis set of Wachters (15s11p6d1f)/[10s7p4d1f] for Cu^{+}.[203-205]

Table 3.1 Relative energies (in kcal/mol) of the ground and low-lying electronic states of Cu^{2+}-H_2O at different levels of theory. In parenthesis the percentage of the exact HF exchange.

Symmetry	State	Value	G96LYP (0%)	BLYP (0%)	B3LYP (20%)	MPW1PW91 (25%)	BHLYP (50%)	CCSD(T)
C_{2v}	$^2A_1$	ΔE_{rel}	0.0	0.0	0.0	0.0	0.0	0.0
		R_{Cu-O}	1.874	1.878	1.844	1.832	1.837	1.841
C_s	$^2A'$	ΔE_{rel}	-10.9	-11.1	-3.7	-1.8		
		R_{Cu-O}	1.976	1.983	1.898	1.866		
C_{2v}	$^2B_1$	ΔE_{rel}	-10.5*	-10.7*	-2.3	0.7	6.6	5.6
		R_{Cu-O}	1.988	1.993	1.917	1.891	1.862	1.865
C_{2v}	$^2B_2$	ΔE_{rel}	23.9	23.4	18.4	17.6	13.2	13.7
		R_{Cu-O}	1.910	1.913	1.908	1.904	1.909	1.919
C_{2v}	$^2A_2$	ΔE_{rel}	28.5	27.8	21.2	20.3	15.7	16.3
		R_{Cu-O}	1.926	1.929	1.917	1.911	1.911	1.922

* First order saddle point.

It can be observed that, at the CCSD(T) level of calculation, the ground electronic state of Cu^{2+}-H_2O is the $^2A_1$ one, in agreement with previous post-HF results.[186, 193] This was to be expected considering that the $3d_{z^2}$ orbital is the one with a larger overlap with H_2O, and thus, doubly occupying the $3d_{xy}$(a_2), $3d_{xz}$(b_2), $3d_{yz}$(b_1), and $3d_{x^2-y^2}$ (a_1) orbitals and maintaining the $3d_{z^2}$ (a_1) orbital singly occupied minimize the Cu^{2+}-H_2O repulsion. At this level of theory, the relative stability of the different electronic states is $^2A_1$ < $^2B_1$ < $^2B_2$ < $^2A_2$, in agreement with what one would expect considering the different overlap between the five *d* orbitals of the metal and H_2O.[167] That is, electronic states become increasingly less stable if metal *d* electrons are allocated in orbitals that have a larger overlap with H_2O, since then metal-ligand repulsion becomes larger. Accordingly, the R_{Cu-O} distance in the different electronic states follows the same trend: $R_{Cu-O}(^2A_1) < R_{Cu-O}(^2B_1) < R_{Cu-O}(^2B_2) < R_{Cu-O}(^2A_2)$.

Results with different density functional methods, however, vary significantly depending on the amount of exact exchange mixed in the functional. First, it should be mentioned that for the $^2B_1$ state and with G96LYP and BLYP the C_{2v} symmetry structure is not a minimum on the potential energy surface but is a first-order saddle point. Symmetry relaxation following the transition vector leads to a C_s symmetry structure and a

$^2A'$ electronic state, with H_2O being somewhat pyramidalized. Moreover, with B3LYP and also with MPW1PW91, in addition to the C_{2v} ($^2A_1$) and C_{2v}($^2B_1$) minima, we have located a C_s($^2A'$) symmetry structure lower in energy, as found in the previous study of El-Nahas with B3LYP.[188] The stabilization gained upon pyramidalization is, however, small, so we will mainly focus on the relative stabilities of the different electronic states assuming C_{2v} symmetry.

The most striking difference observed between the different functionals is the relative energy of $^2B_1$ with respect to $^2A_1$, which ranges from -10.7 for BLYP to +6.6 for BHLYP. Thus, for nonhybrid density functional methods, and assuming C_{2v} symmetry, $^2B_1$ is computed to be the lowest electronic state of Cu^{2+}-H_2O, whereas with the hybrid BHLYP the ground state is the $^2A_1$ one, as predicted by the CCSD(T) level of theory. Note that with the popular B3LYP method the $^2B_1$ state is also wrongly predicted to be lower than the $^2A_1$ one, although with this functional the two states become much closer in energy than with BLYP. Relative energies of the $^2B_2$ and $^2A_2$ states with respect to $^2A_1$ also show significant variations upon increasing the exact HF exchange mixing in the functional. However, changes are not as pronounced as for $^2B_1$, and their relative order is maintained. It can be observed in Table 3.1 that, among all the functionals considered, the one that provides better results compared to CCSD(T) is the BHLYP one, in which the exact exchange mixing is 50%.

It deserves to be commented that all these observations appear to be related to the degree of charge and spin delocalization in the different electronic states. For the $^2B_1$ state the BLYP functional provides an almost completely delocalized picture. As the amount of exact HF exchange mixing increases, the spin density becomes more localized at the metal centre and the monoocupied orbital presents larger contributions of the d_{yz}(b_1) metal orbital (see Figure 3.3)

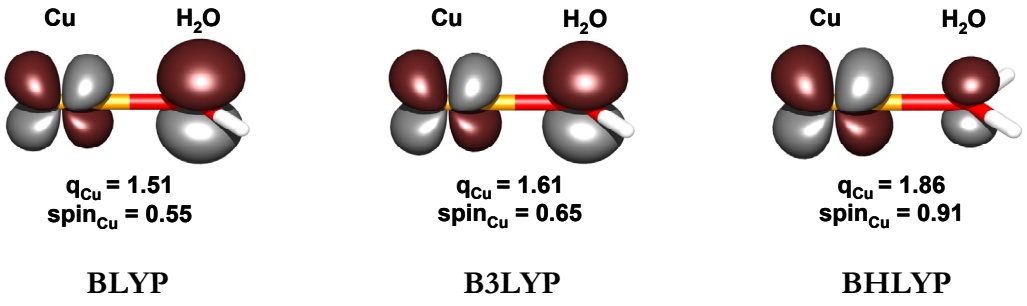

Figure 3.3 SOMO of the $^2B_1$ state computed at the BLYP, B3LYP and BHLYP density functionals. The net charge (q_{Cu}) and the spin density ($spin_{Cu}$) on the metal cation are also included.

The overstabilization of the $^2A_1$ ground electronic state is not as important as for $^2B_1$, because the degree of delocalization is smaller. However, it is non-negligible and it can lead to a too large Cu^{2+}-H_2O binding energy. To evaluate how much this important magnitude is affected by the functional used, we have computed the Cu^{2+}-H_2O ($^2A_1$) interaction energy with the different functionals tested in this work. Results are given in Table 3.2. The values computed with GGA functionals are about 18-20 kcal/mol larger than the CCSD(T) one. Hybrid functionals show smaller deviations (from 12 to 4 kcal/mol), the differences depending on the amount of exact exchange included in the functional; that is, the larger the percentage of HF exchange, the smaller the interaction energy and the better the agreement with CCSD(T). In particular, it is observed that BHLYP provides a Cu^{2+}-H_2O interaction energy in good agreement with CCSD(T).

Table 3.2 Interaction energies for the $^2A_1$ state of Cu^{2+}-H_2O, in kcal/mol.

	G96LYP	BLYP	B3LYP	MPW1PW91	BHLYP	CCSD(T)
D_e	122.1	124.4	115.8	112.8	107.4	103.8
D_o	120.6	122.9	113.7	109.6	105.7	102.6
ΔH^0_{298}	121.8	124.1	114.9	110.9	106.8	103.9

This study was carried out in collaboration with Dr. J. Poater and Dr. M. Solà from Universitat de Girona.[206] In order to analyze these energetic changes according to the functional used, we calculated the different electronic states of Cu^{2+}-H_2O by varying monotonically the proportion of exact exchange introduced (for further details see ref [206] and Appendix C). These results indicated that the ground state of Cu^{2+}-H_2O changes from $^2B_1$ to $^2A_1$ between 20 and 30 % of exact exchange. Furthermore, the parameter set that give the closest results to the CCSD(T) values are those having percentage between 40 and 50 %.

In summary, this work shows that Cu^{2+}-H_2O presents C_{2v} symmetry and the relative order of the electronic states is $^2A_1 < {}^2B_1 < {}^2B_2 < {}^2A_2$. However, density functional results show that the relative stability of these states varies depending on the degree of mixing of exact HF and DFT exchange functionals. For GGA and also for hybrid functionals with low percentages of HF mixing (up to 20-25%), the $^2B_1$ state becomes more stable than the $^2A_1$ one. Instead, the relative energies of the electronic states obtained by the BHLYP approach are in good agreement with the computed at CCSD(T), the $^2A_1$ state being thus the most stable one. These changes are related to the spin delocalization in the different

electronic state; the overstabilization of the $^2B_1$ state and the degree of delocalization become diminished by adding more contribution of the exact HF exchange, indicating that the error is related to the exchange functional. On the other hand, the optimized R_{Cu-O} distance in this state appears to be quite sensitive to the functional used (see Table 3.1); the larger the amount of exact exchange mixing, the smaller the metal-ligand distance (at least until 50%). This situation is similar to that found in delocalized radical systems; i.e. two center-three electron bond systems,[207-209] which present too large interaction energies and too long bond lengths with LDA or GGA functionals. Such overstabilization is attributed to a bad cancellation of the self-interaction (SI) included in the Coulomb energy by the exchange-correlation functional, due to its delocalized electron hole. Therefore, the admixture of exact exchange reduces the degree of delocalization and also the overstabilization and similarly to the two centre-three electron systems BHLYP is found to be the functional that provides the closest results to CCSD(T).

3.1.4 OTHER Cu^{2+} SYSTEMS

As mentioned, the performance of density functional methods for studying transition metal dications has been much less analyzed than singly positive cations. In this sense, the B3LYP technique has been usually used to study the interactions between neutral small biomolecules and transition metal dications. In particular, for Cu^{2+}-glycine[112] and Cu^{2+}-oxime analogues systems,[210] although the relative energies of the different structures investigated obtained at the B3LYP level were in reasonably agreement with those estimated using CCSD(T) method when comparing structures of similar spin distribution, the B3LYP binding energies were substantially higher, a fact that clearly indicates the propensity of the B3LYP method to overestimate the binding energies when dealing with Cu^{2+}-systems. This overbinding, also found when using LDA and GGA functionals, can be attributed to these methods (LDA, GGA and hybrid functionals with low admixture percentages of HF) to overstabilize electronically delocalized situations as a result of a bad cancellation of the self-interaction part by the exchange correlation functional[207-209], usual situation when Cu^{2+} interacts with small ligands. It was shown that the use of functionals with large amounts of exact exchange reduces the error. Indeed, the BHLYP Cu^{2+} binding energies to glycine and to the oxime analogues systems were in excellent agreement with the CCSD(T) ones. It is worth noting that similar facts were observed by the Co^{2+}-glycine system[113] but in a lesser extent and that for the Fe^{2+}-glycine[211] system the functional that gives similar results to CCSD(T) (both relative and binding energies) is the BHLYP one.

3.2 CONFORMATIONAL FLEXIBILITY

Flexible ligands such as amino acids and peptides may exist in different conformations and thus, in order to identify the most stable one a conformational analysis is mandatory.

Conformational methods can be divided into different categories such as systematic search algorithms, random approach or molecular dynamics. In this work the random method, in particular the Monte Carlo Multiple Minimum (MCMM)[212] search, was used and thus it will be briefly discussed next.

In a random search, one moves from a region of the energy surface to a completely unconnected region in a single step; that is, the exploration of the conformational space is performed in an unpredictable way. At each iteration, a random change is made on an initial conformation and the new structure is redefinied by energy minimisation. If the new minimised conformation has not already been found previously, it is then stored and used as the starting point for the next iteration. Otherwise, the structure is rejected. This procedure continues until a given number of iterations have been performed or until it is decided that no new conformations can be found.

The criteria to reject structures are not univocal and depend on the interests of the user. Particularly, MCMM search criteria are based on several constraint tests that involve energy-minimised structures and interatomic parameters.[213] Structures rejected according to the energetic test are those whose energy lie outside the selected energetic upper bound relative to the instant global minimum, that is, the energy is high enough that the conformer is not significant. Rejections according to the second test are fulfilled if the geometry parameters of the new structure are very similar to those of another one previously located, in such a way that they are considered as the same conformer.

3.3 SURFACE MODELLING

When modelling surfaces, one can use four different approaches: the free cluster, the ONIOM cluster, embedded clusters and periodic calculations.

The free cluster approach is the simplest method to represent a solid. It consists on performing quantum chemical calculations on a small fragment of the solid, called cluster. The substitution of an infinite solid by a finite cluster is justified assuming that the chemical problem studied depends mainly on local properties of the solid. Accordingly, this cluster represents the active site of the solid. However, the elimination of the rest of the solid can

induce three types of errors: i) the selected cluster may not consider the essential chemistry involved in the system, ii) constraints produced by the infinite structure are not considered, which can lead to extra (un)stabilization of the system leading to wrong results, and iii) the long-range effects are not included in the calculations, a fact that in some solids may be important. To correct these deficiencies larger clusters could be considered but the computational cost rapidly increases with the size of the cluster. Thus, alternative approaches should be applied.

The ONIOM[214-217] (our own n-layered integrated molecular orbital and molecular mechanics) approach allows to use larger clusters. This approach subdivides the whole system (real) in different layers, usually 2 or 3, each one being treated at different computational levels. The most important part, which includes the active site of the solid, is called the model system and it is described at a high level of theory, whereas the rest of the solid is computed at a lower level. This allows the study of large clusters and thus to get a better description of the system. However, this approach presents some critical points. One of them is how bonds between atoms of different layers are treated. Normally, these bonds are broken and the model part is saturated with link atoms, typically hydrogens. A second critical point is how the system is partiotinated and which combination of high and low-levels of theory should be used. To validate both the partition and the levels of theory one can perform a test that involves the optimization of the global system at the high level of theory for at least one case. However, in some cases this is not possible and the test is given by comparing with experimental data or full periodic calculations. For the particular case of silicates and aluminosilicates it is well described that an optimum level of theory for the model part is DFT(B3LYP) while for the real part it are the semiempirical methods (MNDO and AM1) or HF.[218-222]

The embedded cluster approach also divides the system in two parts, but in contrast to ONIOM clusters, the second layer includes periodic conditions to represent the whole solid. That is, the local part where the majority of the chemistry is included is described at an accurate level of theory, whereas the long-range effects are evaluated at a lower level. This fact, however, introduces a disadvantage because the long-range effects are introduced indirectly and at a low level such as the use of point charges to reproduce the Madelung constant, the introduction of a correcting electrostatic potential, or the use of force fields with periodic boundary conditions. One example of the latter case is the QM-

pot scheme developed by Sauer and coworkers,[223, 224] which is probably the embedded cluster approach that have provided more satisfactory results in a great variety of situations.

Finally, fully ab-initio periodic calculations can also be done. They include both the local properties and the long-range effect in a solid at the quantum level. Accordingly, this approach is the best one if the level of theory used is accurate enough. Unfortunately, at present, for silicates and aluminosilicates they can only be applied taking relatively small unit cells.

4. INTERACTION OF Cu^+ AND Cu^{2+} TO AROMATIC AMINO ACIDS. AN EXPERIMENTAL AND THEORETICAL STUDY

4.1 INTRODUCTION

There are 20 natural amino acids, among which 4 have an aromatic chain (AA_{arom}): phenylalanine (Phe), tyrosine (Tyr), tryptophane (Trp) and histidine (His), as is represented in Figure 4.1. As described by Ruan and Rodgers,[81] the most stable conformation of these amino acids present a hydrogen bond between the proton of the carboxylate group and the nitrogen of the amino group. Furthermore, His possesses two tautomeric forms, His(ε) and His(δ) depending on wether the non-protonated N of the imidazole ring is Nε or Nδ, respectively. Gas phase calculations have shown that the most stable tautomer is His(ε) by 2.8 kcal/mol (relative enthalpies computed at the G3(MP2)/6-31G(d)),[225] that is, with the proton on Nδ (as shown in Figure 4.1).

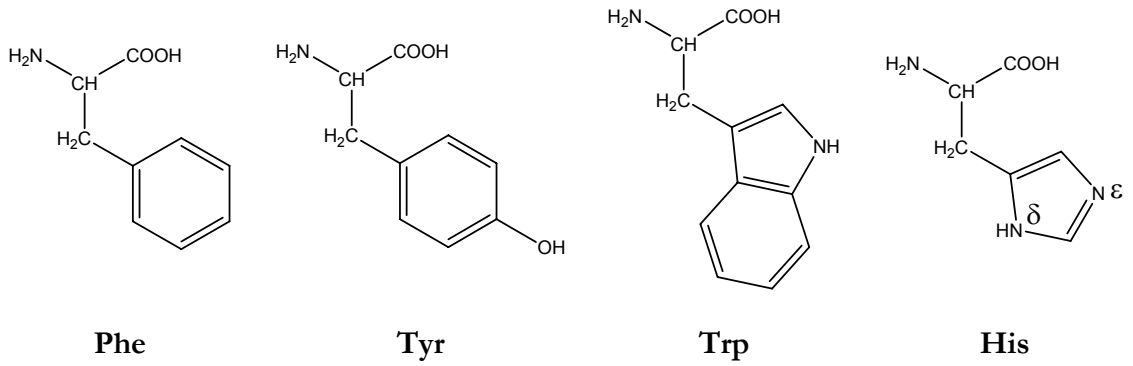

Figure 4.1 Schematic representation of the four aromatic amino acids (AA_{arom}): phenylalanine (Phe), tyrisone (Tyr), tryptophane (Trp) and histidine (His).

The aromatic groups enable these amino acids to establish an additional interaction with metal cations: the cation-π interactions.[226, 227] This kind of interactions are non-covalent binding forces that occur between cations and the π-face of the aromatic amino acid. Since cation-π interactions were first observed and recognized, they have attracted considerable attention because of its relevance in many biological systems.[228] For instance, they are responsible for the functioning and selectivity in variable ion channels, in which Na^+ and K^+ are the cations,[229-233] or they are often involved in biological recognition.[234, 235]

In addition, recent studies have suggested that the interactions between aromatic amino acids and various metal cationic centres are common motifs in protein structures.[236-239]

The nature of this interaction has been the subject of several theoretical studies.[107, 229, 240-245] According to Dougherty and co-workers, cation-π interactions are basically electrostatic, the interaction of the cation with the large quadrupole moment of the aromatic moiety accounting for 60 – 90 % of the overall binding.[228, 240, 241] For small cations, ion-dipole and ion-induced dipole interactions may also contribute to the binding.[107] Other smaller contributions are due to charge transfer, and dispersion forces. According to these bonding factors, transition metal cation-π interactions are not usually catagorized as cation-π interactions because of the interaction between the aromatic rings with transition metal *d* orbitals.[228]

Recently, studies on the complexation of alkaline, alkaline-earth and transition metal cations to aromatic amino acids, both experimental and theoretical, have been reported in the literature.[68, 72, 74-76, 81-85, 89, 93, 105-107, 123-127, 129, 130, 246] The interaction of Li^+, Na^+, and K^+ to Phe, Tyr and Trp has been considered by the experimental kinetic method, exchange equilibria and by density functional calculations.[82, 84, 85] Additionally, Ruan and Rodgers studied the complexation energies of Na^+ and K^+ with these aromatic amino acids by means of threshold CID techniques,[81] and Polfer at al. investigated the structure of K^+-Phe complex using IRMPD spectroscopy and DFT methods.[246] All these works agree that the most stable structure has the metal cation interacting with the neutral form of these amino acids (so-called charge solvation form) through the nitrogen amine, the carbonyl oxygen and the π system of the side chain. Among the works that have considered transition metal cations it deserves to be mentioned those published by Polfer et al., in which the IRMPD technique was applied to singly charged complexes involving Ag^+ and Zn^{2+} with Phe,[124] and Ag^+ with Trp.[123] Both DFT calculations and the experimental spectrum supported a charge solvation tridentate structure as the predominant one (similarly to alkali and alkaline-earth metal cations), whereas results ruled out a significant presence of zwitterionic conformations (so-called salt-bridge form) in gas phase.

On the other hand, the reactivity in the gas phase of transition metal cations with amino acids has been studied by several authors from an experimental point of view.[56, 89, 90, 125-130, 135-138] Harrison and co-workers reported the fragmentation reactions of several Cu^+-cationized amino acids generated by FAB[125] and Lavannant et al.[129] studied the formation and fragmentation of α-amino acids complexed by Cu^+ in PD mass spectrometry. It was

proposed that these fragmentations were induced by an insertion of the metal cation into the amino acid bonds. For all of them the loss of mass 46 u was mostly observed under CID conditions. This loss was also observed with other metal cations such as Ni^+ and Fe^+.[56, 126, 127] Recently, Hoppiliard et al.[138] have presented an exhaustive theoretical study of the fragmentation mechanisms of the complexes of Cu^+ with glycine (Cu^+-Gly) generated by ESI, which suggests that this mass of 46 u is associated to the losses of H_2O and CO, in agreement with a previous theoretical study for the fragmentation of the Ni^+-Gly system.[56] Focusing on the gas phase reactions of Ag^+-Phe studied both from experimental and theoretical points of view,[68, 72] the fragmentation spectra obtained by ESI-CID showed the loss of H_2O followed by CO, the loss of NH_3 and CO and the simultaneous loss of CO_2 and NH_3. They also observed the formation and the loss of AgH and a peak belonging to the Ag^+-NH_3 complex. To our knowledge there are no works addressed to the formation and reactivity of the gas phase complexes ions of Cu^+-AA_{arom} by means of ESI-CID techniques.

As commented, Cu^{2+} is an open-shell system with a d^9 (^{2}D) ground state that can easily be reduced to Cu^+ closed-shell d^{10} (^{1}S) ground state. The preferred coordination environment varies depending on the oxidation state, which provides a very rich chemistry. Because of the relevance of copper cations in some biochemical processes such as electron transfer or dioxygen transport,[247] the study of the nature of bonding and its reactivity between copper cations and biomolecules is of great importance.

The present chapter will show the experimental results from an ESI-MS analysis of the copper cations with the four aromatic amino acids; that is, the ions generated in the source as well as the gas phase reactivity of the Cu^+-AA_{arom} systems. Complementing such experimental results, a detailed analysis of the gas phase binding chemistry between Cu^+ and Cu^{2+} and these aromatic amino acids will be presented by means of DFT and CCSD(T) calculations. Additionally, with the aim of proposing an interpretation of the low energy decompositions experimentally observed for Cu^+-AA_{arom} systems, the fragmentations mechanisms have been investigated for Cu^+-Phe as a model system.

As aforementioned in the Outlook, the experiments were carried out in a short stay of three months during the spring of 2004 at the Université of Évry-Val d'Essonne under the supervision of Dr. Jeanine Tortajada.

4.2 METHODOLOGY

4.2.1 EXPERIMENTAL DETAILS

Electrospray mass spectra were recorded on an Applied Biosystems/MDS Sciex API2000 triple-quadrupole instrument fitted with a "turboionspray" ion source. Samples were introduced in the source using direct infusion with a syringe pump, at a flow rate of 8 μl/min. Ionization of the samples was achieved by applying a voltage of 5.0 kV on the sprayer probe and by the use of a nebulizing gas (GAS1, air) surrounding the sprayer probe, intersected by a heated gas (GAS2, air) at an angle of approximately 90°. The operating pressure of GAS1 and GAS2 are adjusted to 2.0 bar, by means of an electronic board (pressure sensors), as a fraction of the air inlet pressure. The curtain gas (N_2), which prevents air or solvent from entering the analyzer region, was similarly adjusted to a value of 2.0 bar. The temperature of GAS2 was set to 70 °C. MS/MS spectra were carried out by introducing nitrogen as collision gas in the second quadrupole at a total pressure of 3×10^{-5} mbar, the background pressure being around 10^{-5} mbar. As detailed later, the declustering potential (DP), defined as the difference of potentials between the orifice plate and the skimmer (grounded), and typically referred to as the "cone voltage" for other electrospray interfaces, was fixed to 100 V to perform MS/MS experiments (110 V in case of *Phe*).

Sample solutions were prepared from $CuSO_4 \cdot 5H_2O$/amino acid mixture with concentrations of 10^{-4} mol L^{-1} in a methanol/water 1:1 solvent.

Unless otherwise noted, mass to charge ratios mentioned in throughout this chapter refer to as peaks that include the most abundant Cu isotope (^{63}Cu).

4.2.2 COMPUTATIONAL DETAILS

Molecular geometries and harmonic frequency calculations of the considered structures have been obtained using the non-local hybrid three-parameter B3LYP density functional approach.[195, 197] For the reactivity in gas phase, in some cases intrinsic reaction coordinate (IRC) calculations at the same level of theory have been carried out in order to corroborate the minima connected by a given transition state. As commented in Chapter 3, B3LYP has been widely used to study transition metal containing complexes, particularly Cu^+-L systems, and it has been shown to be a cost-effective method.[176, 248] However, as it has been observed in Cu^{2+}-H_2O (section 3.1.3) and also in other works,[206, 210] for the open shell Cu^{2+}-L systems, hybrid functionals with a larger percentage of exact exchange, such as

BHLYP, provide better results compared to the highly correlated CCSD(T) method. Thus, for Cu^{+2}-AA_{arom} systems, in addition to B3LYP, we have also carried out calculations with BHLYP.[195, 201] Furthermore, in order to confirm the reliability of DFT results, for some selected cases we have performed single point CCSD(T)[202] calculations at the B3LYP geometries.

In order to explore the conformation space of this kind of systems, a previous search of the Na^{+}-AA_{arom} complexes has been performed to model the electrostatic interaction of the metal cation with the AA_{arom}. This primary study was carried out using the MCMM procedure,[212] with the AMBER* force field,[249, 250] as implemented in the Macromodel 7.0 package.[213] Among all the possible structures obtained, only those lying within a range of 10 kcal/mol above the most stable one have been calculated at the DFT level. Moreover, some structures not obtained in this initial conformational search but chemically important and derived from experience and chemical intuition have also been computed.

The following basis set was used. For Cu we have employed the Watcher's primitive set (14s9p5d),[203] supplemented with one s, two p, and on d diffuse functions,[204] and one f polarization function, the final basis set being (15s11p6d1f)/[10s7p4d1f]. For C, N, O and H the standard 6-31++G(d,p) basis set has been employed. Binding energies have been corrected for basis set superposition error using the counterpoise method.[251]

All density functional calculations have been performed using the Gaussian 03 set of programs.[252] Open-shell calculations were based on an unrestricted formalism. Thermodynamic corrections have been obtained assuming an ideal gas, unscaled harmonic vibrational frequencies and the rigid rotor approximation by standard statistical methods.[253] Electron spin densities and net atomic charges on the atoms have been obtained using the population analysis of Weinhold et al.[254]

4.3 RESULTS AND DISCUSSION

4.3.1 COMPLEXES GENERATED IN THE ION SOURCE

The electrospray spectra of the copper sulfate/amino acid mixtures is dependent on the cone voltage, also referred to as declustering potential (DP) in our instrument. At all low values of DP the spectra are dominated by different Cu^{+} and Cu^{2+} hydrated complexes. Instead, at high values of DP some species of interest appear. The presence of the two isotopes of Cu (^{63}Cu and ^{65}Cu) leads to an easy identification of the Cu containing ions.

Figure 4.2 shows the source spectra recorded at DP = 100 V, with the exception of Phe, for which DP = 110 V since this DP gave optimum intensities of the ion of interest.

The main peaks do not correspond to the copper/amino acids products but to the protonated forms of the amino acids and some of its related fragments. However, the most intense peaks in which copper cations are involved correspond to the Cu^{+}-AA_{arom} complexes. Interestingly and with the exception of Phe, the peaks belonging to the Cu^{II} adducts of the deprotonated forms of the aromatic amino acids $[Cu^{II}(AA_{arom}\text{-}H)]^{+}$ are observed one unit mass lower than Cu^{+}-AA_{arom}. The addition of one molecule of amino acid to these complexes produces the $[Cu^{II}(AA_{arom}\text{-}H)(AA_{arom})]^{+}$ ions. Following the same procedure but adding one molecule of methanol the $[Cu^{II}(AA_{arom}\text{-}H)(CH_3OH)]^{+}$ ions are also observed. However, for this case, another possibility could be considered arising from the transfer of the proton of methanol to the deprotonated amino acid, which leads to the $[Cu^{II}(AA_{arom})(CH_3O^{-})]^{+}$ adduct. It is noticeable that for Phe and Tyr cases the peak of the dinuclear ion of $[Cu^{I}_{2}(AA_{arom}\text{-}H)(\ AA_{arom})]^{+}$ is also observed. In Table 4.1 the most interesting ions are classified according to the m/z ratio for each amino acid.

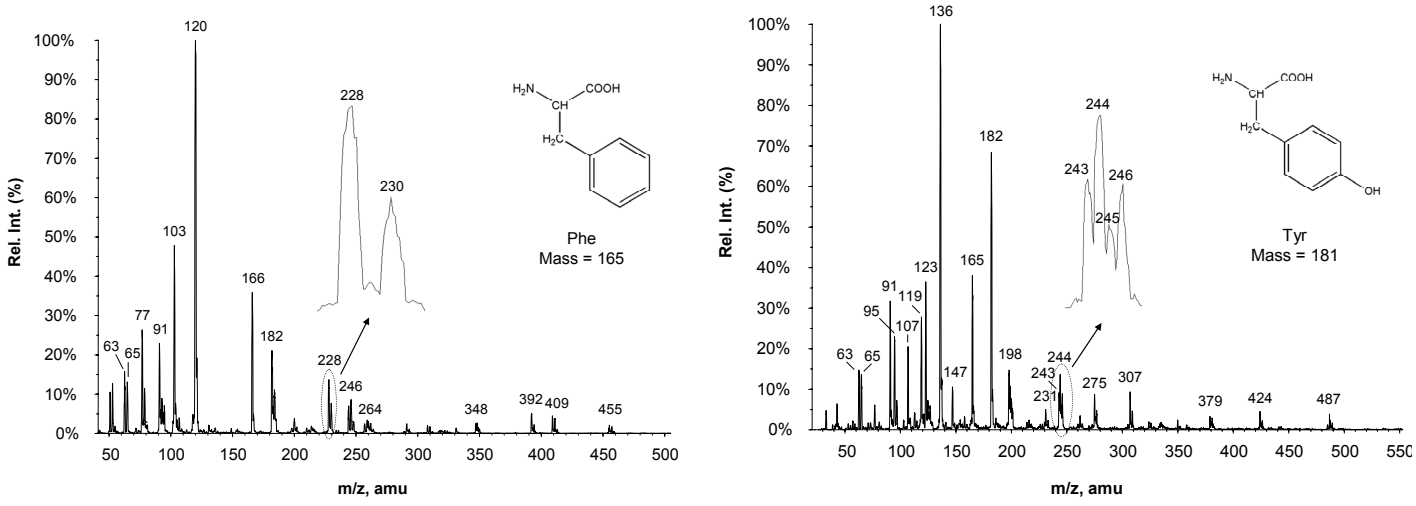

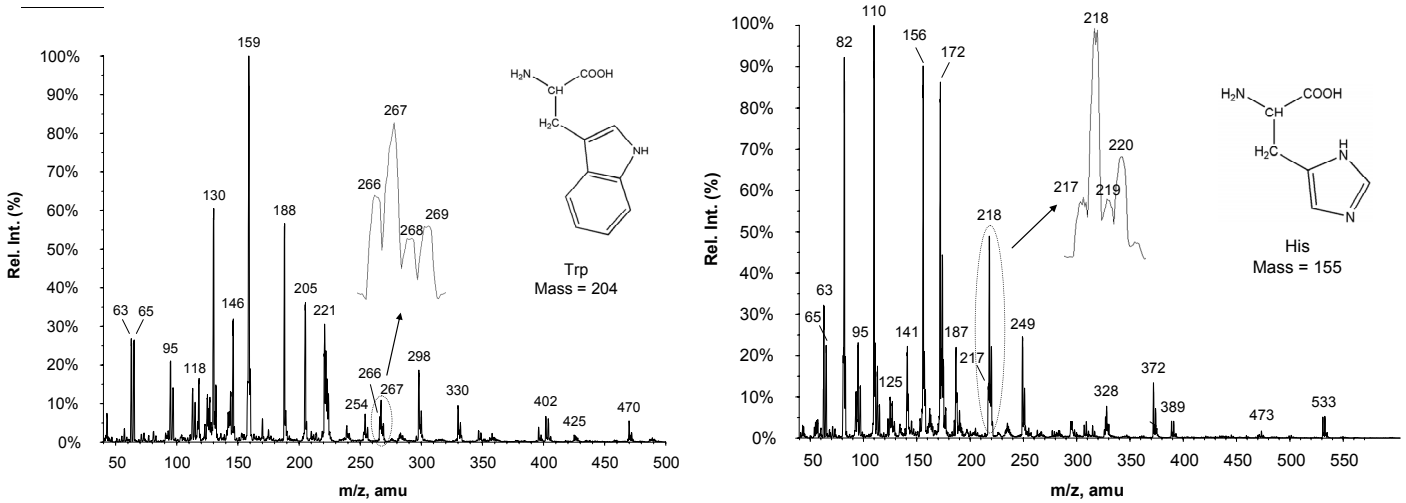

Figure 4.2 ESI source spectra of the solutions of each amino acid and $CuSO_4$ in water/methanol 1:1 solvent.

Table 4.1 Copper adducts with AA_{arom} observed in the ion source.

Ion	*m/z*			
	Phe	Tyr	Trp	His
$AA_{arom}H^+$	166	182	205	156
$[Cu^{II}(AA_{arom}\text{-}H)]^+$	-	243	266	217
$Cu^+\text{-}AA_{arom}$	228	244	267	218
$[Cu^{II}(AA_{arom})(CH_3O^-)]^+$ or $[Cu^{II}(AA_{arom}\text{-}H)(CH_3OH)]^+$	-	275	298	149
$[Cu^{II}(AA_{arom}\text{-}H)(AA_{arom})]^+$	392	424	470	372
$[Cu^{I}_2(AA_{arom}\text{-}H)(AA_{arom})]^+$	455	487	-	-

It is worth to note that neither doubly charged complexes (such as $Cu^{2+}\text{-}AA_{arom}$) nor organic radical cations have been observed in the ion source by the interaction of Cu^{2+} with the aromatic amino acids, suggesting that to generate such active species auxiliary ligands would be required, as found in the literature.[65, 74, 75, 140-144]

4.3.2 THE $Cu^+\text{-}AA_{arom}$ SYSTEMS

As it was shown, the $Cu^+\text{-}AA_{arom}$ complexes are the most important adducts observed in the source. Thus, this section concerns to a conformational analysis of the

possible isomers of these systems and also to a discussion of the nature of bonding established in the complexes.

It must be commented that only the most significant structures of the Cu^+-AA_{arom} systems will be presented. The whole conformational analysis of each system is included in Appendix D.

Structures have been named as Cu^+-AA_{arom}n, where n is a number associated to a given coordination and follows the increasing order of energy for Cu^+-Phe.

4.3.2.1 Cu^+-Phe and Cu^+-Tyr

The behaviour of the Cu^+-Phe and Cu^+-Tyr complexes is very similar, so the discussion for such systems is presented together. Main geometry parameters of B3LYP-optimized structures as well as relative potential energies including the ZPE are given in Figure 4.3. Table 4.2 summarizes the relative potential energies including the ZPE (ΔU_0), the relative enthalpies (ΔH_{298}) as well as the relative free energies (ΔG_{298}) of the isomers presented.

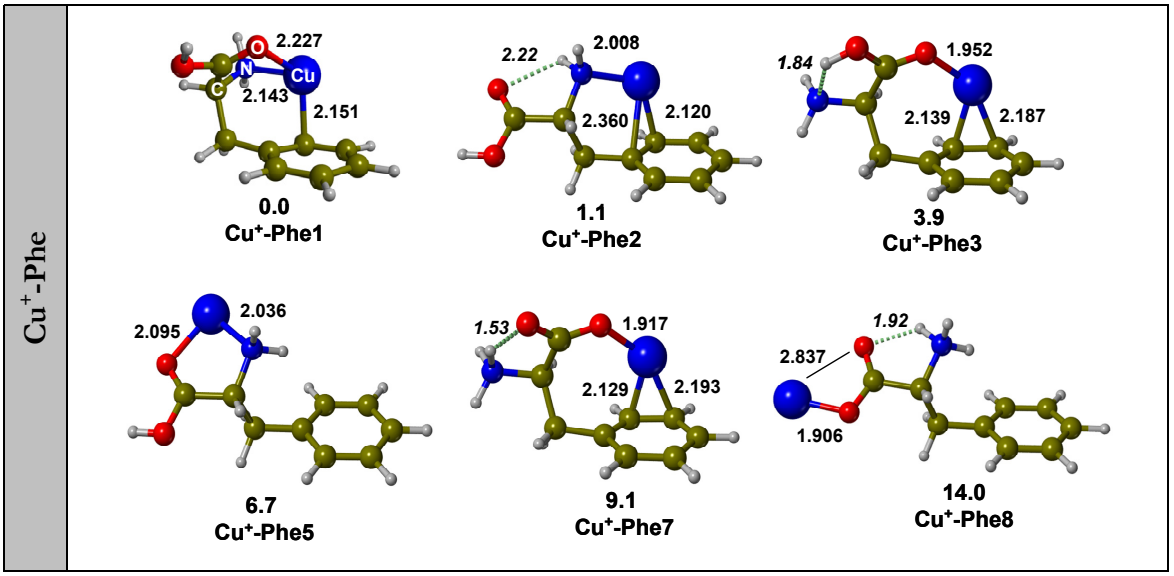

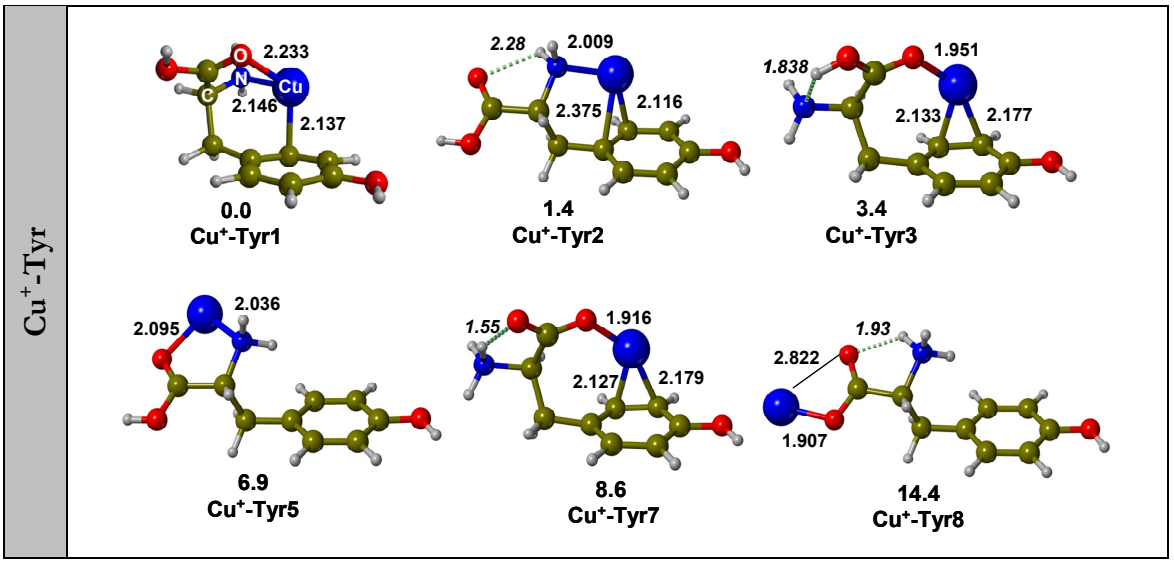

Figure 4.3 B3LYP-optimized geometries of the Cu^+-Phe and Cu^+-Tyr isomers. Relative potential energies including the ZPE values, in kcal/mol. Distances in Å.

Table 4.2 Relative potential energies including ZPE values (ΔU_0), relative enthalpies (ΔH^0_{298}) and relative free Gibbs energies (ΔG^0_{298}) of the isomers presented for the Cu^+-Phe and Cu^+-Tyr systems. In kcal/mol.

structure	coordination	ΔU_0	ΔH^0_{298}	ΔG^0_{298}
Cu^+-Phe1	(N/O/ring)	0.0	0.0	0.0
Cu^+-Phe2	(N/ring)	1.1	1.2	0.3
Cu^+-Phe3	(O/ring)	3.9	4.0	3.8
Cu^+-Phe5	(N/O)	6.7	6.8	5.6
Cu^+-Phe7	$(O^-/ring)_{zwit}$	9.1	9.1	9.1
Cu^+-Phe8	$(O^-)_{zwit}$	14.0	14.3	12.1
Cu^+-Tyr1	(N/O/ring)	0.0	0.0	0.0
Cu^+-Tyr2	(N/ring)	1.4	1.6	0.4
Cu^+-Tyr3	(O/ring)	3.4	3.4	3.6
Cu^+-Tyr5	(N/O)	6.9	7.0	5.8
Cu^+-Tyr7	$(O^-/ring)_{zwit}$	8.6	8.6	8.7
Cu^+-Tyr8	$(O^-)_{zwit}$	14.4	14.8	12.5

In both cases, the most stable structure found (**Cu^+-Phe1** and **Cu^+-Tyr1**) is similar to that previously obtained for alkali-AA_{arom} [81, 82, 84, 85, 105-107, 246] and Ag^+-Phe;[124] that is, Cu^+ interacts with the amino N, the carbonyl O and the π system of the aromatic group. However, while for the alkaline systems metal cations are centred above the aromatic ring, for Cu^+ complexes the metal cation interaction occurs only with one C of the ring. This can be understood considering that alkali metals are positively charged spheres that interact with the entire electronic cloud of the π system, whereas Cu^+, with fully occupied *d* orbitals, has the ability to efficiently reduce repulsion with the ligand through *sd* and *dp* hybridization. In this particular case, the $3d_{xz}$ orbital of Cu^+ (assuming N-Cu-C_{ring} in the *xz* plane) is hybridized with the $4p_z$ orbital in order to reduce the repulsion with the donor sites, especially those of the amino acid backbone (see Figure 4.4). As a consequence, the aromaticity of the ring is partially broken, the distance of the adjacent C-C bonds being increased around 0.013 – 0.022 Å.

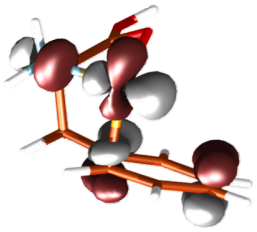

Figure 4.4 HOMO of the Cu^+-Phe isomer.

Both for Phe and Tyr, the second most stable form found involves the coordination of the metal cation to the amine and the π system (**Cu^+-Phe2** and **Cu^+-Tyr2**), which lies 1.1 and 1.4 kcal/mol above the ground state structure, respectively. In these cases a hydrogen bond interaction between the proton of the amino group, more acidic due to its coordination to Cu^+, and the oxygen of the carbonyl group is observed.

Other important structures are those in which the oxygen of the carbonyl group and the aromatic ring interact with the metal cation (**Cu^+-Phe3** and **Cu^+-Tyr3**). In these cases, a strong hydrogen bond between the proton of the hydroxyl group and the nitrogen of the amine of the most stable form of the amino acid in gas phase is observed. All attempts to optimize a structure in which the **π** system and both oxygens of the carboxylic group were coordinated to the metal collapsed to forms "3".

Cu^+-Phe5 and **Cu^+-Tyr5** present similar metal cation coordination than **Cu^+-Phe1** and **Cu^+-Tyr1** but without the interaction between the metal cation and the **π** system of the side chain. This mode of coordination is the most stable found for Cu^+-Gly.[93, 112] The fact

that **Cu^+-Phe5** and **Cu^+-Tyr5** are 6.7 and 6.9 kcal/mol less stable than their respective ground states conformers suggests that the additional stabilization conferred by the aromatic side chains interacting with the metal cation is around 7 kcal/mol. Since Cu-N and Cu-O distances are longer in forms "1" than in forms "5" this value is probably a lower limit.

Cu^+-Phe7, **Cu^+-Tyr7**, **Cu^+-Phe8** and **Cu^+-Tyr8** correspond to the zwitterionic form interacting with Cu^+. In forms "7" the metal cation is bound both to one oxygen of the carboxylate and to the π system, whereas in forms "8" the metal is only unsymmetrically coordinated to the carboxylate group. According to the relative energies of these pairs of structures it can be anew observed that coordinating to the π system confers an additional stabilization of about 5-6 kcal/mol.

It is interesting to pay attention to the energy difference between neutral and zwitterionic structures. It is well known that the zwitterionic form of glycine does not exist in gas phase.[255] However, zwitterionic forms can be stabilized by the presence of any metal cation, the higher the charge of the cation is, the more stabilized is the zwitterionic form.[102, 112, 113, 256] Thus, the energy difference between neutral and zwitterionic species may be influenced by the coordination environment of the metal cation. For instance, results for forms "3" and "7", for which Cu^+ interacts also with the side chain, show that the neutral structures (**Cu^+-Phe3** and **Cu^+-Tyr3**) are 5.2 kcal/mol more stable than the zwitterionic forms (**Cu^+-Phe7** and **Cu^+-Tyr7**). This is different to what was observed for Cu^+-Gly,[112] for which the zwitterionic form was found to be more stable by 1.6 kcal/mol and can be attributed to the screening effect that the side chains exerts on the metal cation.

4.3.2.2 Cu^+-Trp

Figure 4.5 shows the B3LYP-optimized geometries of the different conformers along with the relative potential energies with the ZPE values and Table 4.3 summarizes the ΔU_0, ΔH^0_{298} and ΔG^0_{298} values of the isomers found. It can be observed that the coordination modes of the four most stable conformers are analogous to those obtained for Cu^+-Phe and Cu^+-Tyr, the ground state conformer being **Cu^+-Trp1**, where the coordinating groups are the amino nitrogen, the carbonyl oxygen and the π system. **Cu^+-Trp1** is followed by the **Cu^+-Trp2** and **Cu^+-Trp3** conformers (0.3 and 5.3kcal/mol above the former structure). It should be noted that when entropic effects at 298K are included, **Cu^+-Trp2**, N/ring biccordinated, becomes the most stable structure by 0.4 kcal/mol. On the other hand, it can be observed that for all conformers in which the π system is involved

in the coordination, the metal cation prefers to coordinate to the six member ring than to the five member ring of the indole group. This fact was observed in other works and was attributed to the larger electrostatic potential in the six-membered ring,[228] and also because it implies a smaller deformation energy of the amino acid.

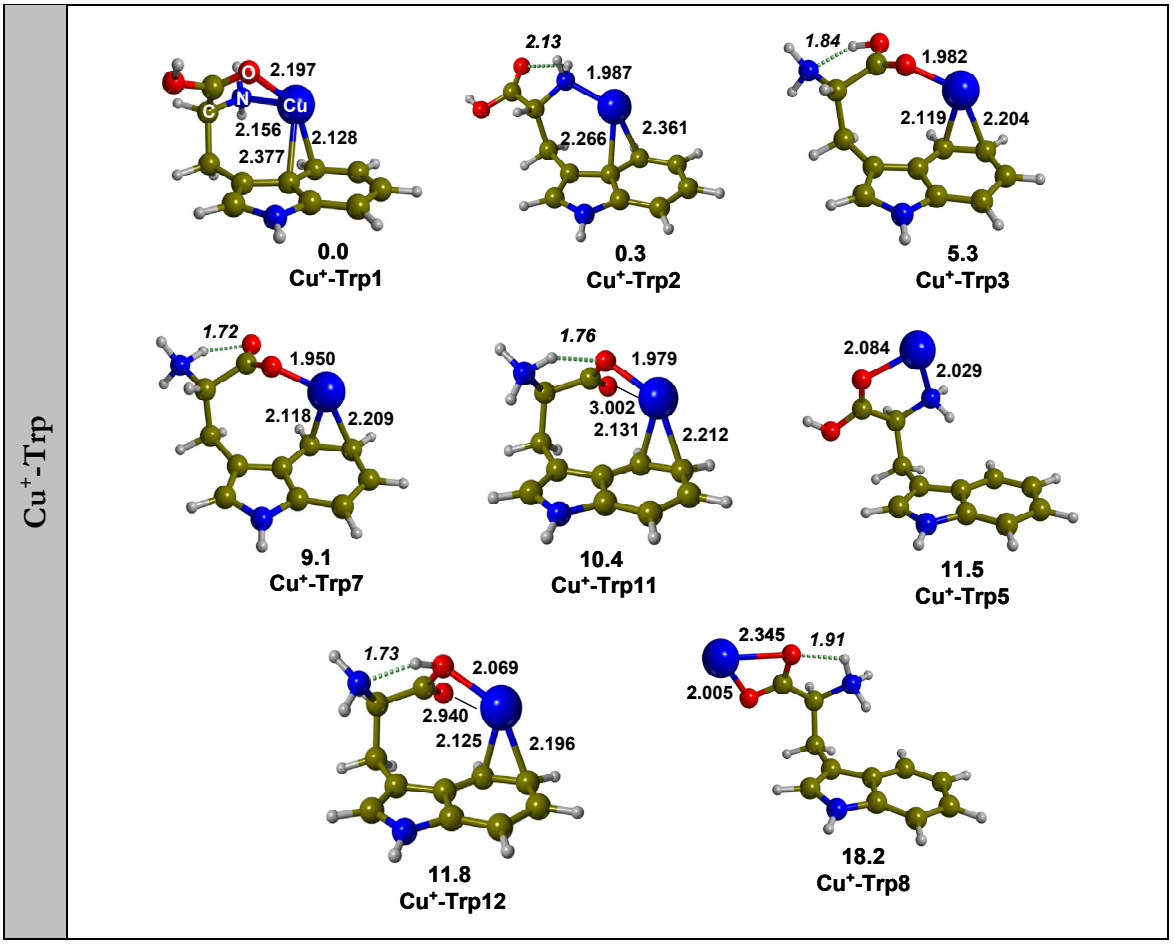

Figure 4.5 B3LYP-optimized geometries of the Cu^+-Trp isomers. Relative potential energies including the ZPE values, in kcal/mol. Distances in Å.

Table 4.3 Relative potential energies including ZPE values (ΔU_0), relative enthalpies (ΔH^0_{298}) and relative free Gibbs energies (ΔG^0_{298}) of the isomers presented for the Cu^+-Trp system. In kcal/mol.

structure	coordination	ΔU_0	ΔH^0_{298}	ΔG^0_{298}
Cu^+-Trp1	(N/O/ring)	0.0	0.0	0.0
Cu^+-Trp2	(N/ring)	0.3	0.4	-0.4
Cu^+-Trp3	(O/ring)	5.3	5.3	5.1
Cu^+-Trp7	$(O^-/ring)_{zwit}$	9.1	9.0	9.0
Cu^+-Trp11	$(O^-/ring)_{zwit}$	10.4	10.3	10.7
Cu^+-Trp5	(O/N)	11.5	11.6	10.4
Cu^+-Trp12	(OH/ring)	11.8	11.7	12.1
Cu^+-Trp8	$(O^-/O^-)_{zwit}$	18.2	18.5	16.0

The energy difference between **Cu^+-Trp5**, N/O coordinated, and **Cu^+-Trp1**, N/O/ring coordinated, is 11.5 kcal/mol. As mentioned, this value can be considered as a qualitative measure of the additional stabilization that the side chain confers when it coordinates to the metal cation. This value is larger than that obtained for the Cu^+-Phe and Cu^+-Tyr systems (~7 kcal/mol), which suggests that the interaction between Cu^+ and indole is more stabilizing than that with phenyl and phenol groups.

In addition to the zwitterionic **Cu^+-Trp7** and **Cu^+-Trp8** forms, also found in Cu^+-Phe and Cu^+-Tyr systems, another zwitterionic form has been located: **Cu^+-Trp11**. This structure is similar to **Cu^+-Trp7**, in which the metal cation interacts with the aromatic system and with the carboxylate group unsymmetrically, but now the shortest Cu^+-O distance correspond to the oxygen that is acting as proton acceptor in the intramolecular hydrogen bond with $-NH_3^+$. The neutral/zwitterionic pair **Cu^+-Trp7**/**Cu^+-Trp3** follows the same trend found for Cu^+-Phe and Cu^+-Tyr; that is, the neutral form is more stable due to the screening of Cu^+ by the side chain. However, for the **Cu^+-Trp12**/**Cu^+-Trp11** pair, the neutral form system is less stable than the zwitterionic form (even though there is also a screening effect by the side chain) because now the metal cation coordinates to the hydroxyl group.

4.3.2.3 Cu^+-His

Figure 4.6 shows the most significant optimized parameters of Cu^+-His conformers with its relative potential energies including the ZPE values and Table 4.4 summarizes the ΔU_0, ΔH^0_{298} and ΔG^0_{298} values of the isomers found. His presents a very rich coordination chemistry due to its potential binding sites, which are: i) the amino and carboxylic groups, ii) the π system and iii) either the Nδ or Nε of the imidazole ring (see Figure 4.1). In the gas phase the Nε-tautomeric form was the most stable one.[225] However, both from experimental (Cu^{2+} in solution)[257, 258] and theoretical points of view (Na^+ and Ag^+),[76, 84, 114] the most stable structure of His has the Nδ unprotonated available for coordinating the metal cation. Thus, we have considered the interaction of the two tautomers of His to the metal cation.

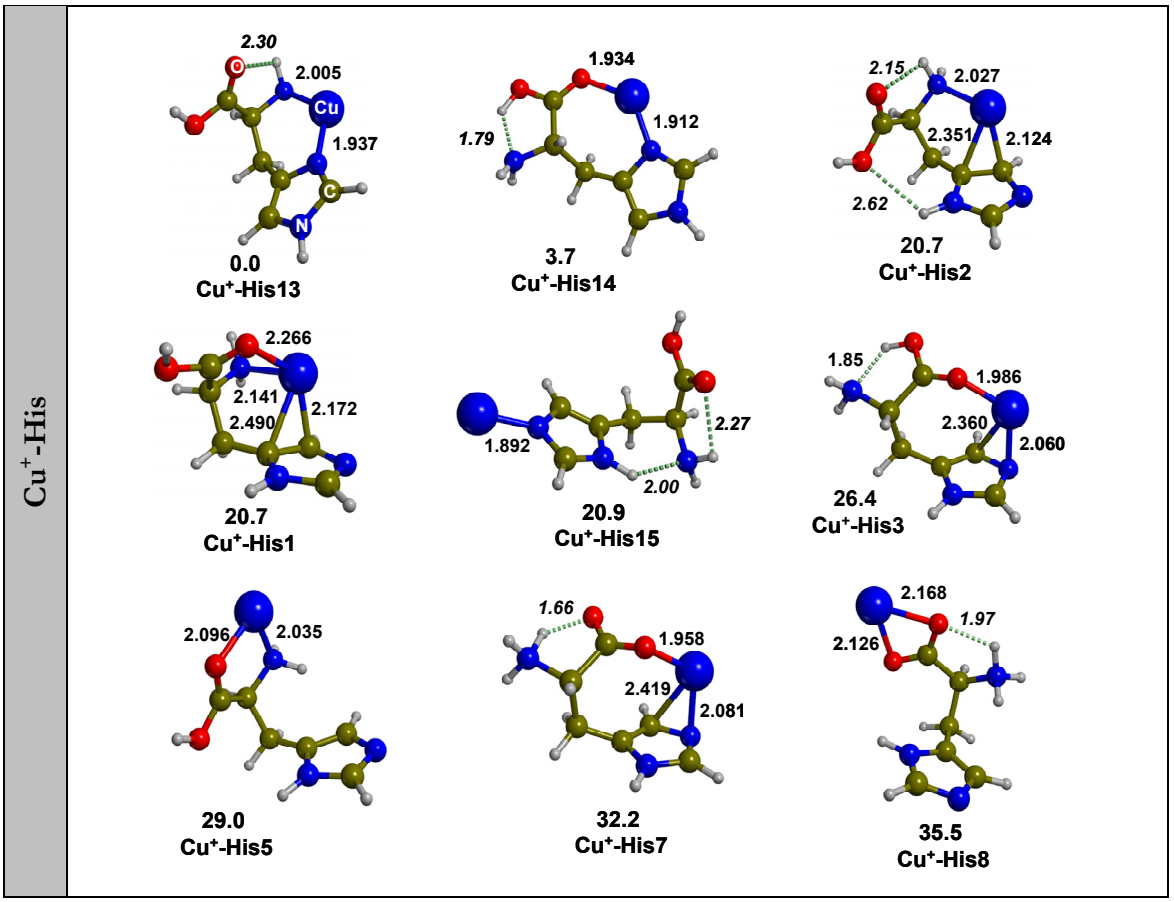

Figure 4.6 B3LYP-optimized geometries of the Cu^+-His isomers. Relative potential energies including the ZPE values, in kcal/mol. Distances in Å.

Table 4.4 Relative potential energies including ZPE values (ΔU_0), relative enthalpies (ΔH^0_{298}) and relative free Gibbs energies (ΔG^0_{298}) of the isomers presented for the Cu^+-His system. In kcal/mol.

structure	coordination	ΔU_0	ΔH^0_{298}	ΔG^0_{298}
Cu^+-His13	(N/Nδ)	0.0	0.0	0.0
Cu^+-His14	(O/Nδ)	3.7	3.7	4.2
Cu^+-His2	(N/ring)	20.7	20.7	21.1
Cu^+-His1	(N/O/ring)	20.7	20.8	21.1
Cu^+-His15	(Nε)	20.9	21.1	20.3
Cu^+-His3	(O/ring)	26.4	26.6	26.2
Cu^+-His5	(N/O)	29.0	29.1	28.5
Cu^+-His7	$(O^-/ring)_{zwit}$	32.2	32.3	32.5
Cu^+-His8	$(O^-/O^-)_{zwit}$	35.5	35.9	34.6

It can be observed in Figure 4.6 that, as for [Cu^{2+}-His_n] species in solution[257, 258] as well as Na^+-His[84] and Ag^+-His[76] the most stable structure (**Cu^+-His13**) corresponds to the interaction of Cu^+ with His(δ), that is, the metal cation interacts with Nδ and the NH_2 group. Next in energy, 3.7 kcal/mol above, we have located another conformer in which the metal cation also coordinates to Nδ and to the carbonyl oxygen. The remaining structures are all more than 20 kcal/mol higher in energy than the ground state structure and arise from the interaction of Cu^+ to the other tautomer of histidine, His(ε). These structures are less stable because now the N available for coordination in the imidazole ring is Nε, which does not permit a simultaneous interaction of the metal cation with this site and the NH_2 or COOH of the backbone. Among these conformers, the first two (**Cu^{2+}-His1** and **Cu^{2+}-His2**) present cation-π interactions (in addition to NH_2 and CO binding) and lie 20.7 kcal/mol above the ground state. In particular, in **Cu^+-His1**, the coordination to Cu^+ is through the NH_2, the CO, and the aromatic ring; that is, analogous to the most stable isomers of Cu^+-Phe, Cu^+-Tyr and Cu^+-Trp. In the remaining conformers, the metal cation is either monocoordinated through the imidazole Nε, presents cation-π interactions with the ring or does not interact with the side chain.

It should be mentioned that the zwitterionic forms have only been located when Cu^+ interacts with His(ε). For Cu^+ interacting with His(δ) all attempts have collapsed to the neutral form (**Cu^+-His14**). This is not surprising considering that in these cases the metal cation is largely screened by the coordination of Nδ and thus, the zwitterionic form is less stabilized.

4.3.2.4 Binding energies of Cu^+-AA_{arom}

The computed D_e, D_0, ΔH^0_{298} and ΔG^0_{298} values for the lowest energy structure of Cu^+-AA_{arom} are given in Table 4.5.

Table 4.5 Binding energies (D_e, D_0, ΔH^0_{298} and ΔG^0_{298}) of Cu^+-AA_{arom}, in kcal/mol. In parenthesis counterpoise corrected values.

		D_e	D_0	ΔH^0_{298}	ΔG^0_{298}
Phe	B3LYP	84.8 (82.9)	83.5 (81.6)	84.0 (82.1)	74.4 (72.3)
	CCSD(T)	84.2			
Tyr	B3LYP	85.6 (83.6)	84.2 (82.4)	84.8 (82.8)	75.1 (73.1)
	CCSD(T)	85.2			
Trp	B3LYP	91.1 (89.1)	89.7 (87.7)	90.3 (88.3)	80.3 (78.3)
His	B3LYP	100.6 (98.9)	98.8 (97.1)	99.3 (97.6)	90.8 (89.1)
	CCSD(T)	97.7			

According to these values, the order of Cu^+ affinity is: His > Trp > Tyr ≈ Phe. The strongest binding is given by His due to the fact that the interaction of the side chain with the metal cation takes place through the Nδ imidazole, which is highly stabilizing, and not through the π system of the aromatic ring, as for Trp, Tyr and Phe. In these three latter cases the interaction of Cu^+ with the π system determines the order of the binding energies. Note that by comparing the energy difference between structures "5" and "1" (see Figure 4.3 and Figure 4.5) one can estimate the degree of stabilization that the π-coordinating side chain confers to the complex. The order of π stabilization (in kcal/mol) is: Trp (11.5) > Tyr (6.9) ≈ Phe (6.7), which is similar for naked Cu^+ cation interacting with the bare rings (indole, phenol and benzene). Other experimental and theoretical studies with alkali metal cations interacting with aromatic amino acids also agree with the trend M^+-Trp > M^+-Tyr ≈ M^+-Phe.[81-84, 105]

The computed order for the Cu^+ affinity is also in agreement with the experimental data which determine the Cu^+ affinity of His, Trp, and Tyr to be 5.4, 3.4 and 0.3 kcal/mol higher than that of Phe.[89] However, the computed energy differences at 298K and considering the counterpoise correction, 15.5, 6.2 and 0.7 kcal/mol, are larger than those determined experimentally, especially for His. At the CCSD(T) level the Cu^+ affinity of His is 13.5 kcal/mol larger than that of Phe, which seems to confirm the B3LYP results. The larger affinity of His compared to other amino acids is attributed to its different interaction with the side chain since it does not interact with the π system but with the imidazole N. On the other hand, as found for many other ligands,[101] Cu^+ affinities to aromatic amino acids are much larger than those of alkali metal ions, which are 48-52 kcal/mol for Na^+ or 35-38 kcal/mol K^+ interacting with Phe, Tyr and Trp.[105]

4.3.2.5 Vibrational features of the computed infrared spectra

As mentioned, IRMPD spectroscopy has been employed to obtain binding information on singly charged metal ions to phenylalanine and tryptophan.[123, 124, 246] Metal ions considered up to now are alkaline cations and Ag^+ and Zn^{2+} transition metal ions. In all cases the spectra are consistent with a charge solvation structure and rule out the presence of the salt bridge tautomer. However, the spectra obtained for transition metals show significant differences from that of alkaline ones. Thus, it is interesting to provide and discuss the computed IR spectra of the most stable structures of Cu^+ interacting with Phe and His. The vibrational frequencies have been scaled by the factor of 0.96.[259, 260] IR spectra corresponding to the three most stable structures of Cu^+-Phe are shown in Figure 4.7. These structures correspond to **Cu^+-Phe1** (tricoordinated N/O/ring), **Cu^+-Phe2** (bicoordinated N/ring) and **Cu^+-Phe3** (bicoordinated O/ring). According to Table 4.2 the relative energies including zero point energy are 0.0, 1.1 and 3.9 kcal/mol, respectively. However, if entropic effects are considered at 298 K, relative Gibbs free energies are 0.0, 0.3 and 3.8 kcal/mol, respectively; that is, the tricoordinated N/O/ring and the bicoordinated N/ring become almost degenerate. This last structure, not considered in previous works, seems relevant for Cu^+ complexes and presents some spectroscopic differences with respect to the other two coordinations.

The most important features observed in these three spectra are:

i) Coordination to the carbonylic oxygen induces a red shift of 80 and 103 cm^{-1} in structures **Cu^+-Phe1** (tricoordinated N/O/ring) and **Cu^+-Phe3** (bicoordinated O/ring), leading to an intense C=O stretching band at 1682 cm^{-1} and 1659 cm^{-1}, respectively.

ii) There is an intense peak at 1400 cm^{-1} in **Cu^+-Phe3** (bicoordinated O/ring) spectra that mainly corresponds to the in plane COH bending. This peak decreases in intensity for the other two **Cu^+-Phe1** (N/O/ring) **Cu^+-Phe2** (N/ring) structures.

iii) There is a moderate peak at 1150 cm^{-1} in the **Cu^+-Phe1** (N/O/ring) spectra that corresponds to OH bending + NH_2 wagging. This peak increases significantly in **Cu^+-Phe2** (N/ring), and can be used as a diagnostic N binding vibration to identify this kind of coordination. Moreover, the fact that the C=O stretching in **Cu^+-Phe2** (N/ring), is not red-shifted can further confirm that CO is not involved in the binding to Cu^+.

iv) Both for **Cu^+-Phe1** and **Cu^+-Phe2** there is a peak of moderate intensity at 617 and 594 cm^{-1}, respectively, that corresponds to an out of plane COH bending. In contrast, for **Cu^+-Phe3** this peak decreases in intensity and is shifted to higher energies (949 cm^{-1}) owing to the OH···NH_2 intramolecular hydrogen bond. This can be used to further confirm that NH_2 group is not interacting with the metal cation but, instead is involved in a hydrogen bond with OH.

In summary, for **Cu^+-Phe1** and **Cu^+-Phe3** we find the same vibrational features than those observed in previous studies for alkaline and Ag^+ cations in which the authors beautifully pointed out that the (N/O/ring) and (O/ring) conformers could be easily distinguished based on diagnostic vibrations at ~ 1150 (N/O/ring) and 1400 (O/ring) cm^{-1}, respectively.[123, 124] In this context it is worth to note that a third relevant N/ring conformer, at least for transition metal cations such as Cu^+, but not for alkaline ones, could be distinguished by noting that the band at 1150 cm^{-1} becomes more intense and the CO stretching frequency becomes almost unshifted.

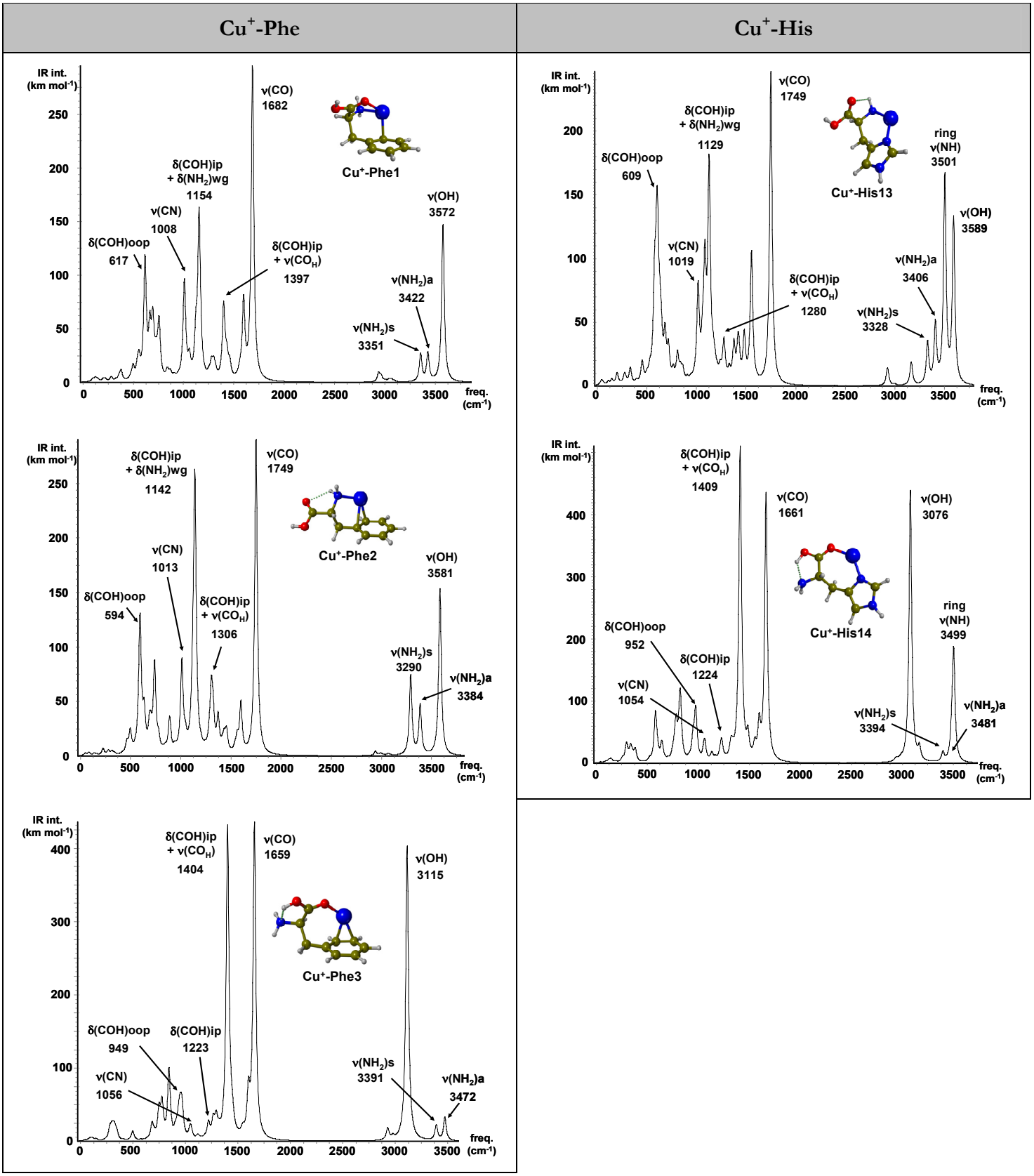

Figure 4.7 Calculated infrared spectra for charge solvated structures of Cu^+-Phe1 (N/O/ring), Cu^+-Phe2 (N/ring), Cu^+-Phe3 (O/ring), Cu^+-His13 (N/Nδ) and Cu^+-His14 (O/Nδ).

In addition to Cu^+-Phe, the spectra of **Cu^+-His13** (bicoordinated N/Nδ) and **Cu^+-His14** (bicoordinated O/Nδ) are also presented (see Figure 4.7) since the low-lying of Cu^+-His structures are significantly different from those of the other aromatic amino acids. Becasue relative Gibbs free energy at 298 K of **Cu^+-His14** with respect to **Cu^+-His13** is 4.2 kcal/mol, the former isomer is the most likely structure to be found in the gas phase. Similar features to those previously mentioned for Cu^+-Phe are observed. For N/Nδ coordination there is a quite intense band at 1130 cm^{-1} corresponding to in-plane COH bending + NH_2 wagging and the CO stretching frequency is unshifted. However, for the O/Nδ isomer an intense band at 1409 cm^{-1} corresponding to the in-plane COH bending is observed and the CO stretching frequency is shifted by 87 cm^{-1}. Thus, coordination of the ring through the Nδ instead of the π system does not seem to modify significantly the diagnostic bands. For the out-of-plane COH bending is observed that while in **Cu^+-His13** the band is at 609 cm^{-1}, for **Cu^+-His14** it is shifted to the higher value of 952 cm^{-1} showing the presence of the strong intramolecular $OH\cdots NH_2$ hydrogen bond, as was observed previously in Cu^+-Phe. Finally, further experiments on Cu^+-AA_{arom} to confirm low-lying Cu^+-N/ring coordinating structures would be desirable.

4.3.3 GAS PHASE REACTIVITY OF Cu^+-AA_{arom}

Once the possible isomers for the Cu^+-AA_{arom} systems have been computationally studied, the ground state conformer distinguished, and the nature of the bonding described, the next step to perform is to study the reactivity of such systems in gas phase in order to rationalize the metal induced activation as well as to examine the existing differences on reactivity when comparing with other amino acids or other metal cations.

4.3.3.1 Experimental reactivity

Collisional activation experiments were carried out on the Cu^+-AA_{arom} complexes at m/z = 228, 244, 267 and 218 u for Phe, Tyr, Trp and His amino acids, respectively. Low energy CID spectra have been recorded at different collision energies. Several new ions are observed on the collision spectra of each amino acid. Figure 4.8 shows the CID spectra recorded at collision energy of 20 eV. The breakdown graphs associated to the abundances of the various fragment ions relative to the parent as a function of the collision energy are also represented.

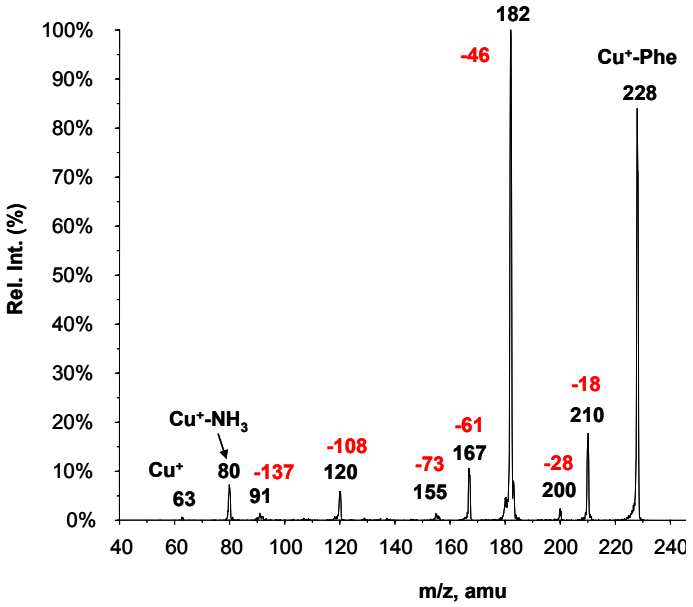
Rel. Int. (%)
m/z, amu
Cu⁺-Phe
228
182
-46
Cu⁺-NH3
Cu⁺
63
80
-137
91
-108
120
-73
155
-61
167
-28
200
-18
210

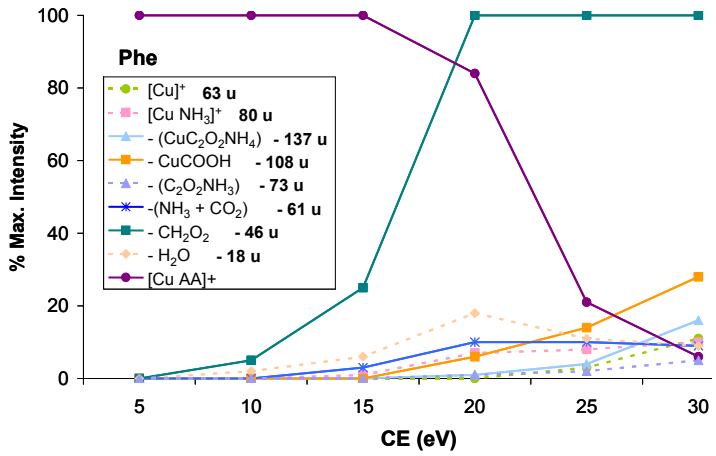
Phe
% Max. Intensity
CE (eV)
[Cu]⁺ 63 u
[Cu NH3]⁺ 80 u
- (CuC2O2NH4) - 137 u
- CuCOOH - 108 u
- (C2O2NH3) - 73 u
-(NH3 + CO2) - 61 u
- CH2O2 - 46 u
- H2O - 18 u
[Cu AA]+

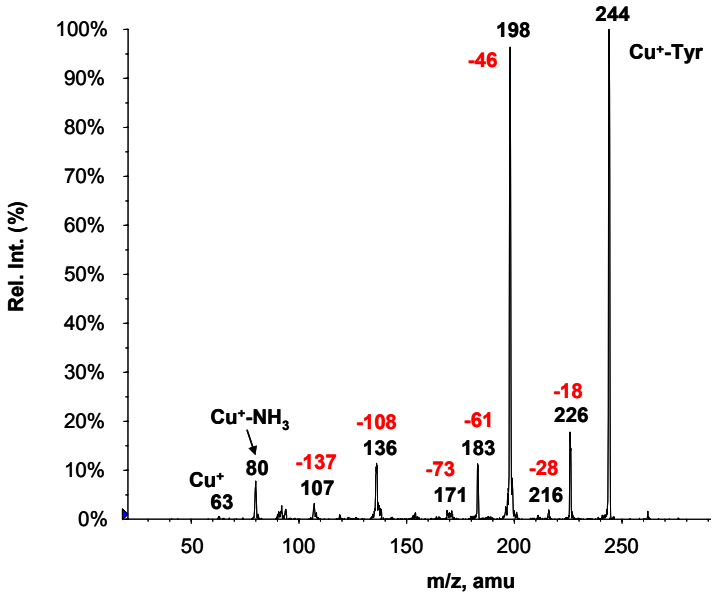
Rel. Int. (%)
m/z, amu
Cu⁺-Tyr
244
198
-46
Cu⁺-NH3
Cu⁺
63
80
-137
107
-108
136
-73
171
-61
183
-28
216
-18
226

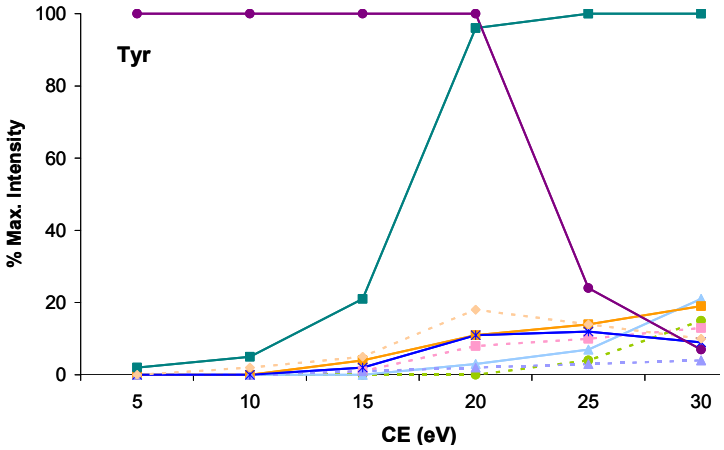
Tyr
% Max. Intensity
CE (eV)

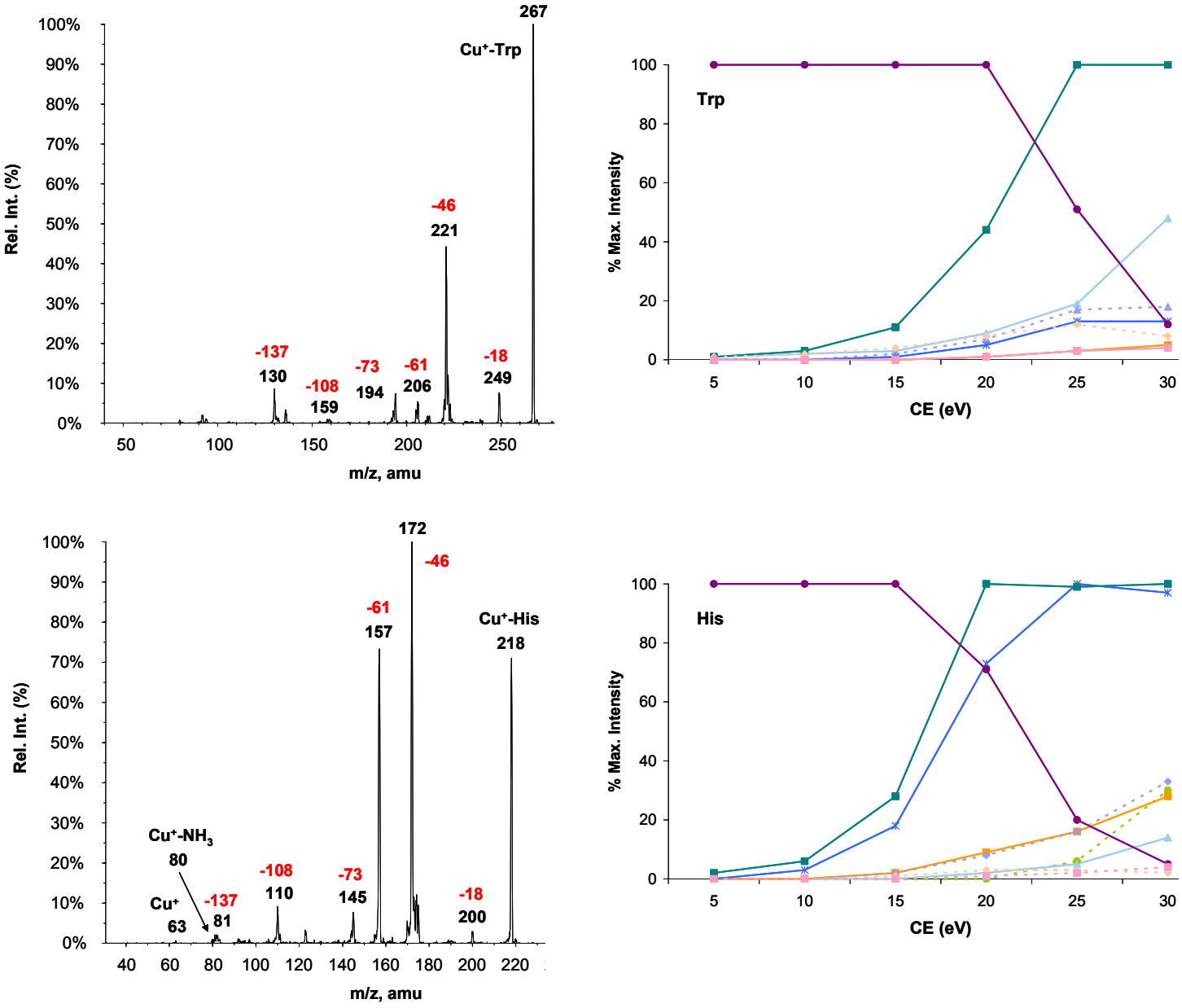

Figure 4.8 Left: fragmentation spectra of the corresponding parent Cu^+-AA_{arom} ions at collision energy of 20 eV (numbers in black belongs to the *m/z* fragment, in red the losses of mass). Right: relative abundances of the observed ions versus the collision energy.

It can be observed that most of the fragmentations are common for all systems. The loss of 46 u (CH_2O_2) is always the most important fragmentation and could come from the consecutive elimination of 18 u and 28 u, corresponding to the loss of H_2O and CO, respectively, since the peaks for the elimination of these fragments are also observed, although they disappear rapidly as the collision energy increases. The loss of 61 u belongs to the elimination of a fragment with a CO_2NH_3 composition, likely the consecutive elimination of NH_3 and CO_2 as proposed before for the Ag^+-Phe system.[68, 72] It should be

noted that in all cases this loss is a minor fragmentation of the complex except in the case of His where it is a major fragmentation channel at high collision energies (see Figure 4.8). Collision spectra also show the loss of 73 u corresponding to the elimination of a fragment with $C_2O_2NH_3$ composition. This elimination can result from the consecutive elimination of CH_2O_2 (the main fragmentation in all cases as noted above) and HCN, or the direct elimination of $C_2O_2NH_3$. The loss of 108 u is probably associated to the elimination of CuCOOH to give the NH_2CHR^+ imonium ion. Finally, for the elimination of 137 u different mechanisms could be accounted for, which can be either the direct loss of the $CuC_2O_2NH_4$ group or the consecutive elimination of CuCOOH and $NH{=}CH_2$. Calculations will help identify the most favourable mechanisms for these intriguing fragmentations.

Two other peaks can be also observed in the spectra. These are at m/z 63 (Cu^+) and m/z 80 (Cu^+-NH_3). It should be noted that at higher collision energies (not shown) only the peak corresponding to Cu^+ (m/z 63) rises in intensity, while the other ones decline. As pointed out Hopilliard et al.,[138] this is due to the fact that at high collision energies the direct dissociation becomes favoured over rearrangements involving one or several energy barriers. Therefore, the values of the binding energies of the Cu^+-AA_{arom} complexes (reported in Table 4.5) can be taken as an approximate limit to distinguish which processes can occur; i. e., transition or final states with energies above this limit will be considered as unfavourable.

4.3.3.2 Theoretical elucidation of the fragmentation mechanisms

The observed losses are very similar for all the aromatic systems and only differ in their relative intensities. Consequently, it seems that losses do not involve the breaking of the side chain of the amino acid. Therefore, we have selected only one of the considered systems, Cu^+-Phe, for the study of its PES (including the ZPE corrections) in order to rationalize the experimental findings by means of the B3LYP approach.

As it has been shown in section 4.3.2.1, the lowest energy structure of Cu^+-Phe is **Cu^+-Phe1**, which is a charge solvation tridentate form whose coordinating groups are the NH_2, the CO and the aromatic ring. This structure has been taken as reference for the calculations of the different mechanisms. The interaction energy for this system is 83.5 kcal/mol at the B3LYP level so that this value will be taken as the limit to consider if a process is favourable or not.

The initial steps for the metal-induced fragmentations of amino acids and peptides have been traditionally invoked to occur via the insertion of the metal cation into the bonds of the backbone of amino acids. These are the C_α-COOH, C_α-NH_2 or OC-OH insertions. However, since the structure that results upon complexation to the OH and NH_2 lies 16.4 kcal/mol above **Cu^+-Phe1** and that for Cu^+-Gly the OC-OH insertion was found to be less favourable than the C-COOH one, the OC-OH insertion has not been considered for the present case.

Loss of 46 u mechanisms

The composition associated with 46 u is CH_2O_2 and the corresponding ion resulting from this fragmentation is commonly observed both in cationized and protonated amino acids. Different mechanisms have been proposed in the literature that account for this fragmentation in cationized amino acids: consecutive loss of H_2O and CO, loss of formic acid (HCOOH), or consecutive loss of CO_2 and H_2, the former being generally accepted as the most probable mechanism.[136, 138] Because it was found that the elimination of CO_2 and H_2 has an activation barrier considerably higher than the other two channels,[138] the mechanisms have been focused on the elimination of HCOOH and H_2O+CO.

Figure 4.9 shows the mechanisms arising from the C_α-COOH metal cation insertion that leads to the elimination of 46 u. Such an insertion yields an intermediate (**CC46-1**) through the transition state **CC46-TS1**. The IRC calculation from this structure indicates that the transition state does not connect with the **Cu^+-Phe1** structure but with another isomer, **Cu^+-Phe6**, that is 8.4 kcal/mol higher in energy than the most stable one. Any attempt to locate a transition state for the C_α-COOH insertion connecting with **Cu^+-Phe1** collapsed to **CC46-TS1**. However, the interconversion barrier leading to **Cu^+-Phe6** (11.1 kcal/mol) is much lower than the other steps of the mechanism.

The intermediate **CC46-1** can evolve through two different pathways. The most energetic one proceeds via a hydrogen transfer from the amine group to the carbon of carboxylic group through a transition structure (**CC46-TS4**) whose energy barrier is 40.8 kcal/mol and producing an intermediate containing formic acid as a ligand (**CC46-7**), which is the most stable stationary point of the PES, -9.7 kcal/mol respect to **Cu^+-Phe1**. Detachment of formic acid leads to the loss of 46 u product, **CC46-8** located at 15.1 kcal/mol above **Cu^+-Phe1**. The second possible pathway proceeds via a hydrogen transfer from the amine group to the OH group of **CC46-1** resulting in the formation of **CC46-2**. This is a quite stable tricoordinated complex where the metal cation is

coordinated to CO, H_2O and to the aromatic ring. The fragmentation of **CC46-2** can produce the elimination of one or two of these ligands. Elimination of H_2O via **CC46-TS3** produces the **CC46-3** intermediate (5.9 kcal/mol above **Cu^+-Phe1**), while direct elimination of CO leads to **CC46-5** being 22.8 kcal/mol above **Cu^+-Phe1**. Finally, loss of CO from **CC46-3** leads to **CC46-4** (Cu^+RCH=NH), which is 42.0 kcal/mol higher in energy than **Cu^+-Phe1**.

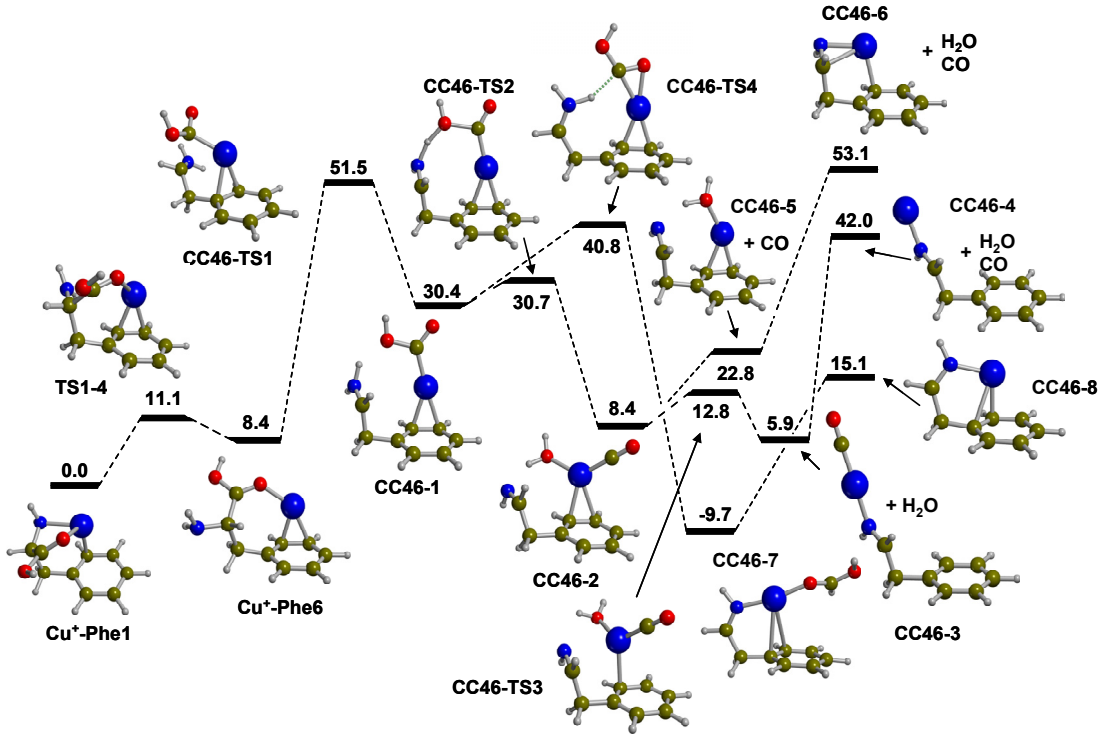

Figure 4.9 Potential energy profiles including the ZPE corrections for the loss of 46 u starting with the Cu^+ insertion into the C_α-COOH bond

The limiting step of both mentioned pathways, elimination of HCOOH and consecutive elimination of H_2O and CO, is the metal cation insertion to produce **CC46-1** (51.5 kcal/mol) in such a way that the following steps after the insertion will have enough internal energy to decompose directly to the final products in agreement with the rapid extinction of the peaks corresponding to the loss of CO and H_2O. Since the C_α-COOH insertion barrier is the highest one, both paths are energetically viable for the elimination of mass 46.

Elimination of CH_2O_2 can also be achieved through another mechanism without any metal insertion. In this case a hydrogen transfer from the amine to the OH group of **Cu^+-Phe2** (after rotation of the C_α-COOH bond to reach **Cu^+-Phe4**) leads to the direct

elimination of H_2O and CO. The barrier for this fragmentation is 57.8 kcal/mol, a value significantly higher than those involved in the C_α-COOH insertion mechanism. Thus, this mechanism can be discarded.

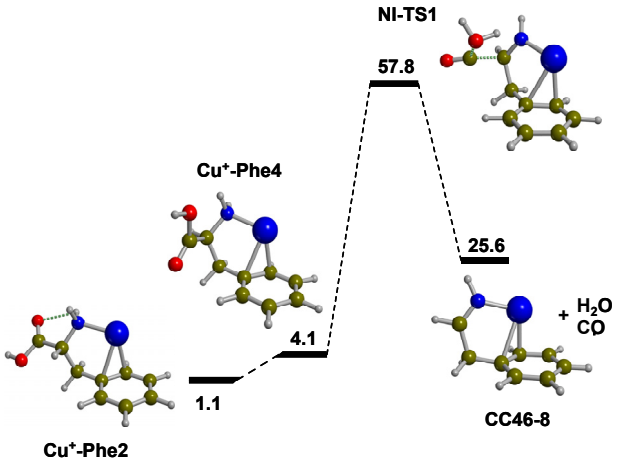

Figure 4.10 Potential energy profile including the ZPE values for the loss of 46 u via non-insertion metal mechanism.

Loss of 108 u mechanism

The mass of 108 u belongs to the CuCOOH fragment that leads to the formation of the immonium ion NH_2CHR^+. The mechanism associated to the formation of this product ion is shown in Figure 4.11 and, similar to the loss of 46 u, starts with the insertion of the metal cation into the backbone C_α-COOH. The direct loss of CuCOOH from **CC46-1** yields to the immonium ion **[I-1]**$^+$.

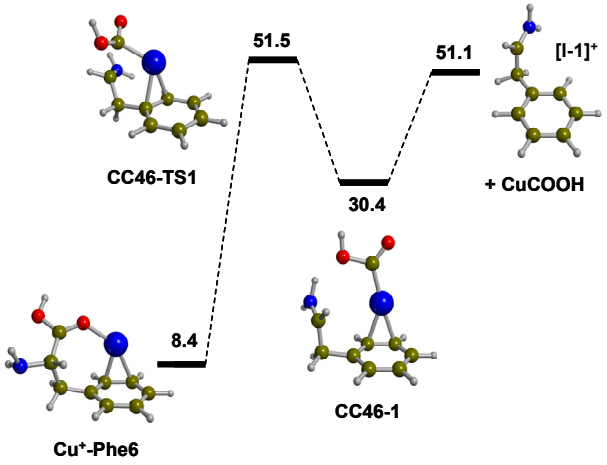

Figure 4.11 Potential energy profile with the ZPE corrections for the loss of 108 u.

The energy barrier of the limiting step in this mechanism (51.5 kcal/mol) is the same than that of the loss of 46 u mechanism. However, Figure 4.8 shows very different intensities for the peaks corresponding to these losses. This is probably due to the fact that for the loss of 108 the energy of the asymptote is of the same order than the C_α-COOH insertion barrier, in contrast to the loss of 46 for which the asymptote is much lower in energy (42.0 kcal/mol).

Loss of 137 u mechanisms

This fragmentation corresponds to the loss of a fragment with a $CuC_2O_2NH_4$ composition and two possibilities have been explored for this reaction. The first possibility implies a consecutive elimination of CuCOOH and $NH{=}CH_2$. The elimination of $NH{=}CH_2$ from **[I-1]$^+$**, which is the product ion after losing CuCOOH (Figure 4.11), is more than 140 kcal/mol above **Cu$^+$-Phe1**, enormously higher than the dissociation energy of Cu^+-Phe so that this pathway can be discarded.

The second possibility is the direct elimination of the $COOHCHNH_2Cu$ fragment (Figure 4.12). This mechanism starts with the insertion of the metal cation into the C_α-R bond leading to the **CR137-1** complex with an energy barrier of 45.3 kcal/mol. The decomposition of **CR137-1** directly leads to $COOHCHNH_2Cu$ + **[I-2]$^+$** asymptote. The energy of this asymptote is 83.4 kcal/mol above the most stable isomer, very similar to the binding energy of Cu^+-Phe (83.5 kcal/mol). This fact agrees with the experimental observations because both peaks of 63 u (Cu^+) and loss of 137 u appear at high collision energies (about 25 eV). In addition, it can also be observed that the intensity of the loss of 137 u is higher in the case of Cu^+-Trp than in the other amino acids. This is probably due to the presence of a second aromatic ring in the side chain of Trp, which can delocalize more efficiently the positive charge located in the eliminated side chain **[I-2]$^+$**.

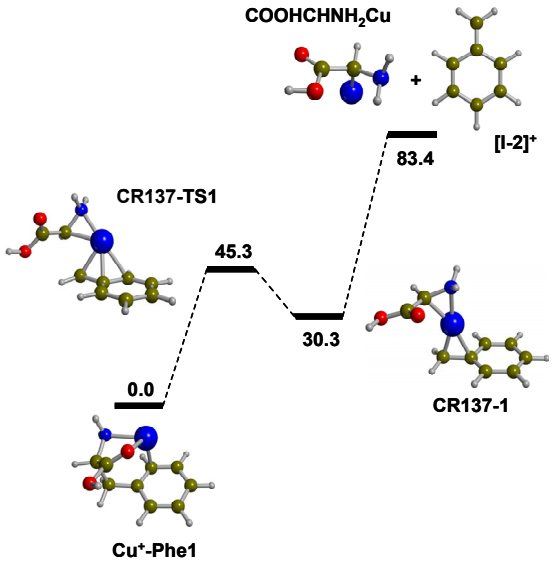

Figure 4.12 Potential energy profile including the ZPE values for the loss of 137 u.

Loss of 73 u mechanisms

The neutral moiety for this fragmentation corresponds to a composition of $C_2O_2NH_3$. The loss of this fragment can occur through two different ways. In the first case, the product ion from the initial loss of 46 u could eliminate HCN. However, the energy barriers associated to these mechanisms are always larger than 114 kcal/mol and thus, they would not occur.

Another more probable path is the loss of the NH=CH-COOH fragment. This elimination starts from the Cu^+ inserted intermediate **CR137-1**, which can evolve through two different paths depending on the proton transfer that takes place: i) hydrogen transfer from NH_2 group to the CH_2 group of R, or ii) hydrogen transfer from COOH group to CH_2 group of R. In the first case, a previous rotation of the Cu-CN bond should be required to facilitate the proton transfer. Unfortunately, all attempts to find a transition state corresponding to this step failed, and thus, it is assumed that this process cannot proceed. In the second case (shown in Figure 4.13) the hydrogen transfer in **CR137-1** leads to a high stable complex **CR73-2**, through a barrier of 76.7 kcal/mol. This is a complex where the cation is bound to the aromatic ring and to one oxygen of the CO_2CHNH_2 moiety. The direct decomposition of this complex would lead to **CR73-3** + $^+NH_2CHCO_2^-$ but such zwitterionic structure is unstable in gas phase and very likely it rearranges during the disscociation process to lead **CR73-3** + NH=CH-COOH. This final asymptote is 43.6 kcal/mol with regard to **Cu^+-Phe1**.

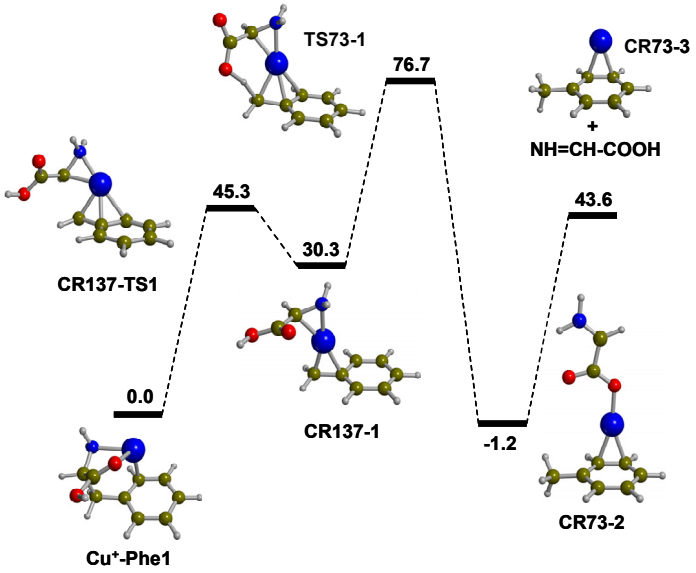

Figure 4.13 Potential energy profile with the ZPE values for the loss of 73 u.

The limiting step of the calculated process has a barrier of 76.7 kcal/mol, higher than the loss of 46 u mechanism, and therefore in agreement with the intensities of the spectra.

Loss of 61 u mechanisms

This loss must correspond to the elimination of NH_3 and CO_2. The optimal starting structure for such fragmentation appears to be the zwitterionic one because the NH_3 and CO_2 groups are already formed. Consequently, **Cu^+-Phe1** should evolve to **Cu^+-Phe7** (its zwitterionic form) through several steps, represented in Figure 4.14, whose highest barrier is around 21 kcal/mol. Interestingly, the **TS3-7** structure has a transition state character only on the electronic PES because **Cu^+-Phe7** becomes higher in energy after adding the ZPE corrections. The elimination from **Cu^+-Phe7** starts with the metal cation insertion into the C_α-COOH bond leading to **CC61-1** with a barrier of 44.7 kcal/mol above **Cu^+-Phe1**. Two different pathways can occur from this intermediate (Figure 4.14). The first one implies a direct and consecutive elimination of CO_2 and NH_3 that leads to an asymptote of 59.8 kcal/mol above **Cu^+-Phe1**. The second pathway leads to **CC61-2** through a transition state, **CC61-TS2**, which is 36.8 kcal/mol above the most stable conformer. **CC61-2** can lose CO_2 without reverse activation barrier yielding **CC61-3** (15.3 kcal/mol less stable than **Cu^+-Phe1)**. Via a three-member ring opening of **CC61-3** with an activation barrier of 8.6 kcal/mol respect to **CC61-3,** the **CC61-4** + CO_2 fragments are obtained. Fragmentation of **CC61-4** can take place through the elimination of NH_3 leading to **CC61-6** + CO_2 + NH_3

(26.8 kcal/mol higher than the energy of the ground state structure), or through the elimination of **CC61-5** leading to NH_3Cu^+ + **CC61-5** + CO_2, 1.5 kcal/mol more stable than the previous asymptote.

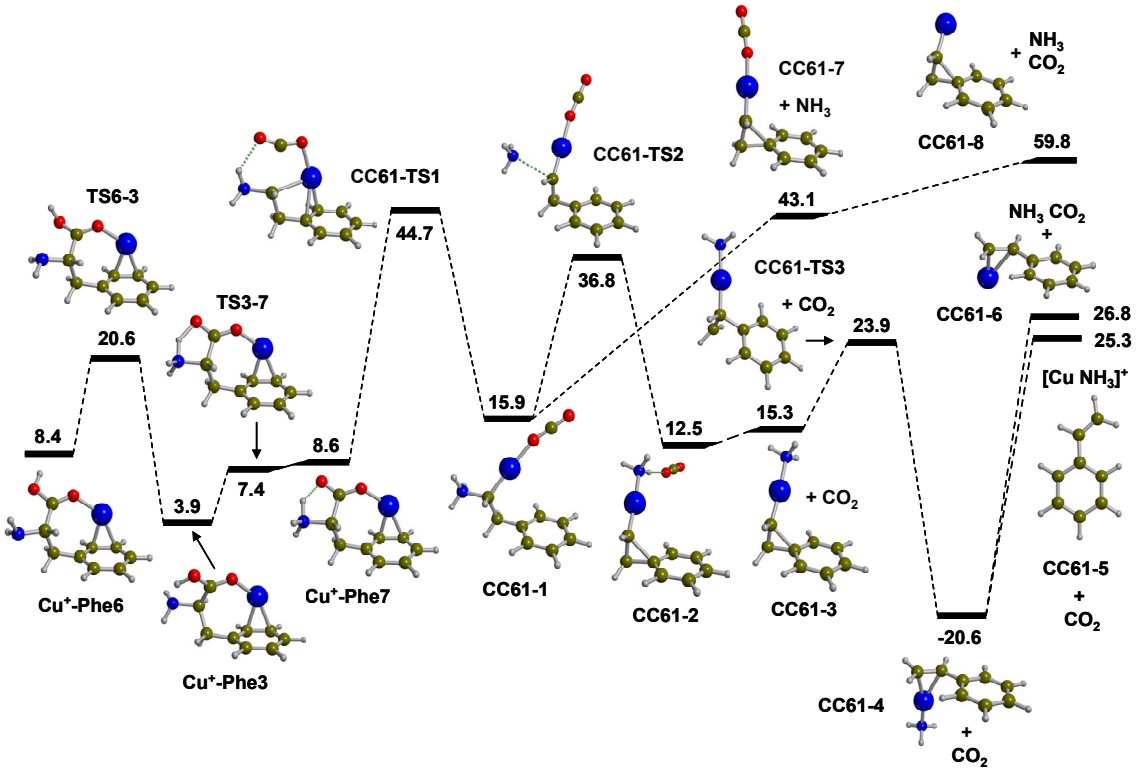

Figure 4.14 Potential energy profile including the ZPE values for the loss of 61 u.

Comparing both highest energy barriers it seems clear that the second elimination channel would be the preferred mechanism. However, the step **CC61-1 → CC61-2** through the **CC61-TS2** transition state implies a very important reorientation of the NH_3 and CO_2 moieties. The excess of internal energy into the system would favour the direct cleavage of the C-NH_3 bond in **CC61-TS2** leading to **CC61-7**, which is 43.1 kcal/mol above **Cu^+-Phe1**. Further elimination of CO_2 yields **CC61-8** + CO_2 + NH_3, 59.8 kcal/mol higher in energy than the most stable complex. As a consequence, the limiting step in this mechanism has an energy barrier of 59.8 kcal/mol, much larger to that found in the case of the loss of 46 u, in agreement with the intensities found for both peaks in the CID spectra (see Figure 4.8).

Differences with Cu^+-His fragmentations

It is interesting to note that the peak corresponding to the elimination of NH_3 + CO_2 is always a minor fragmentation channel of the complexes except in the case of Cu^+-His, whose intensity is very similar to that for the loss of 46 u. As shown previously,

the differences of Cu^+-Phe, Cu^+-Tyr and Cu^+-Trp respect to Cu^+-His lie in the type of metal coordination of the ground state isomers (see Figure 4.3, Figure 4.5 and Figure 4.6). This different coordination of the metal cation in the case of Cu^+-His will probably induce differences in the reaction mechanisms for the observed fragmentations and therefore, differences in the intensities.

In that vein, the fragmentation mechanisms for the losses of 46 and 61 u have been computed and the profiles are shown in Figure 4.15 and Figure 4.16, respectively.

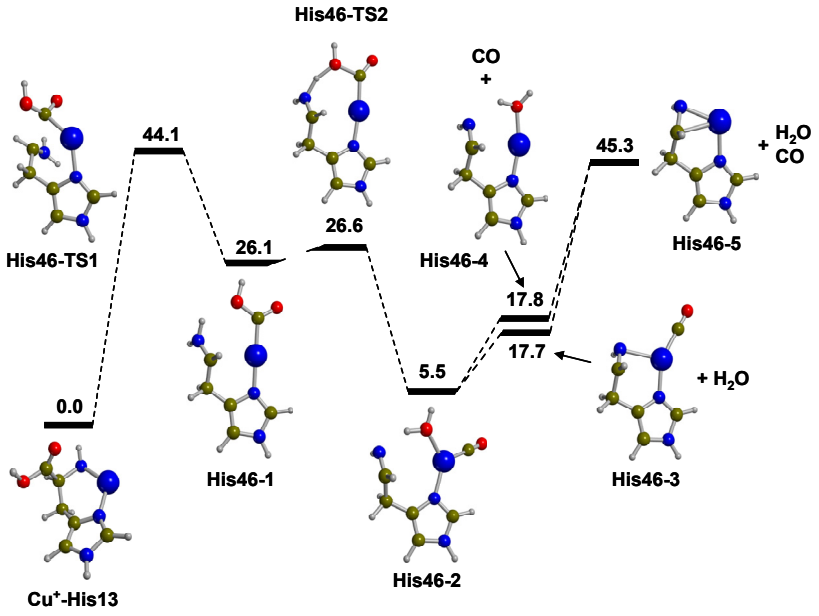

Figure 4.15 Potential energy profile with the ZPE corrections for the loss of 46 u for the Cu^+-His system.

The profile for the loss of 46 u and associated to the loss of $CO+H_2O$ is similar to the analogous for the Cu^+-Phe system. The fragmentation starts with a metal cation insertion into C_α-COOH bond through a barrier of 44.1 kcal/mol with respect to **Cu^+-His13** and is followed by a proton transfer from the NH_2 group to the OH one, giving rise to the **His46-2** intermediate. From this structure the losses of H_2O and CO are produced with a final asymptote lying 45.3 kcal/mol above the lowest energy isomer of Cu^+-His, which is the highest energy state of the profile.

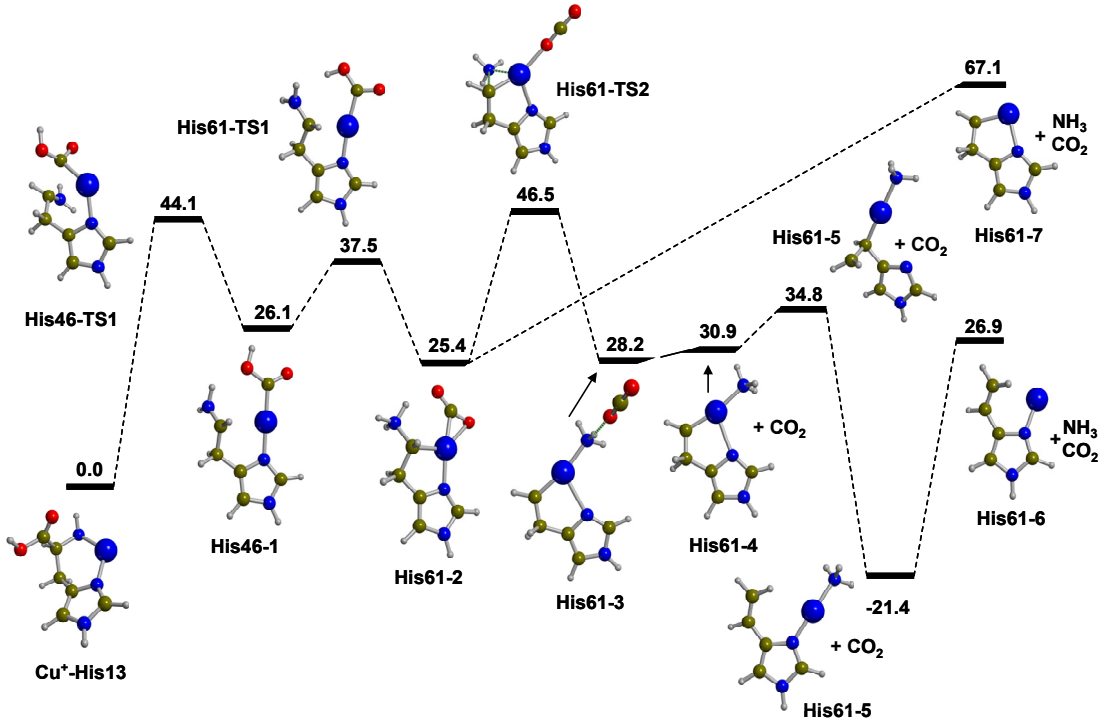

Figure 4.16 Potential energy profile including the ZPE values for the loss of 61 u for the Cu^+-His system.

Due to the lack of zwitterionic forms when Cu^+ coordinates to His(δ), the loss of 61 starts with the same insertion as for the loss of 46 u, that is, by producing the intermediate **His46-1**. In order to obtain a structure with the NH_3^+ and COO^- moieties, His46-1 evolves via proton transfer from OH to NH_2 yielding the **His61-2** intermediate. From **His61-2** two possible paths can take place: i) direct elimination of NH_3 and CO_2 to reach **His61-7**, which is 67.1 kcal/mol above **Cu^+-His13**, or ii) cleavage of the Cu-CO_2 bond and formation of the Cu-NH_3 one, giving rise to **His61-3**. Since this intermediate is analogous to **CC61-2**, the elimination of the NH_3+CO_2 through this path follows the same profile as in Cu^+-Phe system, the highest barrier lying 46.5 kcal/mol (**His61-TS2**) to the ground state isomer.

There is a crucial step when losing 61 u for both mechanisms of Cu^+-Phe and Cu^+-His that leads to two possible paths: a) direct loss of CO_2+NH_3 from **CC61-TS2** and **His61-TS2**, or b) intracomplex rearrangement leading to **CC61-2** and **His61-3**. Which path is favoured depends on the excess of internal energy transferred during collision into the systems. Thus, the different intensities for this loss of 61 u when comparing Cu^+-Phe and Cu^+-His systems could depend on this fact. An analysis of the transition structures **CC61-TS2** and **His61-TS2** provides an important clue related to which path is followed by these

two systems. Indeed, while the C-N and N-Cu bond distances in **CC61-TS2** are 2.78 and 2.95, respectively, for **His61-TS2** these values are 2.59 and 2.57, respectively (Figure 4.17). This subtle fact suggests that since the leaving NH_3 fragment is closer to the remaining ion in **His61-TS2** than in **CC61-TS2**, the direct cleavage of the C-NH_3 bond is more favourable than CO_2 elimination in Cu^+-Phe rather than in Cu^+-His. Accordingly, the activation barrier corresponding to the loss of 46 and 61 u for this latter case would be 44.1 and 46.5, respectively kcal/mol, two similar values that would explain the similar intensities observed in Cu^+-His. This explanation, which is based on energy barriers obtained by statical calculations, allows to rationalize the differences of intensities experimentally observed for the loss of 61 u. However, more rigorous explanations may be achieved by means of dynamic calculations. Indeed, through these theoretical techniques one can analyze in which degrees of freedom the energy transferred by the inert gas is accumulated. Accordingly, two different systems distribute differently the energy giving rise to different fragmentations and intensities. For the present case, since the ground state isomer of Cu^+-His differs to the remaining systems, one should expect different energy distribution and thus, different intensities for a same elimination.

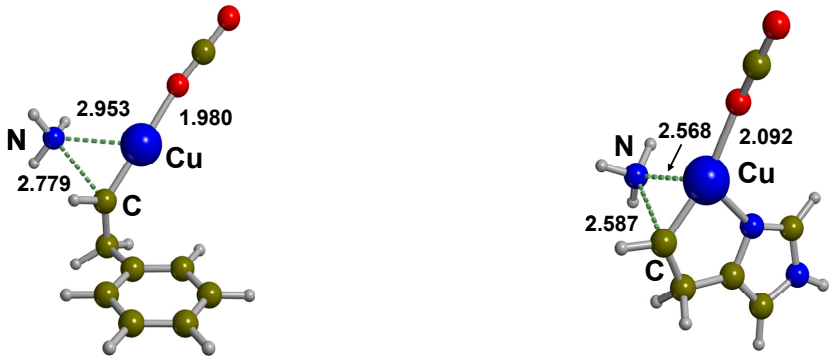

CC61-TS2 **His61-TS2**

Figure 4.17 B3LYP-optimized geometry of the key transition structures for the loss of 61 u in Cu^+-Phe (CC61-TS2) and Cu^+-His (His61-TS2) systems.

Comparison with other systems

It is worth noting that the fragmentation patterns observed in the ESI-CID spectra of Cu^+-AA_{arom} systems is somewhat different to those observed for Cu^+-Gly.[138] Although the most intense peak corresponding to the loss of 46 u is common for both Cu^+-Gly and Cu^+-AA_{arom} systems, appreciable differences are distinguished; these are, eliminations in which the aromatic side chains are implicated (loss of 73 and 137 u) and consecutive

elimination of NH_3 and CO_2. Nonetheless, the side chain interaction with the Cu^+ cation has a minor influence on the fragmentation pattern for all cases.

On the other hand comparing the peaks observed in the ESI-CID spectrum for Cu^+-Phe and Ag^+-Phe,[68, 72] one can observe that different metal cations induce different reactivity of the aromatic amino acids. The common eliminations for both systems are loss of H_2O, consecutive loss of $CO+H_2O$ (or elimination of HCOOH) and consecutive loss of CO_2+NH_3. The formation of the M^+-NH_3 ion is also commonly observed. In contrast, while in Ag^+-Phe system the elimination of NH_3+CO and loss of AgH fragments were found, in Cu^+-Phe system new eliminations corresponding to the loss of CuCOOH (leading to the formation of the immonium ion), to the loss of HOOC-CHCu-NH_2 and to the loss of NH=CH-COOH are observed. Therefore, low collisional decomposition experiments of Phe interacting with these two metal ions produces metal-specific fragmentations, and thus, Cu^+ and Ag^+ can be considered as two complementary metals to elucidate structures that contain AA_{arom}.

4.3.4 THE Cu^{2+}-AA_{arom} SYSTEMS

Despite that in the ion source doubly charge systems have not been observed, it is interesting to analyze the structures and the nature of the bonding between Cu^{2+} and the AA_{arom}. In fact, since Cu^{2+} is recognized to be an oxidising agent in some biochemical processes,[29, 30, 247, 261] the study of the oxidative effects induced by the $Cu^{+/2+}$ pair is of paramount importance. For example, it is believed that the interaction between amyloid-β peptide with Cu^{2+}, a process suggested to play an important role in the oxidative neurotoxicity of this peptide, is established with two histidine amino acids. As mentioned previously, Cu^{2+} (d^9,^{2}D)-L systems presents some computational difficulties. In particular, it was shown that functionals with a larger amount of exact exchange than B3LYP perform better compared to CCSD(T).[206, 210] Because of that, it is also of interest to compare the B3LYP results with those obtained at BHLYP level for the Cu^{2+}-AA_{arom} systems.

Similarly to Cu^+-AA_{arom}, only the most significant structures of the Cu^{2+}-AA_{arom} systems will be presented, the whole conformational analysis for each system being shown in the Appendix D.

4.3.4.1 Cu^{2+}-Phe and Cu^{2+}-Tyr

Optimized geometries with the relative potential energies with the ZPE values are summarized in Figure 4.18 and Table 4.6 shows the computed relative potential energies

including the ZPE (ΔU_0), relative enthalpies (ΔH^0_{298}) as well as the relative free energies (ΔG^0_{298}) at the B3LYP [BHLYP] levels.

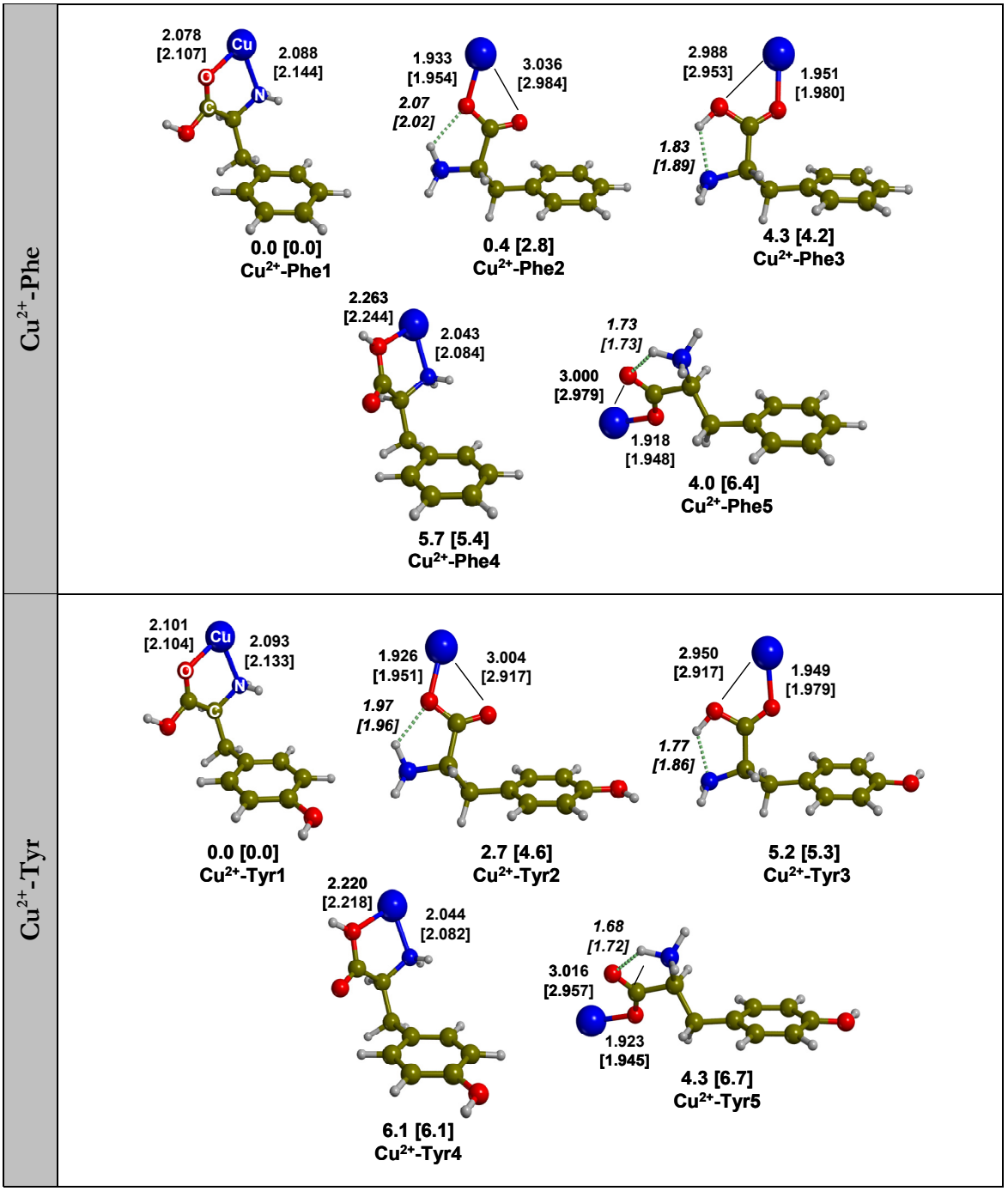

Figure 4.18 B3LYP [BHLYP]-optimized geometries of the Cu^{2+}-Phe (top) and Cu^{2+}-Tyr (bottom) isomers. Relative potential energies including the ZPE values, in kcal/mol. Distances in Å.

Table 4.6 B3LYP [BHLYP] values of the relative potential energies including ZPE values (ΔU_0), relative enthalpies (ΔH^0_{298}) and relative free Gibbs energies (ΔG^0_{298}) of the isomers presented for the Cu^{2+}-Phe and Cu^{2+}-Tyr systems. In kcal/mol.

structure	coordination	ΔU_0		ΔH^0_{298}		ΔG^0_{298}	
Cu^{2+}-Phe1	(N/O)	0.0	[0.0]	0.0	[0.0]	0.0	[0.0]
Cu^{2+}-Phe2	$(O^-)_{zwit}$	0.4	[2.8]	0.6	[3.0]	0.4	[2.3]
Cu^{2+}-Phe3	(O)	4.3	[4.2]	4.5	[4.4]	4.0	[3.6]
Cu^{2+}-Phe4	(N/OH)	5.7	[5.4]	5.8	[5.4]	5.9	[5.5]
Cu^{2+}-Phe5	$(O^-)_{zwit}$	4.0	[6.4]	4.2	[6.6]	3.4	[5.6]
Cu^{2+}-Tyr1	(N/O)	0.0	[0.0]	0.0	[0.0]	0.0	[0.0]
Cu^{2+}-Tyr2	$(O^-)_{zwit}$	2.7	[4.6]	3.0	[4.9]	2.2	[3.7]
Cu^{2+}-Tyr3	(O)	5.2	[5.3]	5.4	[5.6]	4.4	[4.4]
Cu^{2+}-Tyr4	(N/OH)	6.1	[6.1]	6.2	[6.2]	5.7	[6.0]
Cu^{2+}-Tyr5	$(O^-)_{zwit}$	4.3	[6.7]	4.5	[7.0]	3.7	[5.7]

First, it should be mentioned that for these two systems both functionals provide similar relative energies and optimized parameters. The largest differences (~ 2 kcal/mol) are observed for the zwitterionic species and are not due to differences on spin density upon metal coordination. Calculations for isolated glycine show that the relative energy between the zwitterionic form (obtained by freezing the NH distances of the NH_3^+ moiety) and the full optimized neutral glycine (21.3 and 23.9 kcal/mol, with B3YLP and BHLYP, respectively) already differs by 2.6 kcal/mol, this difference carrying over to the metal complex.

Compared to the monovalent analogous, the main difference observed for Cu^{2+} complexes is that we have not localized any structure with the metal cation interacting with the π system, even though all optimizations have been performed taking as starting point the optimised structures of Cu^+-Phe and Cu^+-Tyr systems. To rationalize the lack of cation-π interactions we have analysed the highest monoocupied molecular orbital of **Cu^{2+}-Phe1** (see Figure 4.19). As one can observe, this open shell orbital is mainly localized on the aromatic ring; that is, the amino acid has been oxidized by the metal cation, the π system becoming positively charged with radical character. Accordingly, the metal cation Cu^{2+} is

practically reduced to a monocharged cation (Cu^+). With this scenario, the metal cation and the positively charged π system establish a repulsive electrostatic interaction that moves the metal cation away from the side chain. The value of the net charge of the metal cation and the lateral chain (0.93 and 1.00, respectively) and the fact that the spin density is basically localized on the aromatic ring reinforces the validity of this explanation.

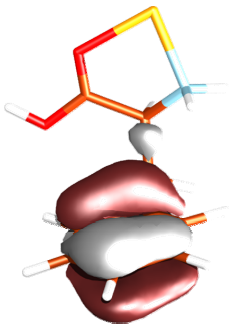

Figure 4.19 SOMO of the Cu^{2+}-Phe1 isomer

Both for Phe and Tyr amino acids, the most stable conformer has the metal cation binding to the oxygen of the carbonyl group and to the nitrogen of amine (**Cu^{2+}-Phe1** and **Cu^{2+}-Tyr1**). A similar coordination was found in Cu^{2+}-Gly system[112] but not as the ground state conformer. In the second most stable structure, **Cu^{2+}-Phe2** and **Cu^{2+}-Tyr2**, the amino acids are in their respective zwitterionic forms and the metal cation binds unsymmetrically to the carboxylate groups, a clear difference with respect to the zwitterionic structure in Cu^{2+}-Gly, for which the interaction with CO_2^- was bidentate. This difference is due to the fact that the copper cation has been reduced upon interacting with Phe and Tyr and thus, it prefers to interact with the carboxylate group in a similar way to that found for Cu^+; that is, unsymmetrically. Because of that, and similar to Cu^+-Gly system, forms "1" (bidentate with NH_2 and CO) are more stable than forms "2" (monodentate to CO_2^-).

As a consequence of the oxidation of the π system, in the zwitterionic **Cu^{2+}-Phe2** and **Cu^{2+}-Tyr2** structures, a new stabilizing interaction between the oxygens not bonded to the metal cation and the positive charge of the aromatic ring is established, which explains the larger stabilization (around 6-7 kcal/mol) found for such structures compared to the other zwitterionic **Cu^{2+}-Phe5** and **Cu^{2+}-Tyr5** forms.

In the remaining structures the metal cation binds either to the COOH group (**Cu^{2+}-Phe3** and **Cu^{2+}-Tyr3**) or to the hydroxyl oxygen and the amine nitrogen (**Cu^{2+}-Phe4** and **Cu^{2+}-Tyr4**). These structures lie 4-6 kcal/mol above the ground state structure.

4.3.4.2 Cu^{2+}-Trp

Figure 4.20 summarizes the structures found for this system and Table 4.7 summarizes the ΔU_0, ΔH^0_{298} and ΔG^0_{298} values of the isomers presented. In this case, both B3LYP and BHLYP provide similar relative energies except when the ring is involved in the interaction.

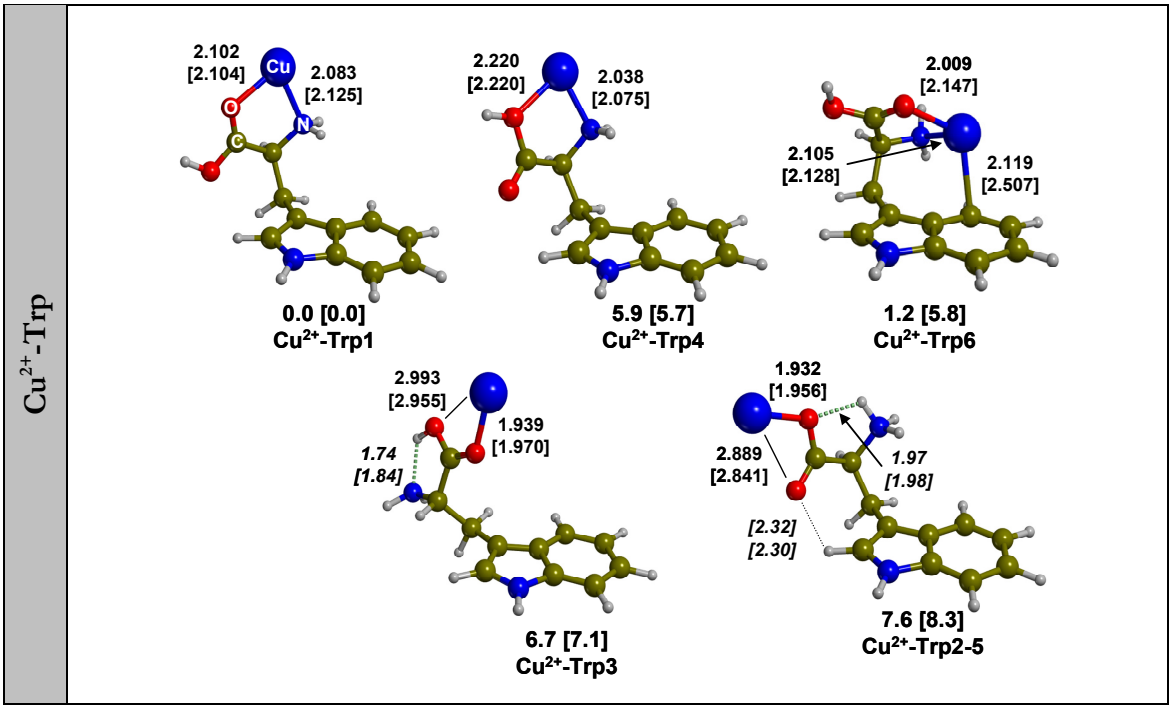

Figure 4.20 B3LYP [BHLYP]-optimized geometries of the Cu^{2+}-Trp isomers. Relative potential energies including the ZPE values, in kcal/mol. Distances in Å.

Table 4.7 B3LYP [BHLYP] values of the relative potential energies including ZPE values (ΔU_0), relative enthalpies (ΔH^0_{298}) and relative free Gibbs energies (ΔG^0_{298}) of the isomers presented for the Cu^{2+}-Trp system. In kcal/mol.

structure	coordination	ΔU_0		ΔH^0_{298}		ΔG^0_{298}	
Cu^{2+}-Trp1	(N/O)	0.0	[0.0]	0.0	[0.0]	0.0	[0.0]
Cu^{2+}-Trp4	(N/OH)	5.9	[5.7]	5.9	[5.7]	5.8	[5.6]
Cu^{2+}-Trp6	(N/O/ring)	1.2	[5.8]	0.9	[5.8]	2.9	[6.2]
Cu^{2+}-Trp3	(O)	6.7	[7.1]	6.9	[7.4]	6.0	[6.0]
Cu^{2+}-Trp2-5	$(O^-)_{zwit}$	7.6	[8.3]	7.8	[8.5]	7.2	[7.9]

The most striking difference observed compared to Cu^{2+}-Phe and Cu^{2+}-Tyr, is that more structures have been found to be stable. These new structures have the particularity that interactions with the indole ring are established, even though natural population analysis indicate that the aromatic ring has also been oxidized upon Cu^{2+} binding in all cases. Figure 4.20 only presents the most stable structure of them, the remaining ones being shown in the Appendix D. Comparing the most stable conformer (**Cu^{2+}-Trp1**), which presents a CO and NH_2-metal cation coordination, with its homologous in which the metal cation also interacts with the aromatic side chain (**Cu^{2+}-Trp6**), it is observed that the latter structure is 1.2(5.8) kcal/mol less stable than the former at the B3LYP(BHLYP) levels. Furthermore, the remaining structures in which the metal cation interacts with the π system are the most unstable isomers found along this conformational exploration (shown in the Appendix D). This is not surprising considering the repulsive interactions between the positive charge of the ring and the metal cation. The fact that these structures are, however, stable, in contrast to Cu^{2+}-Phe and Cu^{2+}-Tyr, can be understood considering that the indole ring can better delocalize the positive charge than benzene or phenol. Moreover, the net charge localized on the five and six membered rings of **Cu^{2+}-Trp6** indicates that the latter ring supports less charge than the former. In addition, the spin density shows that the radical character mainly lies at the five membered ring.

Three more conformers in which the metal cation does not interact with the side chain have been found (**Cu^{2+}-Trp4**, **Cu^{2+}-Trp3** and **Cu^{2+}-Trp2-5**). Special attention deserves **Cu^{2+}-Trp2-5**. In this isomer, the amino acid is in its zwitterionic form and the metal cation is unsymmetrically coordinated by the carboxylate group, similar to forms "2" and "5" of the Cu^{2+}-Phe and Cu^{2+}-Tyr systems. However, the orientation of $Cu{-}COO^{-}$ and NH_3^{+} is quite different respect to forms "2" and "5". Note that in **Cu^{2+}-Trp2-5**, a hydrogen bond between the acidic CH of oxidized indole ring and one of the carboxylate oxygens is established.

4.3.4.3 Cu^{2+}-His

Figure 4.21 shows the optimized geometries of Cu^{2+}-His with their respective relative potential energies including the ZPE values and Table 4.8 summarizes the ΔU_0, ΔH^0_{298} and ΔG^0_{298} values of the isomers found. For this system, the values computed with B3LYP and BHLYP show important variations. See for example the relative energy of **Cu^{2+}-His13** which is 9.4 with B3LYP and 15.3 kcal/mol with BHLYP or the relative energies of **Cu^{2+}-His14** structure which vary in more than 7 kcal/mol depending on the

functional. In general, these differences are due to the fact that B3LYP provides a too delocalized picture of the electron, which is overstabilized by DFT methods due to a bad cancellation of the self-interaction part by the exchange functional. Nevertheless, some structures with quite different coordination environments and thus, spin distribution, show similar relative energies, probably due to error cancellations. Thus, in order to check the reliability of B3LYP and BHLYP methods CCSD(T)//B3LYP single-point energy calculations for **Cu^{2+}-His11** and **Cu^{2+}-His13** structures have been performed. The computed relative energy at the CCSD(T) level (15.1 kcal/mol) is in much better agreement with the BHLYP value (15.3 kcal/mol) than with the B3LYP one (9.4 kcal/mol). These differences are related to the changes on the spin density of Cu^{2+}, the obtained values being around 0.7 – 0.8 and 0.5 – 0.6 with BHLYP and B3LYP, respectively. Thus, BHLYP results are expected to be more accurate and from now the discussion will only refer to the BHLYP values. In any case, it should be mentioned that both B3LYP and BHLYP provide **Cu^{2+}-His11** to be the ground state structure.

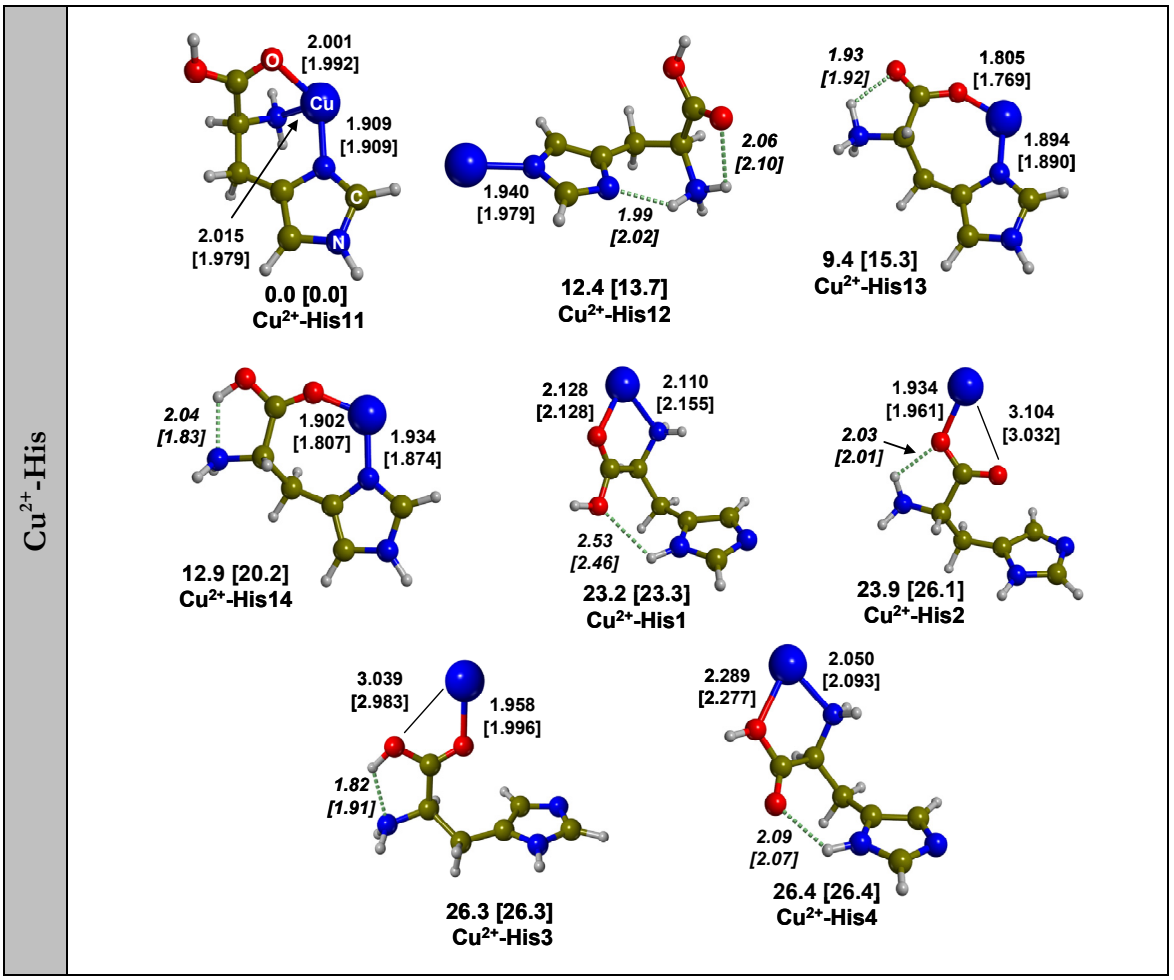

Figure 4.21 B3LYP [BHLYP]-optimized geometries of the Cu^{2+}-His isomers. Relative potential energies including the ZPE values, in kcal/mol. Distances in Å.

Table 4.8 B3LYP [BHLYP] values of the relative potential energies including ZPE values (ΔU_0), relative enthalpies (ΔH^0_{298}) and relative free Gibbs energies (ΔG^0_{298}) of the isomers presented for the Cu^{2+}-His system. In kcal/mol.

structure	coordination	ΔU_0		ΔH^0_{298}		ΔG^0_{298}	
Cu^{2+}-His11	(N/O/Nδ)	0.0	[0.0]	0.0	[0.0]	0.0	[0.0]
Cu^{2+}-His12	(Nε)	12.4	[13.7]	13.3	[14.6]	10.5	[11.7]
Cu^{2+}-His13	$(O^-/N\delta)_{zwit}$	9.4	[15.3]	9.9	[15.7]	8.5	[14.7]
Cu^{2+}-His14	(O/ Nδ)	12.9	[20.2]	13.5	[20.5]	12.1	[19.9]
Cu^{2+}-His1	(N/O)	23.2	[23.3]	24.0	[24.2]	21.0	[21.4]
Cu^{2+}-His2	$(O^-)_{zwit}$	23.9	[26.1]	25.0	[27.2]	21.5	[23.6]
Cu^{2+}-His3	(O)	26.3	[26.3]	27.3	[27.4]	23.7	[23.6]
Cu^{2+}-His4	(N/OH)	26.4	[26.4]	27.2	[27.2]	24.6	[24.7]

The ground state **Cu^{2+}-His11** has the metal cation coordinating to the carbonyl and the amino group (as in the previous Cu^{2+}-AA_{arom} systems), and to the Nδ of imidazole. That is, the metal cation is tricoordinated, in contrast to the ground structure of Cu^+-His, which is dicoordinated. In this case, the metal cation behaves as Cu^{2+} since the spin density mainly lies at the metal cation (0.79). The same occurs for **Cu^{2+}-His13** and **Cu^{2+}-His14**. However, for the remaining structures the spin density lies at the amino acid. In these situations the metal cation presents either only monocoordination through Nε of imidazole or coordination with the donor atoms of the backbone, which favours the electron hole to be in the amino acid, especially in the side chain. This induces an increase of the imidazole NH acidity[262] which in **Cu^{2+}-His12** results in a spontaneous intramolecular proton transfer from the NH group of the imidazole ring to the amino group. It is worth mentioning that, in some cases, however, the radical character of the amino acid does not lie at the side chain but in the backbone, the nature of the electron hole depending on the conformation. In other Nε-monocoordinated structures, the open shell orbital is mainly centred at the amino group. In these latter cases, the NH_2 group becomes more planar and due to its increase of acidity it establishes a new hydrogen bond in which it acts as proton donor (see Appedinx D), as described in the literature.[263]

Particularly interesting are structures **Cu^{2+}-His13** and **Cu^{2+}-His14**, which correspond to the metal cation interacting with the zwitterionic and neutral species of His. In contrast to other bidentate forms, these structures have the metal cation acting as Cu^{2+}, the spin density mainly lying at copper. This is due to the fact that Nδ imidazole is a better coordinating site than NH_2, which stabilizes Cu^{2+}. It should be mentioned, however, that an analogous structure to **Cu^{2+}-His14** have been localized but with the spin density at the amino acid. This structure lies about 4 kcal/mol above **Cu^{2+}-His14** and presents Cu-N and Cu-O distances 0.2 Å larger. This shows that the coordination environment, and in particular the metal ligand distance, can determine whether the amino acid is oxidized (or not) by the metal cation. In fact, unsaturated coordination will favour oxidation and formation of Cu^{+}, whereas full coordination will stabilize Cu^{2+}. It is well known that the kind of coordination, square-planar or tetrahedral, can determine the oxidation state of the metal cation. In that vein, the oxidative effects of biological systems due to its interaction with Cu^{2+} are of particular interest. For instance, it is believed that development of Alzheimer's disease is related to the interaction of Cu^{2+} with Amyloid-β (a peptide that contains His and Tyr), which can induce βA aggregation and subsequent neurotoxicity,[264, 265] due to oxidative damage.

Remaining coordination modes follow either the same features found in Cu^{2+}-Phe and Cu^{2+}-Tyr systems (CO and NH_2 in **Cu^{2+}-His1**, COO^- in **Cu^{2+}-His2**, COOH in **Cu^{2+}-His3**, and OH and NH_2 in **Cu^{2+}-His4**) or the coordination is given through the Nε imidazole such as **Cu^{2+}-His12** or other isomers presented in the Appendix D.

4.3.4.4 Binding energies of Cu^{2+}-AA_{arom}

The computed D_e, D_0, ΔH^0_{298} and ΔG^0_{298} values for the lowest energy structure of Cu^{+}-AA_{arom} are given in Table 4.9.

Table 4.9 Binding energies (D_e, D_0, ΔH^0_{298} and ΔG^0_{298}) of Cu^{2+}-AA_{arom}, in kcal/mol. In parenthesis counterpoise corrected values.

		D_e	D_0	ΔH^0_{298}	ΔG^0_{298}
Phe	B3LYP	285.7 (284.8)	285.9 (285.0)	286.0 (285.1)	278.6 (277.7)
	BHLYP	261.6 (260.2)	262.1 (260.7)	262.1 (260.7)	254.8 (253.4)
Tyr	B3LYP	304.9 (304.0)	303.7 (302.8)	304.1 (303.2)	295.9 (295.0)
	BHLYP	280.5 (279.2)	279.5 (278.2)	279.9 (278.6)	271.8 (270.5)
Trp	B3LYP	322.6 (321.7)	321.3 (322.4)	321.7 (320.8)	313.5 (312.6)
	BHLYP	297.7 (296.3)	296.7 (295.3)	297.1 (295.7)	289.0 (287.6)
His	B3LYP	310.2 (308.0)	308.0 (305.8)	309.0 (306.8)	298.7 (296.5)
	BHLYP	288.6 (286.2)	286.0 (283.6)	287.1 (284.7)	276.9 (274.5)
	CCSD(T)	289.8			

For Cu^{2+}-AA_{arom} systems, interaction energies provide a different trend than the observed for the Cu^+-AA_{arom}. Indeed, the order of Cu^{2+} cation affinities is Cu^{2+}-Trp > Cu^{2+}-His > Cu^{2+}-Tyr > Cu^{2+}-Phe. Although the Cu^{2+}-Trp, -Tyr and -Phe systems follow the same trend than that observed for Cu^+, in this case, however, the order is not determined by cation-π interactions with the side chain since, as shown, Cu^{2+} binding induces the oxidation of the amino acid. In fact, the order arises from the ability to oxidize the amino acid (IE(Trp) < IE(Tyr) < IE(Phe)) and from the efficiency in delocalizing the positive charge. The IE of His is similar to Phe but due to the different kind of coordination and to the fact that in the ground state structure the amino acid is not oxidized, the binding energy is much larger.

Concerning the two functionals it is observed that the binding energy computed with B3LYP is about 22-26 kcal/mol larger than with BHLYP. This important variation mainly arises from the large differences in the second IE of Cu which is computed to be 20.8 eV with B3LYP and 19.9 eV with BHLYP. That is, the Cu^{2+} + AA_{arom} asymptote lies too high in energy with B3LYP and consequently, the computed Cu^{2+}-AA_{arom} binding energy is too large. The computed CCSD(T) value for Cu^{2+} binding to His indicates that the values obtained by the BHLYP functional are more reliable.

5. INTERACTION OF Cu^+ AND Cu^{2+} TO $(GLYCYL)_n$GLYCINE OLIGOPEPTIDES (n = 1-3).

5.1 INTRODUCTION

In this chapter a computational analysis of the gas phase binding chemistry between Cu^+ and Cu^{2+} with $(glycyl)_n$glycine oligopeptides, with *n* varying from 1 to 3, is analyzed; i. e., the exploration of the existing isomers for these mono and doubly charged systems. Therefore, this chapter is fully addressed to the use of density functional calculations to determine the intrinsic gas phase properties of the complexes formed between transition metal cations and models of relevant biological macromolecules. That is, to accurate describe these transition metal complexes in order to establish the preferred metal coordination environment, to examine the metal specific sites, or to obtain metal cation affinities. This kind of studies allow to obtain trends and new insights at a molecular level that provide important clues and help understand the behaviour of more complicated systems of biological relevance.

Particularly interesting is the study of the $Cu^{+/2+}$-peptides interaction due to the important role that they have been invoked to play in some neurodegenerative diseases, in particular, the pathogenesis of Alzheimer's disease (AD).[266, 267] Indeed, there is accumulating evidences that Cu(II) is directly associated to a neurotoxicity of a 40-42 amino acid peptide called Amyloide-β (Aβ), either by inducing the aggreagation and deposition of Aβ or by serving as cofactor in the generation of oxidative stress, both processes leading to neuronal death.[268-273] Since poliglycines are the backbone of more complex peptides, the use of glycine oligomers as models is a logical choice for initial studies to analyze the interaction of copper cations with peptides.

Up to present, both from experimental and theoretical point of view, most of the works addressed to metal cation interactions with small peptides have dealt with alkali,[87, 88, 114, 274-277] alkaline-earth[278] and closed-shell[64, 67, 130, 131, 134, 279] transition metal cations, whereas only few works have analyzed the interaction of open-shell transition metal cations [65, 117, 130, 131, 134, 279-281] and none of them has considered the binding of Cu^{2+} to peptides. The aim of this chapter is to gain more insights on the interaction of copper cation with peptides by analyzing the influence of both the electronic configuration of the metal cation and the elongation of the peptide chain.

5.2 METHODS

Full geometry optimizations and harmonic frequency calculations for different isomers of $Cu^{+/2+}$-(glycyl)$_n$glycine (n=1-3) have been performed using DFT calculations. The B3LYP approach[195, 197] has been used for Cu^+-poliglycine since as aforementioned, this functional provides results in fairly good agreement with CCSD(T) and experimental values.[101, 177] In contrast, it has been demonstrated along this thesis, that for Cu^{2+}-H_2O the BHLYP functional performs better than the B3LYP one when comparing to CCSD(T) results. Moreover, recent studies performed in our group for Cu^{2+}-$(H_2O)_n$ (n=1-6) have shown that, for a given number of water molecules, the relative energy of different structures is better described with BHLYP than with B3LYP. Becasue of that, the Cu^{2+}-poliglycine systems have only been computed using the BHLYP approach.[195, 201]

The exploration of the conformational space of the considered systems has followed the same procedure done in chapter 3. That is, a preliminary conformational search of the Li^+-(glycyl)$_n$glycine systems using the MCMM[212] with the AMBER* force field[249, 250] implemented in Macromodel 7.0 package[213] was carried out to model the electrostatic interactions. The most significant structures were selected and used as starting points computed at the DFT level.

For Cu we have employed the Watcher's primitive basis set (14s9p5d),[203] supplemented with one s, two p, and one d diffuse functions,[204] plus one f polarization function, the final basis set being (15s11p6d1f)/[10s7p4d1f]. For C, N, O and H the standard 6-31++G(d,p) basis set has been employed.

All density functional calculations have been performed using the Gaussian 03 set of programs package.[252] Open shell calculations have been based on an unrestricted formalism. Thermodynamic corrections have been obtained assuming an ideal gas, unscaled harmonic vibrational frequencies and the rigid rotor approximation by standard statistical methods.[253] Electron spin densities and net atomic charges on the atoms have been obtained using the population analysis of Weinhold et al.[254]

5.3 RESULTS AND DISCUSSION

The results are organized in three parts. In the first two the results of $Cu^{+/2+}$-systems will be presented. In the last section, the binding energies of each system will be discussed. For the sake of brevity, the glycylgycine, the glycylglycylgycine and the glycylglycylglycylgycine peptides are designated as GG, GGG and GGGG, respectively. In

addition, we refer to nitrogen atom of the terminal amino group as **N**, the oxygens and nitrogens of the peptide bond as $\mathbf{O_{pn}}$ and $\mathbf{N_{pn}}$, respectively, where **n** is the number of the peptide bond starting from the NH_2 terminus, the terminal oxygen of the carbonyl group as **O**, and the oxygen of the hydroxyl group as $\mathbf{O_H}$.

Figure 5.1 shows the global B3LYP and BHLYP minima of the neutral forms of GG, GGG and GGGG systems. They have been found after considering the most stable structures arising from previous MCMM and DFT calculations. The GG conformer has been described recently as the most stable form.[263] For the GGG and GGGG cases, other conformations close in energy were found. However, since energy difference between them is very small, $Cu^{+/2+}$ binding energies will not substantially be influenced wether we consider one structure or another.

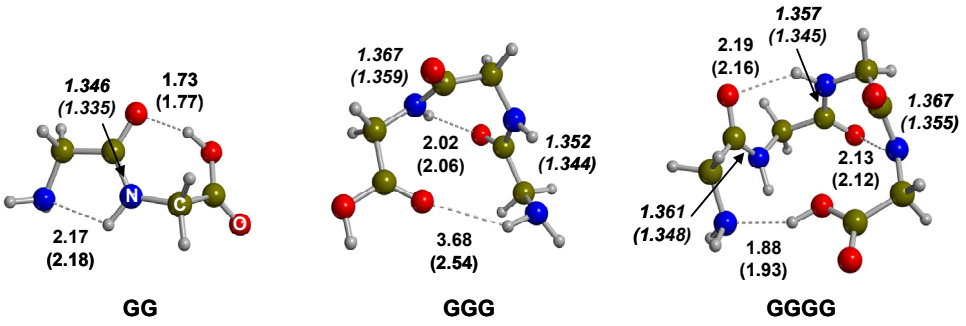

Figure 5.1 B3LYP (BHLYP)-optimized geometries of the most stable conformers of GG, GGG and GGGG systems. Distances in Å.

5.3.1 THE Cu^{+}-GG, -GGG, -GGGG SYSTEMS

The B3LYP-optimized geometries, the main metal-ligand distances and the relative potential energies including the ZPE for the Cu^{+}-GG, Cu^{+}-GGG and Cu^{+}-GGGG systems are given in Figure 5.2, while Table 5.1 summarizes their relative potential energies including the ZPE (ΔU_0), relative enthalpies (ΔH_{298}) and relative free energies (ΔG_{298}).

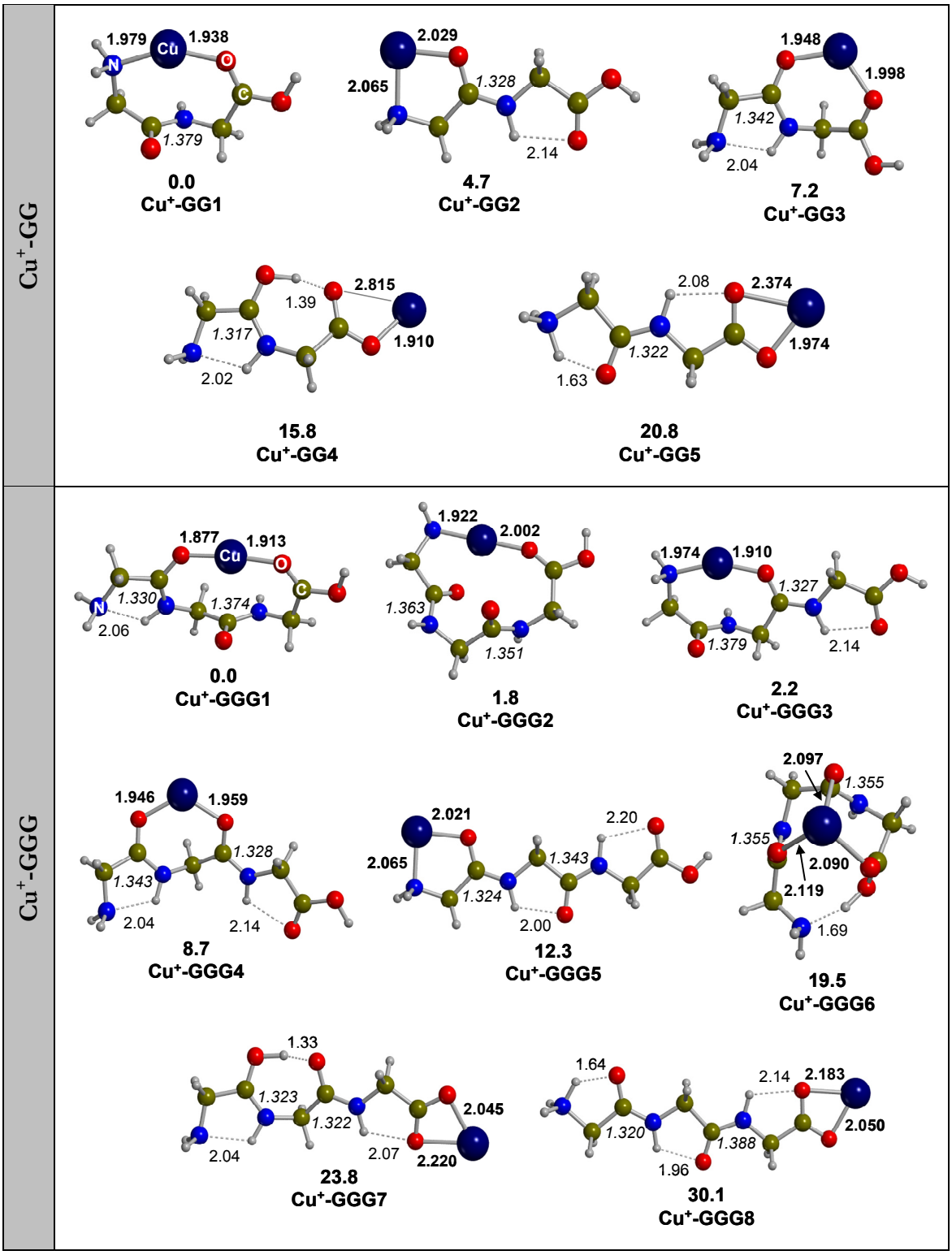
Cu+-GG
1.979
Cu
1.938
N
O
C
1.379
0.0
Cu+-GG1
2.029
2.065
1.328
2.14
4.7
Cu+-GG2
1.948
1.998
1.342
2.04
7.2
Cu+-GG3
2.815
1.39
1.317
1.910
2.02
15.8
Cu+-GG4
2.08
2.374
1.322
1.974
1.63
20.8
Cu+-GG5
Cu+-GGG
1.877
Cu
1.913
O
C
N
1.330
1.374
2.06
0.0
Cu+-GGG1
1.922
2.002
1.363
1.351
1.8
Cu+-GGG2
1.974
1.910
1.327
1.379
2.14
2.2
Cu+-GGG3
1.946
1.959
1.328
1.343
2.04
2.14
8.7
Cu+-GGG4
2.021
2.20
2.065
1.343
1.324
2.00
12.3
Cu+-GGG5
2.097
1.355
1.355
2.090
2.119
1.69
19.5
Cu+-GGG6
1.33
1.323
1.322
2.045
2.04
2.07
2.220
23.8
Cu+-GGG7
1.64
2.14
2.183
1.320
1.388
2.050
1.96
30.1
Cu+-GGG8

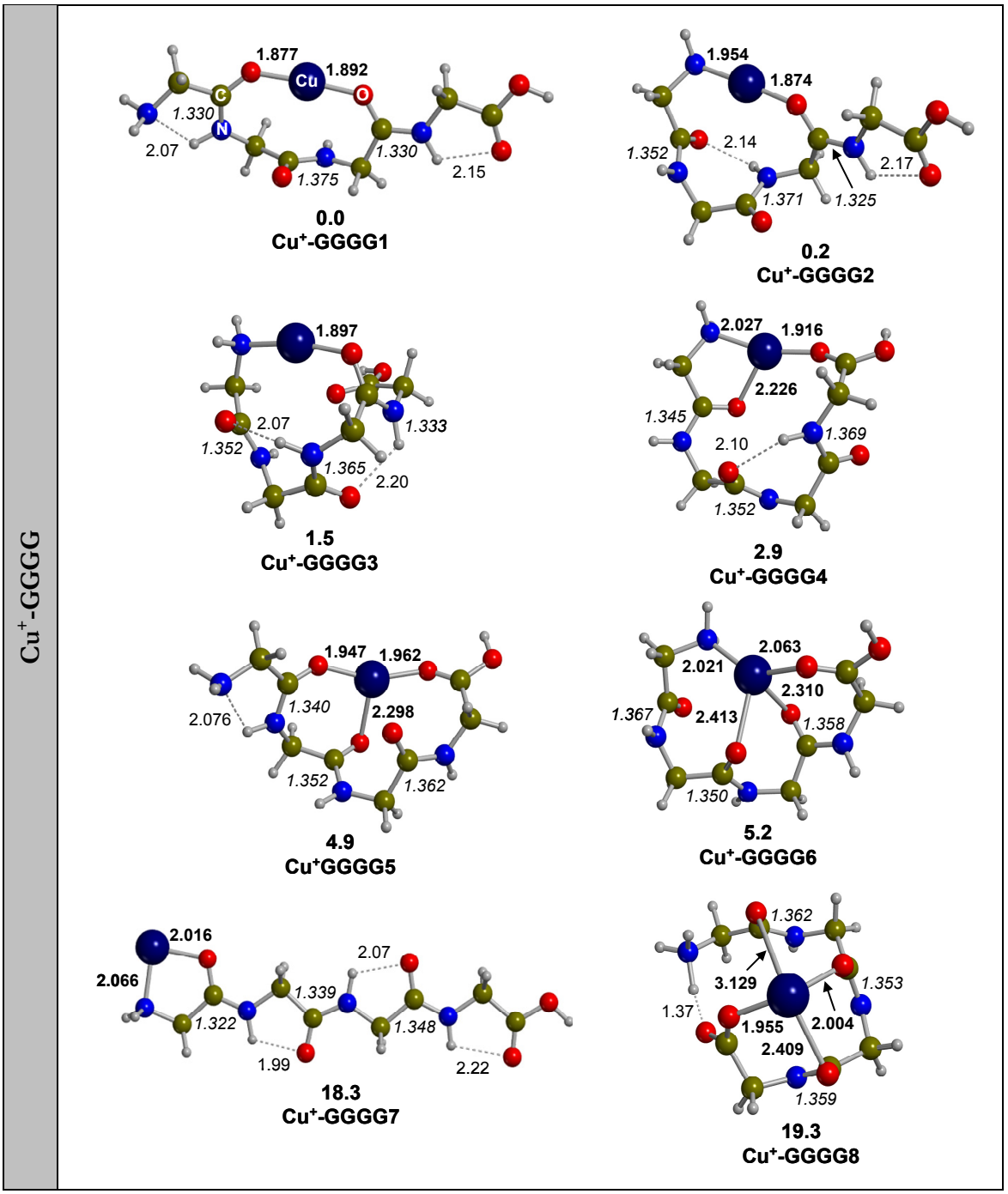

Figure 5.2 B3LYP-optimized geometries of the Cu^{+}-GG, Cu^{+}-GGG and Cu^{+}-GGG isomers. Relative potential energies including the ZPE values, in kcal/mol. Distances in Å.

Table 5.1 B3LYP values of the relative potential energies including ZPE values (ΔU_0), relative enthalpies (ΔH^0_{298}) and relative free Gibbs energies (ΔG^0_{298}) of the isomers presented for the Cu^+-GG, Cu^+-GGG, and Cu^+-GGGG systems. In kcal/mol.

isomers	ΔU_0	ΔH^0_{298}	ΔG^0_{298}
Cu^+-GG1	0.0	0.0	0.0
Cu^+-GG2	4.7	5.0	3.6
Cu^+-GG3	7.2	7.4	6.5
Cu^+-GG4	15.8	16.1	14.2
Cu^+-GG5	20.8	21.3	19.1
Cu^+-GGG1	0.0	0.0	0.0
Cu^+-GGG2	1.8	1.6	1.2
Cu^+-GGG3	2.2	2.0	2.0
Cu^+-GGG4	8.7	8.7	7.8
Cu^+-GGG5	12.3	12.5	10.6
Cu^+-GGG6	19.5	19.0	20.9
Cu^+-GGG7	23.8	23.8	22.4
Cu^+-GGG8	30.1	30.4	28.2
Cu^+-GGGG1	0.0	0.0	0.0
Cu^+-GGGG2	0.2	-0.3	1.2
Cu^+-GGGG3	1.5	0.7	3.3
Cu^+-GGGG4	2.9	2.4	4.4
Cu^+-GGGG5	4.9	4.9	5.1
Cu^+-GGGG6	5.2	4.8	6.1
Cu^+-GGGG7	18.3	18.4	16.4
Cu^+-GGGG8	19.3	18.8	20.8

The most stable isomer of Cu^+-GG corresponds to **Cu^+-GG1,** where Cu^+ is coordinated to the terminal amino (**N**) and the carbonyl oxygen (**O**) groups. When Cu^+ interacts with the GGG peptide the ground-state isomer presents also an almost linear dicoordination where the $\mathbf{O_{p1}}$ and the **O** are the donor atoms (**Cu^+-GGG1**). Finally, the most stable isomer of the Cu^+-GGGG system (**Cu^+-GGGG1**) is also dicoordinated, the Cu^+ cation interacting with the $\mathbf{O_{p1}}$ and $\mathbf{O_{p3}}$ donor centres. Therefore, the trend is clear: Cu^+ prefers to be chelated by two atoms with a coordination angle close to 180º. This trend is reinforced by the fact that the second and the third most stable forms for the two latter systems present also this same way of coordination (**Cu^+-GGG2** and **Cu^+-GGG3** are 1.8 and 2.2 kcal/mol higher in energy respect to **Cu^+-GGG1**, respectively, and **Cu^+-GGGG2** and **Cu^+-GGGG3** lay 0.2 and 1.5 kcal/mol above **Cu^+-GGGG1,** respectively). The mechanism of interaction of these structures is well known. Assuming z as the binding axis, the highest *d* orbital of Cu^+ is the d_{z^2} one, which is hybridized with the 4*s* orbital in order to reduce the repulsion along the metal-ligand axis, and thus the coordination of a third donor centre becomes unfavourable.

In Cu^+-Gly system,[112] the most stable isomer is that in which the **N** and the **O** atoms coordinate to the metal cation forming a five member ring. Similar structures have been found in the present work (**Cu^+-GG2**, **Cu^+-GGG5**, and **Cu^+-GGGG7**) but lying 4.7, 12.3 and 18.3 kcal/mol above the corresponding most stable isomers, respectively. It can be noted that the relative energy of these forms is increased as the peptide chain is elongated and thus, the coordination mode of the most stable isomer of Cu^+-Gly system becomes disfavoured. These results indicate that Cu^+ cation prefers a linear coordination environment rather than an angular coordination. The reason is that to reduce the Pauli repulsion between the metal cation and the ligand, in a linear coordination the d_{z^2} orbital of the metal cation hybridizes with the 4*s* one, while in the angular coordination the hybridization is through the d_{xz} and the 4*p* orbitals. Since the 4*p* orbitals lie higher in energy than the 4*s*, the hybridization is less effective in angular coordination structures and thus, the repulsion minimization is smaller, giving rise to more unstable structures than for linear coordination. For Cu^+-Gly the most stable isomer follows an angular geometry because it is not possible to establish a linear coordination due to geometry restrictions.

Cu^+-GG3 and **Cu^+-GGG4** are dicoordinated structures, in which the metal cation interacts with the $\mathbf{O_{p1}}$ and **O** atoms, and the $\mathbf{O_{p1}}$ and $\mathbf{O_{p2}}$ atoms, respectively, the coordination angle being close to 150º. These structures are quite stable compared to the

respective ground state isomer (7.2 and 8.7 kcal/mol higher in energy). However, if only charge solvated forms are taken into account, structures with this kind of coordination do not exist for Cu^+-GGGG. However, other more coordinated species are observed, such as the tricoordinated **Cu^+-GGGG4** and **Cu^+-GGGG5**, which are 2.9 and 4.9 kcal/mol above **Cu^+-GGGG1**, respectively, and the tetracoordinated **Cu^+-GGGG6**, which is 5.1 kcal/mol above **Cu^+-GGGG1**. Therefore, as the number of donor atoms is increased, the metal cation tends to be coordinated by more than two donor atoms. However, this increment on the cation environment does not imply a loss of the preference of Cu^+ to follow linear coordination.

Finally, the zwitterionic forms localized deserve to be commented. For Cu^+-GG two zwitterionic forms have been found: one in which the proton is transferred from the carboxylic group to the $\mathbf{O_{p1}}$ atom (**Cu^+-GG4**), and another one where the proton is transferred to the **N** atom (**Cu^+-GG5**). These two structures are the most unstable of Cu^+-GG (15.8 and 20.8 kcal/mol higher in energy than the **Cu^+-GG1** isomer, respectively). A similar behaviour is observed for Cu^+-GGG, for which two zwitterionic forms have also been found (**Cu^+-GGG7** with the protonated $\mathbf{O_{p1}}$ atom and **Cu^+-GGG8,** where the protonation takes place at the **N** atom). Once again, these two structures are the most unstable ones (23.8 and 30.1 kcal/mol above the **Cu^+-GGG1** isomer, respectively). In addition, the zwitterionic form in which the proton is on the $\mathbf{O_{p2}}$ atom (not reported here) has also been identified and lies around 37 kcal/mol respect to the **Cu^+-GGG1** isomer. Finally, the only zwitterionic form found for Cu^+-GGGG (**Cu^+-GGGG8)**, which remains 30.1 kcal/mol above the most stable isomer is that where the metal cation is tetraccordinated through the $\mathbf{O_{p1}}$, $\mathbf{O_{p2}}$, $\mathbf{O_{p3}}$ and **O** atoms, while the amino group has received the proton from the hydroxyl group. To sum up, the zwitterionic forms of the Cu^+-GG, Cu^+-GGG and Cu^+-GGGG systems are the most unstable isomers of the explored PES.

Several factors can determine the relative stability of these structures. The main ones are: the deformation energy of poliglycines when coordinating the metal cation, the electrostatic interaction, the metal–ligand repulsion and the charge transfer, which reflects the electronic delocalization between the metal and the ligand. In order to have a deeper insight on the nature of the bonding, the binding energies of the most stable isomers found were computed in two steps. First, we have calculated the deformation energy (E_{def}) of poliglycines by determining the energy difference between the poliglycines at the

geometries of the complexes and free poliglycines in their respective ground-state conformers. Second, we have computed the electrostatic interaction (E_{elec}); that is, the energy lowering of the deformed poliglycines in the presence of a single point charge replacing the cation. In this calculation the electronic relaxation of the ligands is allowed and thus, it also includes the polarization term. The sum of E_{def} + E_{elec} gives us the interaction energy between poliglycines and a point charge ($\Delta E_{int(pc)}$).

The values of these computed terms for the four most stable isomers of Cu^+-GG, Cu^+-GGG and Cu^+-GGGG are summarized in Table 5.2. First, one can observe that the E_{def} term is positive and larger in longer peptide chains, whereas the E_{elec} is, in contrast, negative and larger as the peptide chain is increased. It is interesting to compare the relative energies obtained using a point charge ($\Delta E_{rel(pc)}$) model and those computed for Cu^+-$(glycyl)_n$glycine isomers (ΔE_{rel}). For the "GG" and "GGGG" cases the sequences of the relative energies follow the same trend but the values are somewhat different. Although for the "GGG" cases the relative order is not the same (according to the point charge model the most stable form should be the (+)-GGG3 one), the differences are small. These results point out that the interaction of Cu^+ with poliglycines is not purely electrostatic so that, in contrast to alkali cations, other factors such as Pauli repulsion or charge transfer are also important.

Table 5.2 Contributions to the Total Interaction Energy for the fourth most stable isomers of Cu^+-GG, -GGG and –GGGG systems. In kcal/mol.

Cu^+-G_mX	E_{def}	E_{elec}	$\Delta E_{int(pc)}$	$\Delta E_{rel(pc)}$	ΔE_{int}	ΔE_{rel}
GG1	12.6	-108.7	-96.1	0.0	-87.5	0.0
GG2	10.1	-102.0	-91.9	4.2	-82.4	5.1
GG3	10.4	-100.2	-89.8	6.3	-79.6	7.9
GG4	17.8	-92.7	-74.9	21.2	-69.9	17.6
GGG1	13.7	-118.1	-104.4	0.0	-97.1	0.0
GGG2	21.9	-123.8	-101.9	2.5	-96.2	0.9
GGG3	16.0	-121.5	-105.5	-1.1	-95.6	1.5
GGG4	13.7	-114.1	-100.7	3.7	-88.5	8.6
GGGG1	16.6	-129.5	-112.9	0.3	-104.7	1.3
GGGG2	15.8	-129.0	-113.2	0.0	-106.1	0.0
GGGG3	14.0	-127.0	-113.0	0.2	-105.1	0.9
GGGG4	23.9	-133.4	-109.5	3.7	-103.0	3.0

$\Delta E_{int(pc)}$ = interaction energies of (+)-glycine oligomers: E_{def} + E_{elec}.

$\Delta E_{rel(pc)}$ = relative energies considering $\Delta E_{int(pc)}$.

ΔE_{int} = interaction energy of (Cu^+)-poliglycine isomers.

ΔE_{rel} = relative energies considering ΔE_{int}.

5.3.2 THE Cu^{2+}-GG, -GGG, -GGGG SYSTEMS

Figure 5.3 shows the BHLYP-optimized geometries as well as their relative energies including the ZPE corrections of the structures located for the Cu^{2+}-GG, Cu^{2+}-GGG and Cu^{2+}-GGGG systems. Table 5.3 summarizes the relative potential energies including the ZPE (ΔU_0), relative enthalpies (ΔH_{298}) and relative free energies (ΔG_{298}) for the isomers of these systems.

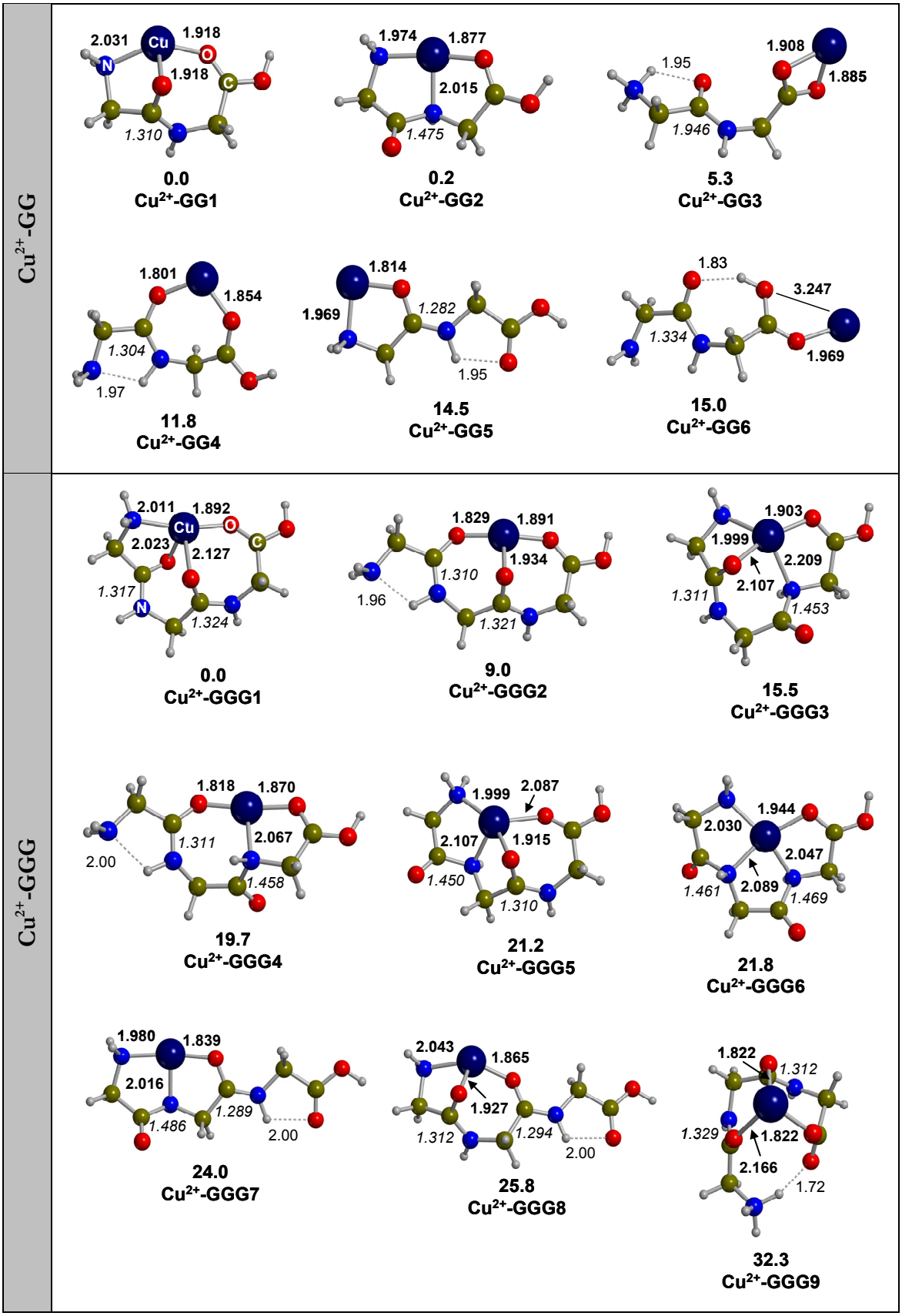
Cu2+-GG
2.031
Cu
1.918
O
N
1.918
C
1.310
0.0
Cu2+-GG1
1.974
1.877
2.015
1.475
0.2
Cu2+-GG2
1.95
1.908
1.885
1.946
5.3
Cu2+-GG3
1.801
1.854
1.304
1.97
11.8
Cu2+-GG4
1.814
1.969
1.282
1.95
14.5
Cu2+-GG5
1.83
3.247
1.334
1.969
15.0
Cu2+-GG6
Cu2+-GGG
2.011
1.892
Cu
O
2.023
2.127
C
1.317
N
1.324
0.0
Cu2+-GGG1
1.829
1.891
1.934
1.310
1.96
1.321
9.0
Cu2+-GGG2
1.903
1.999
2.209
2.107
1.311
1.453
15.5
Cu2+-GGG3
1.818
1.870
1.311
2.067
2.00
1.458
19.7
Cu2+-GGG4
1.999
2.087
2.107
1.915
1.450
1.310
21.2
Cu2+-GGG5
1.944
2.030
2.047
1.461
2.089
1.469
21.8
Cu2+-GGG6
1.980
1.839
2.016
1.289
1.486
2.00
24.0
Cu2+-GGG7
2.043
1.865
1.927
1.312
1.294
2.00
25.8
Cu2+-GGG8
1.822
1.312
1.329
1.822
2.166
1.72
32.3
Cu2+-GGG9

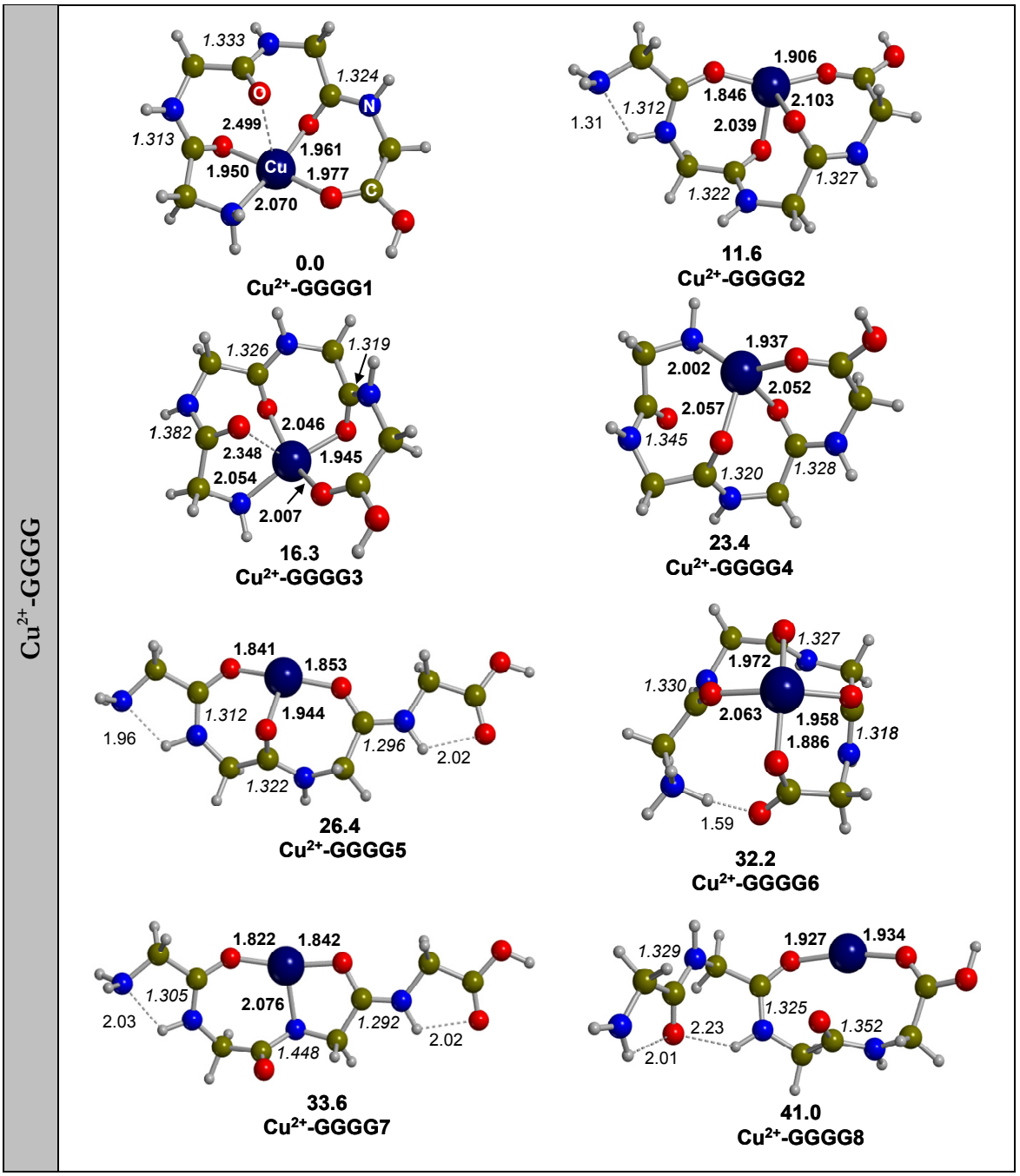

Figure 5.3 BHLYP-optimized geometries of the Cu^{2+}-GG, Cu^{2+}-GGG and Cu^{2+}-GGGG isomers. Relative potential energies including the ZPE values in kcal/mol. Distances in Å.

Table 5.3 BHLYP values of the relative potential energies including ZPE values (ΔU_0), relative enthalpies (ΔH^0_{298}) and relative free Gibbs energies (ΔG^0_{298}) of the isomers presented for the Cu^{2+}-GG, Cu^{2+}-GGG and Cu^{2+}-GGG systems. In kcal/mol.

isomers	ΔU_0	ΔH^0_{298}	ΔG^0_{298}
Cu^{2+}-GG1	0.0	0.0	0.0
Cu^{2+}-GG2	0.2	0.3	-0.1
Cu^{2+}-GG3	5.3	6.2	2.6
Cu^{2+}-GG4	11.8	12.2	10.8
Cu^{2+}-GG5	14.5	15.0	12.9
Cu^{2+}-GG6	15.0	16.4	11.5
Cu^{2+}-GGG1	0.0	0.0	0.0
Cu^{2+}-GGG2	9.0	9.4	8.1
Cu^{2+}-GGG3	15.5	15.6	15.1
Cu^{2+}-GGG4	19.7	20.2	18.2
Cu^{2+}-GGG5	21.2	21.4	20.3
Cu^{2+}-GGG6	21.8	22.0	20.9
Cu^{2+}-GGG7	24.0	24.4	22.0
Cu^{2+}-GGG8	25.8	26.1	24.3
Cu^{2+}-GGG9	32.3	32.5	32.2
Cu^{2+}-GGGG1	0.0	0.0	0.0
Cu^{2+}-GGGG2	11.6	12.0	10.8
Cu^{2+}-GGGG3	16.3	16.3	16.4
Cu^{2+}-GGGG4	23.4	23.6	23.1
Cu^{2+}-GGGG5	26.4	26.9	24.4
Cu^{2+}-GGGG6	32.2	32.0	32.8
Cu^{2+}-GGGG7	33.6	34.2	31.2
Cu^{2+}-GGGG8	41.0	42.4	37.3

Cu^{2+} is a d^9 doubly-charged cation and the highest *d* orbital is monoocupied. In these conditions, the repulsion between the metal and the ligand is lower than for Cu^+ (a d^{10} cation) and the electrostatic interaction larger. Therefore, the interaction with more than two donor centres becomes favourable. In particular, the most stable isomers found for the present systems are tricoordinated (**Cu^{2+}-GG1**) and tetracoordinated (**Cu^{2+}-GGG1** and **Cu^{2+}-GGGG1**).

In Cu^{2+}-GG the most stable form has as a third donor centre the $\mathbf{O_{p1}}$ atom, but this structure is nearly degenerate with **Cu^{2+}-GG2** (0.2 kcal/mol above), where the third basic site is the $\mathbf{N_{p1}}$ atom. The possibility that GG coordinates through the $\mathbf{O_{p1}}$ or the $\mathbf{N_{p1}}$ atoms was also observed in Ni^+-GG and Co^+-GG systems[117] as a consequence of the electronic configuration of the metal. This fact is enhanced as the number of peptide bonds increases. For instance, in Cu^{2+}-GGG system there are two peptide bonds that can interact with the Cu^{2+} cation leading to four different isomers, everyone being tetracoordinated. These are: **Cu^{2+}-GGG1**, **Cu^{2+}-GGG3**, **Cu^{2+}-GGG5** and **Cu^{2+}-GGG6**. From the relative energies of these four structures, it can be observed that Cu^{2+} prefers to interact with $\mathbf{O_p}$ rather than with $\mathbf{N_p}$. Indeed, the most stable isomer presents coordinations with the **N**, $\mathbf{O_{p1}}$, $\mathbf{O_{p2}}$ and **O** atoms (**Cu^{2+}-GGG1**), whereas **Cu^{2+}-GGG3**, **Cu^{2+}-GGG5** and **Cu^{2+}-GGG6** present **N**, $\mathbf{O_{p1}}$, $\mathbf{N_{p2}}$ and **O**; **N**, $\mathbf{N_{p1}}$, $\mathbf{O_{p2}}$ and **O**; and **N**, $\mathbf{N_{p1}}$, $\mathbf{N_{p2}}$ and **O** coordination, which lie 15.5, 21.2 and 21.8 kcal/mol above the ground-state isomer, respectively. Nevertheless, while this trend can be observed in other cases such as the pair **Cu^{2+}-GGG2**/**Cu^{2+}-GGG4** (coordination through the $\mathbf{O_{p1}}$, $\mathbf{O_{p2}}$, **O**, and $\mathbf{O_{p1}}$, $\mathbf{N_{p2}}$, **O** atoms, respectively, the former structure resulting more stable than the latter one), or the pair **Cu^{2+}-GGGG5**/**Cu^{2+}-GGGG7** (coordination through the $\mathbf{O_{p2}}$, $\mathbf{O_{p3}}$, $\mathbf{O_{p4}}$, and $\mathbf{O_{p2}}$, $\mathbf{N_{p3}}$, $\mathbf{O_{p4}}$ atoms, respectively, the former structure being more stable than the latter one), in some cases the trend is not followed, as occurs in the pair **Cu^{2+}-GG1**/**Cu^{2+}-GG2** where, after adding the entropic terms, the latter one becomes more stable than the former one; or in the pair **Cu^{2+}-GGG7**/**Cu^{2+}-GGG8**, in which the former isomer (coordination through the **N**, $\mathbf{N_{p1}}$, $\mathbf{O_{p2}}$ atoms) is more stable than the latter one (coordination through the **N**, $\mathbf{O_{p1}}$, $\mathbf{O_{p2}}$ atoms).

Related to this dichotomy in which the donor atoms are either the $\mathbf{O_{pn}}$ or the $\mathbf{N_{pn}}$ it is worth to focus on the structural changes that result from coordination. As it was observed for Ni^+ and Co^+ cations interacting with GG,[117] when the $\mathbf{O_{pn}}$ atom coordinates to Cu^{2+} as a third site, the peptide bond distance decreases significantly (around 0.02 and 0.04 Å), whereas when the third donor atom is the $\mathbf{N_{pn}}$ the peptide bond distance is

increased (around 0.09 and 0.14 Å). Apart of the effect that the peptide bond suffers depending on the coordination mode, more interesting is to evaluate the changes occurred on the amide hydrogen. When a $\mathbf{O_{pn}}$ atom coordinates the metal cation, the stretching frequency of the amide hydrogen shifts slightly at lower values, around 20 cm^{-1}, enhancing slightly its acidity. However, more important changes are given when the $\mathbf{N_{pn}}$ atom coordinates the metal cation. In such cases, the stretching frequency of the hydrogen amide is substantially shifted towards lower values, around 120 – 150 cm^{-1}, indicating that this hydrogen acquires a significant acid character. This fact is in good agreement with the idea that one of the bonding points between the Cu^{2+} cation and the Aβ takes place through a deprotonated backbone amide nitrogen at neutral pH.[282] Accordingly, the NH amide group in solution, after coordination of Cu^{2+} cation, could lose the proton due to its increased acid character and then, the remaining N (now negatively charged) could coordinate more efficiently the metal cation, enhancing the binding energy. Similar facts were observed by means of EPR experiments, where glycine oligomers in solution establish strong in-plane σ-bonds between Cu^{2+} and the deprotonated nitrogen peptide.[283]

Among the isomers of the Cu^{2+}-GGGG system, one can find dicoordinated, tricoordinated and tetracoordinated structures. These will enable us to establish the preferred coordination modes of the Cu^{2+} cation. The four most stable isomers are tetracoordinated (**Cu^{2+}-GGGG1**, **Cu^{2+}-GGGG2**, **Cu^{2+}-GGGG3** and **Cu^{2+}-GGGG4**, the relative energies being 0.0, 11.6, 16.3 and 23.4 kcal/mol, respectively), and thus, Cu^{2+} cation tends to be coordinated by four basic sites. The main difference between these four isomers arises from the fact that the **Cu^{2+}-GGGG1** and **Cu^{2+}-GGGG3** conformers show a square-planar geometry while the **Cu^{2+}-GGGG2** and **Cu^{2+}-GGGG4** isomers are close to a distorted butterfly structure. Therefore, the preference of the Cu^{2+} cation is to be tetracoordinate adopting a square-planar geometry. Among the charge solvated forms, there are two tricoordinated structures corresponding to **Cu^{2+}-GGGG5** and **Cu^{2+}-GGGG7**, 26.4 and 33.6 kcal/mol higher to **Cu^{+}-GGGG1**, respectively and one dicoordinated structure, **Cu^{2+}-GGGG8**, which lies 41.0 kcal/mol above the most stable one. In this last isomer the ligand has been oxidized by the metal cation (the spin density is located on the amine group, becoming more planar) and the metal becomes a Cu^{+} monocation, which prefers, as aforementioned, a linear dicoordination mode. In summary, the coordination preferences are: tetracoordination (square-planar geometry) > tetracoordination (distorted butterfly geometry) > tricoordination > dicoordination. However, this trend cannot be

taken as a general rule because it is obvious that other factors must be considered, such as the chemical nature of the donor atoms or constraint effects.

It has been observed that the zwitterionic forms for Cu^{+}-poliglycines are the most unstable structures for each system. For the Cu^{2+} systems the salt bridge structures are not the most energetic isomers of the explored potential energy surfaces but as measure the peptide chain increases these forms become more unstable and remain quite high in energy with respect to the most stable ones. In particular, **Cu^{2+}-GGG9** and **Cu^{2+}-GGGG6**, which are coordinatively similar with the metal located over the backbone of the peptide as a crown, lie 32.3 and 32.2 kcal/mol above their respective ground-state conformers, respectively. Following with the zwitterionic forms, it is noteworthy to observe the influence of the metal charge on their stability. The dicationic **Cu^{2+}-GGG9** isomer comes from the monocationic **Cu^{+}-GGG6** structure, in which the proton of the hydroxyl group has migrated to the **N** atom to form the zwitterionic structure. This indicates that this zwitterionic form is stable due to the higher charge of the metal cation. Despite that, in Cu^{+}-GG systems two possible zwitterionic forms are observed, whereas in Cu^{2+}-GG systems only one structure is a salt bridge form: the **Cu^{2+}-GG3** structure (5.3 kcal/mol above the **Cu^{2+}-GG1**). The other zwitterionic form found in Cu^{+}-GG system collapsed into the **Cu^{2+}-GG6** structure after optimizing, the hydrogen of the protonated $\mathbf{O_{p1}}$ atom being transferred to the carboxylate group to form a hydroxyl group.

It is interesting to analyze the spin density of the systems. Only in two cases a total oxidation of the ligand is observed: **Cu^{2+}-GG6** and **Cu^{2+}-GGGG8** isomers. In both cases the spin is located over the amino group. For the remaining systems the spin density values of the metal cation range around 0.60 – 0.80, 0.75 – 0.85 and 0.82 – 0.89 for the Cu^{2+}-GG, -GGG and -GGGG systems, respectively. For Cu^{2+}-Gly[112] the spin density on the metal cation ranged around 0.10 – 0.58. So that, there is a clear fact: the longer the peptide chain is, the smaller the oxidation the ligand undergoes. Similar facts were observed when Cu^{2+} cation interacted with Guanine-Cytosine base pair, in which the degree of oxidation of the pair depended on the coordination environment.[284] These facts can be understood considering the metal–ligand interaction. For the **Cu^{2+}-GGGG1** isomer the optimized geometry corresponds to a square-planar like structure with the **N**, $\mathbf{O_{p1}}$, $\mathbf{O_{p3}}$ and **O** atoms coordinating to the metal cation. The ligand in this plane (*xy*) largely destabilizes the $d_{x^2-y^2}$ orbital of the metal cation and thus, the preferred situation corresponds to that in which this orbital is monoocupied (Figure 5.4a). However, in the **Cu^{2+}-GG1** conformation,

with a trigonal like disposition, the ligand field splitting is smaller than in the square-planar geometry. That is, the 3*d* orbitals are less destabilized, which favours the spin delocalization on the ligand (Figure 5.4b). Thus, the oxidation induced by Cu^{2+} is related to the kind of coordination: more coordinated the metal is, less oxidated the ligand is. The capability of Cu^{2+} to reduce the ligand is an interesting point in the Alzheimer's disease. Indeed, it is thought that the generation of oxygen radicals (oxidative stress), which leads to neuronal death, could be caused by the interaction of Cu^{2+} with the Aβ.[264, 265] These results indicate that in the most stable structures Cu^{2+} does not oxidize the peptide backbone, which suggests that in order to Cu^{2+} induces oxidative stress by interaction with Aβ it is necessary the presence of amino acids with side chains that act as easily electron donors.

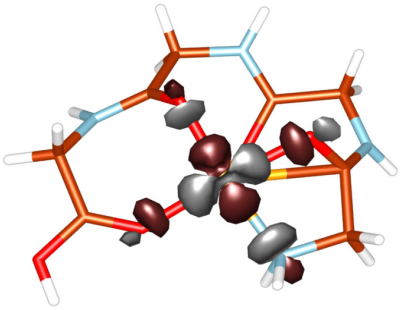

q_{Cu} = 1.81

$spin_{Cu}$ = 0.89

a

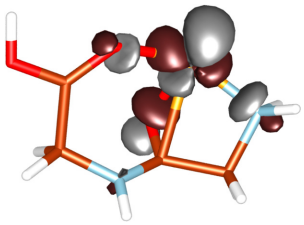

q_{Cu} = 1.61

$spin_{Cu}$ = 0.80

b

Figure 5.4 SOMO of the Cu^{2+}-GGGG1 (a) and Cu^{2+}-GG1 (b) isomers. The net charge (q_{Cu}) and the spin density ($spin_{Cu}$) on the metal cation are also included.

We have also computed the values of the E_{def} and E_{elec} assuming a point charge model of (+2)-ligand, and also the values of ΔE_{int} and ΔE_{rel} for the fourth most stable isomer of each system. In this decomposition (not reported here) it is observed that the relative energies obtained using the point charge model is quite different than the relative energies of the Cu^{2+}-isomers. This great difference is due to the different nature of the bonding of Cu^{+} cation compared to Cu^{2+} one. While in the former case it has been observed that the charge transfer is small, in the latter one the charge transfer is an important factor that greatly contributes in the interaction energies. Furthermore, the metal – ligand repulsion is different owing to the different electron configuration of both metal cations. Therefore, the point charge model does not reproduce well the nature of the bonding in Cu^{2+}-systems, pointing out that it is far from being purely electrostatic.

5.3.3 BINDING ENERGIES OF $Cu^{+/2+}$-GG, -GGG, -GGGG

In Table 5.4 the computed D_e, D_0, ΔH^0_{298} and ΔG^0_{298} values for the most stable $Cu^{+/2+}$-GG, -GGG and -GGGG structures are reported, as well as those of some small molecules that contain the functional groups in peptides (NH_3, HCOOH and NH_2COH). In addition, the calculated interaction energies of the $Cu^{+/2+}$-Gly systems are also shown.

For both metal cations, the binding energies increase as the peptide chain is elongated. In both cases this fact is related to a larger electrostatic interaction although for Cu^+ the most stable structures are always dicoordinated. However, they differ on their coordination angles, which are 90, 150, 180 and 180 degrees for the most stable isomer of Cu^+-Gly, **Cu^+-GG1**, **Cu^+-GGG1** and **Cu^+-GGGG1**, respectively. As previously mentioned, the linear dicoordination is the most favourable one since Pauli repulsion is minimized in this type of geometry. The interaction energy for the two former systems is not as favourable as for the latter ones, for which metal ligand repulsion is efficiently reduced through *sd*σ hybridization, thereby, reducing the metal–ligand distance and thus, increasing the stabilizing electrostatic interaction. Binding energy of **Cu^+-GGG1** is larger than **Cu^+-GGGG1** (although both are 180 degrees linearly diccordinated) because the GGGG ligand is more flexible than GGG, which allows shorter metal–ligand distances. In contrast, for the Cu^{2+} systems, the increase in the binding energies is related to the adopted coordination geometry of the most stable isomer. As mentioned, the preferred geometry of Cu^{2+} dication is a square-planar geometry. The most stable isomer of Cu^{2+}-Glycine is dicoordinated, for **Cu^{2+}-GG1** is tricoordinated, for **Cu^{2+}-GGG1** is tetracoordinated adopting a distorted butterfly structure and for **Cu^{2+}-GGGG1** is tetracoordinated adopting a square-planar geometry. Accordingly, it is not surprising to find that the interaction energy follows the order of **Cu^{2+}-GGGG1** > **Cu^{2+}-GGG1 > Cu^{2+}-GG1**, which is the same than the electrostatic interaction.

It can be slightly appreciated that the binding energy differences between the "GGGG" and "GGG" forms are smaller than the binding energy differences between the "GGG" and "GG" forms, both in Cu^+ and Cu^{2+} systems. This fact suggests that for longer peptides than the presented in this work the binding energies will tend to be similar. In this situation the coordination environment of the metal will be saturated by a number of donor atoms and the binding energy will relatively be independent of the length of the peptide.

Table 5.4 Binding Energies (D_e, D_0, ΔH^0_{298} and ΔG^0_{298}) in kcal/mol of $Cu^{+/2+}$-GG, -GGG and -GGGG, $Cu^{+/2+}$-Gly and $Cu^{+/2+}$-NH_3, -HCOOH and -NH_2COH.

	species	D_e	D_0	ΔH^0_{298}	ΔG^0_{298}
Cu^+	Gly	75.4[a] (68.1)[b]			
	GG	87.5	85.6	86.4	76.8
	GGG	97.1	95.9	96.5	86.3
	GGGG	104.7	104.4	104.4	97.4
	NH_3[c]	59.3	56.6	57.8	49.5
	HCOOH[c]	45.4	44.4	44.7	37.5
	NH_2COH[c]	58.2	56.5	57.1	49.4
Cu^{2+}	Gly	242.7[a] (214.8)[b]			
	GG	256.4	253.9	255.2	244.2
	GGG	301.7	298.6	300.1	287.5
	GGGG	338.1	335.4	336.8	324.7
	NH_3[d]	139.2	136.4	137.7	129.3
	HCOOH[d]	134.4	133.3	133.9	125.9
	NH_2COH[d]	163.5	161.6	162.4	154.1

[a] Ref [112].

[b] Determined at the CCSD(T) level using the B3LYP geometries

[c] Optimized at the B3LYP/6-311++G(2df,2pd) level.

[d] Optimized at the BHLYP/6-311++G(2df,2pd) level.

Finally, in order to have a deeper insight on the nature of the binding energies we have used the interaction energies of the simplest models of the groups that a peptide contains. A priory, we have assumed the binding energies of the real systems as the sum of the interaction energies of the small molecules and the values obtained have been compared by the real computed values. According to the interaction energy values of the small molecules, the maximum binding energy in Cu^+-systems assuming a dicoordination environment would be given by the **N** and the $\mathbf{O_{pn}}$ atoms (the sum of the D_0 values of Cu^+-NH_3 and Cu^+-NH_2COH complexes is 113.1 kcal/mol). However, any of the Cu^+-ground state isomers follows this coordination environment. In addition, according to the

values of the small molecules, the binding energies of the Cu^{+}-GG and Cu^{+}-GGG systems should be equal, around 101 kcal/mol, a fact that is not true in the real cases. Similar facts occur in Cu^{2+}-systems, where the binding energies of the Cu^{2+}-GGG and Cu^{2+}-GGGG systems obtained using the interaction energies of the small molecules should be also equal (around 564.4 kcal/mol). Furthermore, the values of the binding energies for each system given by the small molecules are quite larger than the real systems, especially for the Cu^{2+} ones. These results clearly indicate the non-additive behaviour of the binding energies only considering the interaction between the metal cation and the functional group present in a peptide. Therefore, other factors must be taken in consideration such as the geometry, the deformation of the ligand or the intramolecular hydrogen bonds. Furthermore, the screening effect of the ligands interacting with the metal cation when adding a new ligand will reduce the energy interaction of the small molecules with Cu^{+} and Cu^{2+} cations.